5-1-2016

Solar Energy Storage in Molten Salt Shell Structures

Nathan David Tyrrell Loyd
University of Nevada, Las Vegas, loyd.nate@gmail.com

SOLAR ENERGY STORAGE IN MOLTEN SALT SHELL STRUCTURES

By

Nathan David Tyrrell Loyd

Bachelor of Science in Civil Engineering
University of Nevada, Reno
2013

A thesis submitted in partial fulfillment
of the requirements for the

Master of Science in Engineering – Civil and Environmental Engineering

Department of Civil and Environmental Engineering and Construction
Howard R. Hughes College of Engineering
The Graduate College

University of Nevada, Las Vegas
May 2016

UNLV | GRADUATE COLLEGE

Thesis Approval

The Graduate College
The University of Nevada, Las Vegas

April 11, 2016

This thesis prepared by

Nathan David Tyrrell Loyd

entitled

Solar Energy Storage in Molten Salt Shell Structures

is approved in partial fulfillment of the requirements for the degree of

Master of Science in Engineering – Civil and Environmental Engineering
Department of Civil and Environmental Engineering and Construction

Samaan Ladkany, Ph.D.
Examination Committee Chair

Nader Ghafoori, Ph.D.
Examination Committee Member

Ying Tian, Ph.D.
Examination Committee Member

William Culbreth, Ph.D.
Graduate College Faculty Representative

Kathryn Hausbeck Korgan, Ph.D.
Graduate College Interim Dean

ABSTRACT

SOLAR ENERGY STORAGE IN MOLTEN SALT SHELL STRUCTURES

By Nathan Loyd

An M.S. Thesis Prepared Under the Direction of
Dr. Samaan G. Ladkany, PE
Professor of Civil Engineering

Molten salts (MS) in the 580°C range could be used to store excess energy from solar power stations and possibly from nuclear or coal. The energy can be stored up to a week in large containers at elevated temperature to generate eight hours of electricity to be used at night or during peak demand hours. This helps to reduce the fluctuation experienced at thermal solar power stations due to weather conditions. Our research supported by Office of Naval Research (ONR), presents a survey of salts to be used in molten salt technology and the design of large steel and hybrid molten salt storage shells. The physical characteristics of these salts such as density, melting temperature, viscosity, electric conductivity, surface tension, thermal capacity and cost are discussed. Cost is extremely important given the large volumes of salt required for energy storage at a commercial power station. Formulas are presented showing the amount of salt needed per required megawatts of stored energy depending on the type of salt. The estimated cost and the size of tanks required and the operating temperatures are presented. Recommendations are made regarding the most efficient type of molten salt to use. Commercial thermal solar power stations have been constructed in the US and overseas mainly in Spain for which molten salt is being considered. A field of flat mirrors together with collection towers are presently used in some designs and parabolic troughs used in others to produce electricity commercially.

Two designs of tanks for the storage of excess energy from thermal solar power plants using molten salts (MS) at 580°C is presented. Energy can be stored up to a week in large

containers to generate eight hours of electricity for use at night or to reduce weather related fluctuation at solar thermal energy plants. The research presented in this thesis shows detailed designs of cylindrical shells for the storage of high temperature molten salts. One storage shell consists of an inner stainless steel layer designed to resist corrosion and an external steel structural layer to contain the large pressures resulting from the molten salt with a steel bottom. The other storage shell consists of an inner stainless steel layer and an external reinforced concrete structural layer with a steel bottom. Both cylindrical tanks are 54 feet high and has an 80 foot diameter, with the salt level at a height of 42 feet. Given the heat of the molten salt and the size of the tank, designs include a flat shell cover supported on stainless steel columns and a semispherical utility access dome at the center. Considerations are made for the reduction of strength of steel at elevated temperatures. Layers of external insulation materials are used to reduce heat loss in the storage shells. Designs also present a 120 foot diameter posttensioned concrete foundation with 20 feet high steel side walls for the storage tank for the containment of molten salts in case of an accident. The tanks sit on a layer of sand to allow for thermal expansion.

ACKNOWLEDGEMENTS

I cannot express enough gratitude and thanks for my advisor, mentor, and committee chair, Dr. Samaan G. Ladkany, for providing his support throughout the course of my study. I would also like to thank my research advisory committee members: Dr. Nader Ghafoori, Dr. Ying Tian and Dr. William Culbreth.

I would like to also express my gratitude to the civil and environmental engineering department, graduate college, and the Office for Naval Resarch (ONR), for supporting my study through graduate research assistantships, grants, and scholarships.

In addition, I greatly appreciate the support and cooperation I have gotten from the civil engineering administration and faculty and fellow graduate students throughout my graduate study.

Saving the best for last, I would like to show my deepest gratitude to my parents, Natalie Tyrrell and David Loyd, along with the rest of my family and friends for the support they have provided throughout my higher education.

TABLE OF CONTENTS

ABSTRACT………………………………………………………………………………... iii

ACKNOWLEDGMENTS……………………………………………………………….... v

LIST OF TABLES………………………………………………………………………..ix

LIST OF FIGURES……………………………………………………………………… x

CHAPTER 1 – INTRODUCTION AND LITERATURE REVIEW…………………………….. 1

1.1 INTRODUCTION………………………………………………………………… 1

1.2 PROJECT SUMMARY……………………………………………………………1

1.3 MOLTEN SALT STORAGE……………………………………………………… 2

1.4 MOLTEN SALT PROPERTIES………………………………………………….... 4

REFERENCES……………………………………………………………………….. 5

CHAPTER 2 – MOLTEN SALTS……………………………………………………….. 6

2.1 INTRODUCTION………………………………………………………………… 6

2.2 TYPES OF MOLTEN SALTS…………………………………………………….. 6

2.3 PHYSICAL PROPERTIES OF MOLTEN SALTS……………………………….. 6

2.4 THERMODYNAMIC PROPERTIES OF MOLTEN SALTS……………………..9

2.5 COST OF SOLAR SALTS……………………………………………………….. 10

2.6 CORROSION FROM MOLTEN SALTS………………………………………... 11

2.7 CONCLUSION……………………………………………………………………12

REFERENCES…………………………………………………………………… 12

CHAPTER 3 – STEEL CYLINDRICAL SHELL……………………………………………15

3.1 INTRODUCTION……………………………………………………………... 15

3.2 DESIGN METHODS FOR STEEL MS STORAGE TANKS…………………… 15

3.3 TANK REQUIREMENTS……………………………………………………………...15

3.4 STEEL CYLINDRICAL TANKS…………………………………………………... 17

3.5 STEEL TANK DESIGN CALCULATIONS…………………………………….. 22

3.6 CONCLUSION………………………………………………………………………33

REFERENCES………………………………………………………………………… 33

CHAPTER 4 – CONCRETE CYLINDRICAL SHELL…………………………………………34

4.1 INTRODUCTION……………………………………………………………... 34

4.2 DESIGN METHODS FOR CONCRETE MS STORAGE TANKS………………... 34

4.3 TANK REQUIREMENTS……………………………………………………………...34

4.4 CONCRETE CYLINDRICAL TANKS…………………………………………….. 35

4.5 CONCRETE TANK DESIGN CALCULATIONS…………………………………41

4.6 CONCLUSION………………………………………………………………………52

REFERENCES………………………………………………………………………… 52

CHAPTER 5 – FOUNDATION DESIGN……………………………………………………… 53

5.1 FOUNDATION DESIGN……………………………………………………………53

5.2 CIRCULAR FOUNDATION RADIAL PRE-STRESSING……………………….... 54

5.3 CIRCULAR FOUNDATION CIRCUMFERENTIAL REINFORCEMENT………. 56

5.4 STEEL RING FOR THE CIRCULAR FOUNDATION…………………………….57

5.5 SQUARE FOUNDATION PRE-STRESSING DESIGN……………………………58

5.6 FOUNDATION DESIGN CALCULATIONS………………………………………59

5.7 CONCLUSION………………………………………………………………………71

REFERENCES………………………………………………………………………… 71

CHAPTER 6 – CONCLUSIONS AND FUTURE RESEARCH……………………………….. 72

6.1 CONCLUSIONS………………………………………………………………. 72

6.2 FUTURE RESEARCH…………………………………………………………… 73

REFERENCES………………………………………………………………… 75

APPENDIX A – CHARACTERISTICS OF MOLTEN SALTS AND RECOMMENDATIONS FOR USE IN SOLAR POWER STATIONS…………………………………………….. 76

APPENDIX B – DESIGN OF MOLTEN SALT SHELLS FOR USE IN ENERGY STORAGE AT SOLAR POWER PLANTS…………………………………………………….... 83

BIBLIOGRAPHY………………………………………………………………………..90

CURRICULUM VITAE………………………………………………………………… 93

LIST OF TABLES

Table 2.1: Physical Properties of Solar Salts………………………………………………………. 7

Table 2.2: Physical Properties of Solar Salts at Melting Point………………………………….. 8

Table 2.3: Thermodynamic Properties of Solar Salts…………………………………………… 9

Table 2.4: Costs of Solar Salts………………………………………………………………11

Table 2.5: Corrosion Properties of Stainless Steel Using Molten Salts………………………...11

LIST OF FIGURES

Figure 3.1: Steel Cylindrical Shell Wall M_x Bending Moment……………………………...17

Figure 3.2: Steel Cylindrical Shell Wall N_θ Forces……………………………………………18

Figure 3.3: Stresses at the Bottom of the Steel Shell Wall …………………………………… 18

Figure 3.4: Steel Cylindrical Shell Model Including Top Dome, Supporting Rows of Columns, 2' Sand Layer, 50" Posttension Slab, and Safety Steel Walls at the Edge………………….. 20

Figure 3.5: Volume Calculations for the Cylindrical Steel Tank (Chapter 3) and Concrete Tank (Chapter 4) (1)………………………………………………………………………..23

Figure 3.6: Volume Calculations for the Cylindrical Steel Tank (Chapter 3) and Concrete Tank (Chapter 4) (2)………………………………………………………………………..24

Figure 3.7: Steel Shell Wall Bending and Membrane Force Calculations (1)………………… 25

Figure 3.8: Steel Shell Wall Bending and Membrane Force Calculations (2)………………… 26

Figure 3.9: Top Steel Plate and Column Calculations (1)…………………………………... 27

Figure 3.10: Top Steel Plate and Column Calculations (2)…………………………………… 28

Figure 3.11: Top Steel Plate and Column Calculations (3)…………………………………… 29

Figure 3.12: Top Steel Plate and Column Calculations (4)……………………………………30

Figure 3.13: Top Steel Plate and Column Calculations (5)…………………………………… 31

Figure 3.14: Top Steel Dome Calculations……………………………………………………..32

Figure 4.1: Concrete Cylindrical Shell Wall M_x Bending Moment…………………………… 35

Figure 4.2: Concrete Cylindrical Shell Wall N_θ Forces……………………………………….. 36

Figure 4.3: Stresses at the Bottom of the Concrete Shell Wall ………………………………...36

Figure 4.4: Concrete Cylindrical Shell Model Including Top Dome, Supporting Rows of Columns, 2' Sand Layer, 50" Posttension Slab, and Safety Steel Walls at the Edge………..38

Figure 4.5: Concrete Shell Wall Bending Reinforcement and Shear Calculations (1)…………42

Figure 4.6: Concrete Shell Wall Bending Reinforcement and Shear Calculations (2)…………43

Figure 4.7: Concrete Shell Wall Bending Reinforcement and Shear Calculations (2)…………44

Figure 4.8: Top Concrete Plate and Column Calculations (1)…………………………………45

Figure 4.9: Top Concrete Plate and Column Calculations (2)…………………………………46

Figure 4.10: Top Concrete Plate and Column Calculations (3)……………………………...47

Figure 4.11: Top Concrete Plate and Column Calculations (4)……………………………...48

Figure 4.12: Top Concrete Plate and Column Calculations (5)……………………………...49

Figure 4.13: Top Concrete Plate and Column Calculations (6)……………………………...50

Figure 4.14: Top Concrete Plate and Column Calculations (7)……………………………...52

Figure 5.1: Posttensioning Cable and Circumferential Reinforcement Layout for Concrete Slab Including Inner Steel Ring…………………………………………………………………... 53

Figure 5.2: Inverted Eccentricity for the Circular Slab………………………………………... 55

Figure 5.3: Circumferential Reinforcement Layout per Foot (Six #14 Reinforcement Bars per Foot)……………………………………………………………………………………………56

Figure 5.4: Layout of the Cable and Steel Ring Connection…………………………………... 57

Figure 5.5: Layout of the Pre-Stressing Cable Path for the Square Foundation………………..59

Figure 5.6: Circular Slab Pre-Stressing and Cable Ring Calculations (1)……………………...60

Figure 5.7: Circular Slab Pre-Stressing and Cable Ring Calculations (2)……………………...61

Figure 5.8: Circular Slab Pre-Stressing and Cable Ring Calculations (1)……………………...62

Figure 5.9: Circular Slab Pre-Stressing and Cable Ring Calculations (2)……………………...63

Figure 5.10: Circular Slab Circumferential Reinforcement Calculations………………………64

Figure 5.11: Square Slab Pre-Stressing and Shear Calculations……………………………… 65

Figure 5.12: Square Slab Pre-Stressing and Shear Calculations………………………………. 66

Figure 5.13: Square Slab Pre-Stressing Calculations (X-Direction) (1)………………………..67

Figure 5.14: Square Slab Pre-Stressing Calculations (X-Direction) (2)………………………..68

Figure 5.15: Square Slab Pre-Stressing Calculations (Y-Direction) (1)………………………..69

Figure 5.16: Square Slab Pre-Stressing Calculations (Y-Direction) (2)………………………..70

Figure 6.1: Drop Shell Model………………………………………………………………….. 74

Figure 6.2: Spherical Shell Model……………………………………………………………... 75

CHAPTER 1

INTRODUCTION AND LITERATURE REVIEW

1.1 BACKGROUND

Current energy sources are posing a major problem to society at large. Many of these sources, such as oil and natural gas, exist in only finite quantities and pose major problems to the environment. However, with energy demand at all-time highs, something must be done to break the dependence on these fossil fuels that are fulfilling the bulk of the demand worldwide. Alternative energy is the way to continue to meet Earth's energy demands while minimizing the risk to the environment.

The purpose of this project is to examine the use of molten solar salts to be used for large scale energy storage. The project is being funded by the Office of Naval Research (ONR) with the intent that these molten solar salt systems will be used by the United States Navy to increase their energy independence on military bases and ships.

1.2 PROJECT SUMMARY

The project is divided into three main tasks. Tasks I and II are the primary focus of this thesis as UNLV is responsible for the completion of these two tasks. Task III is being performed by the College of William and Mary in Virginia.

Task I focuses on the examination of the thermophysical properties of molten salts. This task focuses on surveying a variety of molten salt compounds and investigation of their various properties, including density, heat capacity and conductance, and cost. The ideal molten salt mix is one that has a low melting temperature, a low cost and high availability, a heat capacity, a high thermal conductivity, a high temperature limit, and a low corrosion rate.

Task II focuses on the examination of various structural shapes for molten salt storage tanks. This task is determined with investigating the current structural shape, cylindrical shells, with other structural alternatives such as spherical shells and drop shells.

Task III focuses on the corrosion effects of molten salts. This task is focused on investigating the corrosion rates of various molten salts through literature review and laboratory testing.

1.3 MOLTEN SALT STORAGE

In this paper, "Overview of Molten Salt Storage Systems and Material Development for Solar Thermal Power Plants", the authors outline the various systems and methods available for using molten salts for storing solar energy and converting it into electricity (Bauer et al. 2012). Bauer et al. (2012) explains that solar thermal plants are an important technology as an alternative energy source. The use of molten salts allows for the use of detachable power from these sources (Bauer et al. 2012). This is based on the fact that the benefits of molten salts include high heat capacity, a relatively high thermal stability, low vapor pressure, and a relatively low cost (Bauer et al. 2012). Now when considering this process, the big question that needs to be considered is how can this strategy be improved upon to make molten salt use more feasible for storing solar energy?

First of all, molten salts are salts that exists in a liquid state and have high thermal capacities. Most of these salts are the result of mixing nitrites and nitrates derived from four alkali elements: calcium, sodium, potassium and lithium (Bauer et al. 2012).

In showing the main point about the benefits of molten salts, Bauer et al. (2012) provides the results of various experiments examining the thermodynamic properties of solar salt, which is a salt mixture consisting of a mixture of 60 percent (by weight) sodium nitrate and 40 percent potassium nitrate. The data provided shows that solar salt has a high thermal capacity and thermal conductivity, which supports the premise that solar salts have some benefit in storing solar energy. Bauer et al. (2012) also shows that molten salts have high decomposition temperature, supporting the claim that molten salts have a high thermal stability. In addition, Bauer et al. (2012) shows that consistent heating can increase the decomposition temperature of solar salt.

In discussing the current state of molten salt technology, Bauer et al. (2012) states the only commercially available molten salt system is the two tank system, which is a method that uses two steel cylindrical tanks of salt with the tanks at different temperatures and fill levels. However, there is extensive research being performed in developing a single tank system in order to reduce the costs of molten salt storage. The institute responsible for this paper, the DLR, has constructed a single tank system test loop for study. In addition, Bauer et al. (2012) explains that using parabolic troughs to collect solar energy can reduce the costs of molten salt storage systems. Lastly, Bauer et al. (2012) presents phase diagrams showing how the melting temperatures of molten salt mixtures can be lowered.

Ultimately, it is feasible to produce molten salt mixtures that have a low melting temperature, but more work has to be done in order to determine the various thermodynamic properties of these mixtures (Bauer et al. 2012). Also, research shows that it might be possible to produce a single tank storage system (Bauer et al. 2012). As a result, the next step in this area of research is to determine a better salt mixture that has both a low melting temperature and high thermal stability, or higher decomposition temperature. This is being done right now, but the thermodynamic properties of these salts must be determined. In addition, another aspect of the current research is to determine how to reduce the molten salt storage concept into a single tank system. Current research at DLR is examining a single tank test loop with a thermocline system.

1.4 MOLTEN SALT PROPERTIES

In "Thermodynamic Properties of Molten Nitrate Salts" by Cordaro et al. (2011), the paper seeks to determine the validity of the assumption that binary molten salts, which are salt mixtures of consisting of two single salts, observe ideal mixing behavior. This is done by examining the thermodynamic properties of single salts and determining the properties of binary mixtures. In ideal mixing behavior, the apparent heat of melting and heat capacity of a binary mixture is proportional to the molar fraction of the two components of the mixture and their respective thermodynamic properties.

Based on the various test results presented in the paper, the graphs of the heats of fusion and heat capacities versus the molar composition of each of the presented binary salts do not have a linear relationship (Cordaro et al. 2011). In addition, the comparison of the thermodynamic properties of single salts show that the tests performed at Sandia produce similar results to other referenced data (Cordaro et al. 2011).

The main inference made in this paper is that the heats of fusion and heat capacities of various binary salts do not exhibit a linear relationship relative to the molar percentages of the mixtures. The paper explains that this means that the referenced binary salts do not exhibit ideal mixing behavior because the thermodynamic properties of these salts are not proportional to the properties of their component salts (Cordaro et al. 2011). In addition, the tests performed at Sandia of thermodynamic properties of single salts are similar to the results produced by various other tests, which leads to the conclusion that tests performed at Sandia and their results are accurate, which only strengthens the conclusions of the paper (Cordaro et al. 2011).

The paper concludes that many molten salt mixtures do not follow ideal mixing behavior, which would prove the main thesis and assumption as false (Cordaro et al. 2011). Instead, the new data presented relating the thermodynamic properties to their molar percentages can be used to provide more accurate modeling of molten salt storage systems than the previous assumption (Cordaro et al. 2011). Until such point, the properties of specific mixes must be determined through laboratory testing. The various test results of these are explored in further detail in Chapter 2.

REFERENCES

Bauer, Thomas, Nils Breidenbach, Nicole Pfleger, Doerte Laing, and Markus Eck. "Overview of Molten Salt Storage Systems and Material Development for Solar Thermal Power Plants". Institute of Technical Thermodynamics, German Aerospace Center, 2012.

Cordaro, Joseph, Alan Kruizenga, Rachel Altmaier, Matthew Sampson, and April Nissen. "Thermodynamic Properties of Molten Nitrate Salts". Sandia National Laboratories, 2011.

CHAPTER 2

MOLTEN SALTS

2.1 INTRODUCTION

Molten solar salts are a great and effective way to store excess solar energy for future use due to the vast heat storage capacities of solar salts. In order for the solar salts to effectively store heat, the salts must be contained. This is done by storing the solar salts in large insulated tanks in order to keep the molten salts in a closed system.

2.2 TYPES OF MOLTEN SALTS

There are various kinds of salts, all of which can be melted for use as a molten salt. This report will mostly focus on five salts: sodium nitrate, lithium nitrate, potassium nitrate, sodium chloride, and a mixture of 60% sodium nitrate and 40% potassium nitrate. These salts have been most prominently mentioned in the literature and are being used in experimental thermal sun storage facilities since they are cost effective (Janz 1967). Other salts that can be used in these applications, both alone and in mixture form, include calcium nitrate, potassium chloride, and lithium chloride (Janz 1967).

2.3 PHYSICAL PROPERTIES OF MOLTEN SALTS

The first aspect of solar salts that must be considered are there physical properties, including melting point, density, viscosity, surface tension, heat capacity and electrical conductance. The density of these solar salts directly affect the loading exhibited by the storage tanks and any piping used. The melting point reflects an approximation of the temperatures these storage tanks will experience, which can be used to determine thermal expansion, ultimate strength and thickness along with heat shielding requirements of the tanks. The viscosity determines the resistance of the molten salt while flowing through any pipes used. Surface tension is the measure of force a liquid exerts on a surface by interacting with the surface. Lastly, the electrical conductance determines the salt's ability to conduct electricity. Table 2.1 compares the densities and melting points of these various salts.

Table 2.1: Physical Properties of Solar Salts (Haynes 2012a) (Janz et. al. 1972)

Compound or Mixture	Melting Point (°C)	Density at MP (g/cm^3)
Sodium Nitrate – $NaNO_3$	306.5	1.900
Lithium Nitrate – $LiNO_3$	253.0	1.781
Potassium Nitrate – KNO_3	334.0	1.865
Sodium Chloride – NaCl	800.7	1.556
60 % $NaNO_3$ / 40 % KNO_3	225 (approximate)	1.870 (at 625 K)

Comparing the melting points, the 60% sodium nitrate and 40% potassium nitrate mixture has the lowest melting point with an approximate melting point of 225°C (Janz et. al. 1972). The next lowest melting point is lithium nitrate at 253°C (Haynes 2012a). On the other side of the spectrum, sodium chloride (basic table salt) has the highest melting point considered at 800.7°C (Haynes 2012a). The melting point of a salt is an important consideration for solar salt applications, which means that based on melting point, the best salt, for our applications is the 60% sodium nitrate and 40% potassium nitrate mixture since it has the lowest melting point considered while sodium chloride is the worst salt considered since it has the highest melting point.

Comparing the densities of these salts, the salt with the lowest density considered is sodium chloride with a density of 1.556 g/cm^3 (Haynes 2012a). The salt with the next lowest density is lithium nitrate with a density of 1.781 g/cm^3 (Haynes 2012a). At the other end, the salt with the highest density considered is sodium nitrate with a density of 1.900 g/cm^3 (Haynes 2012a). Unlike melting point, density is not as important of a consideration, especially since the relative difference in densities between these salts is small. Table 2.2 compares the viscosities, surface tensions, and electrical conductance of various molten salts.

Table 2.2: Physical Properties of Solar Salts at Melting Point (Janz 1967) (Janz et. al. 1972)

Compound or Mixture	Viscosity (mPa-s)	Surface Tension (mN/m)	Electrical Conductance (S/cm)
Sodium Nitrate – $NaNO_3$	3.038	116.35	0.9713
Lithium Nitrate – $LiNO_3$	7.469	115.51	0.3958
Potassium Nitrate – KNO_3	2.965	109.63	0.6324
Sodium Chloride – NaCl	1.459	116.36	0.8709
60 % $NaNO_3$ / 40 % KNO_3	3.172*	121.80 (at 510 K)	0.7448*

Note: Values with a single asterisk (*) have been extrapolated for the 60% $NaNO_3$ mix at 580 K

Comparing the viscosities, the salt with the lowest viscosity is sodium chloride with 1.459 mPa-s (Janz 1967). The next lowest salt is potassium nitrate with 2.965 mPa-s (Janz 1967). Conversely, the salt with the highest viscosity is lithium nitrate with 7.469 mPa-s (Janz 1967). In comparison with other physical properties considered, viscosity is not the most important property to consider in comparing molten salts. However, it is a property of some importance as the viscosity compares the resistance exerted against the molten salts while flowing through a pipe, which is something the molten salts will have to do in the containment units.

Comparing the surface tension, the salt with the lowest surface tension is potassium nitrate with 109.63 mN/m (Janz 1967). The next lowest salt is lithium nitrate with 115.51 mN/m (Janz 1967). On the other side, the salt with the highest surface tension is the 60% sodium nitrate and 40% potassium nitrate mixture with 121.80 mN/m (Janz et. al. 1972). In comparison with other properties considered, surface tension is also not one of the most important properties to consider in comparing molten salts to be used in our applications. However, it is a property of some importance because it affects the tanks and piping of the containment units

Comparing the electrical conductance, the salt with the highest electrical conductance is sodium nitrate with 0.9713 S/cm (Janz 1967). The next highest salt is sodium chloride with 0.8709 S/cm (Janz 1967). On the other side, the salt with the lowest electrical conductance is lithium nitrate with 0.3958 S/cm (Janz 1967). Compared to the other physical and thermodynamic properties considered, electrical conductance is a minor consideration when comparing solar salts for energy storage applications.

2.4 THERMODYNAMIC PROPERTIES OF MOLTEN SALTS

Solar salts are known for their ability to store heat for long periods of time. The heat of fusion measures the required amount of heat needed to convert a substance from a solid state to a liquid state, or simply the amount of heat needed to melt a substance. The specific heat capacity measures a substance's ability to store heat. Lastly, thermal conductivity measures a substance's ability to conduct heat through said substance. All three properties considered are of major importance since these properties compare how the salts conduct and store heat. Table 2.3 compares the thermodynamic properties of solar salts.

Table 2.3: Thermodynamic Properties of Solar Salts
(Janz 1967) (Cornwell 1970) (Haynes 2012b) (Janz et. al. 1979)

Compound or Mixture	Specific Heat Capacity (J/mol/K)	Thermal Conductivity (kW/mol/K)	Heat of Fusion (kJ/mol)
Sodium Nitrate – $NaNO_3$	131.8	5.66	15.50
Lithium Nitrate – $LiNO_3$	99.6	5.82	26.70
Potassium Nitrate – KNO_3	115.9	4.31	9.60
Sodium Chloride – NaCl	48.5	8.80	28.16
60 % $NaNO_3$ / 40 % KNO_3	167.4 (at 510 K)	3.80	13.77

Note: Since some values were given in calories in some sources, they were converted into joules for this table (1 cal = 4.184 J or 1 kcal = 4.184 kJ) (IUPAC).

Comparing the specific heat capacity, the salt with the highest specific heat capacity is the 60% sodium nitrate and 40% potassium nitrate mixture with 167.4 J/mol/K (Janz et. al. 1979). The next highest salt is sodium nitrate with 131.8 J/mol/K (Janz 1967). On the other side, the salt with the lowest specific heat capacity is sodium chloride with 48.5 J/mol/K (Janz 1967). Based on this comparison, the best salt to use for energy storage is the 60% sodium nitrate and 40%

potassium nitrate mixture since it has the highest heat capacity considered while sodium chloride is the worst salt considered since it has the lowest heat capacity.

Comparing the thermal conductivity, the salt with the highest thermal conductivity is sodium chloride with 8.80 kW/mol/K (Cornwell 1970). The next highest salt is lithium nitrate with 5.82 kW/mol/K (Cornwell 1970). The salt with the lowest thermal conductivity is the 60% sodium nitrate and 40% potassium nitrate mixture with 3.80 kW/mol/K (Cornwell 1970).

Comparing the heat of fusion, the salt with the lowest heat of fusion is potassium nitrate with 9.60 kJ/mol (Haynes 2012b). The next lowest salt is the 60% sodium nitrate and 40% potassium nitrate mixture with 13.77 kJ/mol (Janz et. al. 1979). On the other side, the salt with the highest heat of fusion is sodium chloride with 28.16 kJ/mol (Haynes 2012b). Based on the comparison of salt characteristics presented in Table 1.3, the 60%/40% sodium/potassium nitrates present, for now the most interesting option for molten salt energy storage. However other options will be considered, such as, the addition of Nano silica to the salt mix in order to improve its specific heat capacity by 30% or more.

2.5 COST OF SOLAR SALTS

Ultimately, compared to the other considered salts, the most promising solar salt to use, so far, in molten salt energy storage, is the 60% Sodium Nitrate and 40% Potassium Nitrate mixture since it compares favorably against other salts in terms of thermodynamic and heating properties, which are the primary factors to consider for use as a solar salt.

However, when considering the use of solar salts, one must consider the costs of various types of salts. Table 2.4 compares the 60% sodium nitrate and 40% potassium nitrate mixture to various other solar salt substitutes that are available in the marketplace.

Table 2.4: Costs of Solar Salts (Kearney & Associates 2001)

Compound or Mixture	ΔT (°C)	Cost of Salts ($/kg)	Cost of Power ($/kWH)
Hitec XL in 59% Water (42:15:43 Ca:Na:K)	200 200	1.43 3.49 (w/o H_2O)	18.20 18.20
Hitec (7:53 Na:K: Nitrate, 40 Na Nitrate)	200	0.93	10.70
Solar Salt (60:40 Na:K Nitrate)	200	0.49	5.80
Calcium Nitrate Mixture Dewatered (42:15:43 Ca:Na:K Mixture)	200 150 100	1.19 1.19 1.19	15.20 20.10 30.00
Therminol VP-1 (Diphenyl Biphenyl Oxide)	3.96	100.00	57.50

The solar salt mixture (60% $NaNO_3$ – 40% KNO_3) is both the least expensive in terms of cost to purchase, which is 49 cents per kilogram, and the costs per kilowatt-hour of power generated, which is $5.80 per kilowatt-hour (Kearney & Associates 2001). The next best priced mixture in both aspects is the Hitec mixture, which costs 93 cents per kilogram to purchase and has a power cost of kilowatt-hour of $10.70 (Kearney & Associates 2001). In addition, the mixture that is the most expensive in both aspects is the Therminol VP-1, which costs $100 per kilogram to purchase and has a power cost of $57.50 per kilowatt-hour (Kearney & Associates 2001).

2.6 CORROSION FROM MOLTEN SALTS

In addition to being able to hold large quantities of heat, molten salts can be corrosive. Table 2.5 examines the corrosion properties of stainless steel exposed to various molten salts.

Table 2.5: Corrosion Properties of Stainless Steel Using Molten Salts (Sohal et. al. 2010) (Bradshaw and Goods 2001)

Compound or Mixture	Temp (°C)	Corrosion Rate (mm/y)	
		SS 304	SS 316
60 % $NaNO_3$ / 40 % KNO_3	580	------	0.5
Sodium Chloride – NaCl	845	7.2	7.2
Hitec Salt	538 430 505 550	0.21 ------ ------ ------	<0.03 0.007 0.008 0.074

The solar salt mixture at a temperature of 580°C corrodes the SS 316 stainless steel at 0.5 millimeters per year (Bradshaw and Goods 2001). The sodium chloride at a temperature of 845°C corrodes both types of stainless steel at 7.2 millimeters per year (Sohal et. al. 2010). At 538°C, the Hitec Salt corrodes through SS 304 steel at 0.21 millimeters per year, and through the SS 316 steel at less than 0.03 millimeters per year (Sohal et. al. 2010). In addition, the Hitec Salt corrodes through SS 316 steel 0.007 millimeters per year at 430°C, 0.008 millimeters per year at 505°C, and 0.074 millimeters per year at 550°C (Sohal et. al. 2010).

2.7 CONCLUSION

A survey of molten solar salts for use in energy storage shells is presented, to provide electric generation stations with power for eight hours. Tables are shown providing the characteristics of various molten salts to be used in thermal solar energy stations. Recommendations for the selection of an economical molten salt compound is made using various characteristics, including thermal capacity, availability, melting temperature, and the cost of salts.

REFERENCES

"1.6 Conversion tables for units." IUPAC. Retrieved from http://iupac.org/publications/analytical_compendium/Cha01sec6.pdf on Feb. 3, 2015.

Bradshaw, R.W. and S.H. Goods. "Corrosion Resistance of Stainless Steels during Thermal Cycling in Alkali Nitrate Molten Salts." Sandia National Laboratory, 2001.

Cornwell, K. "The Thermal Conductivity of Molten Salts." Department of Mechanical Engineering, Heriot-Watt University, 1970. Retrieved from http://iopscience.iop.org/0022-3727/4/3/313/pdf/0022-3727_4_3_313.pdf on Nov. 6, 2014.

"Engineering Evaluation of a Molten Salt HTF in a Parabolic Trough Solar Field", pg. 7. Kearney & Associates and Flabeg Solar International, 2001. Retrieved from http://www.nrel.gov/csp/troughnet/pdfs/ulf_herrmann_salt.pdf on Dec. 13, 2014.

Haynes, W. "Density of Molten Elements and Representative Salts". *CRC Handbook of Chemistry and Physics*, 2012. Retrieved from http://www.hbcpnetbase.com//articles/04_07_92.pdf#xml=http://www.hbcpnetbase.com/search/pdfHits.asp?id=04_07_92&DocId=118023&hitCount=10&hits=1984 1980 1969 1965 1386 1382 160 159 141 41 on Nov. 5, 2014.

Haynes, W. "Enthalpy of Fusion." *CRC Handbook of Chemistry and Physics*, 2012. Retrieved from http://www.hbcpnetbase.com//articles/06_26_92.pdf#xml=http://www.hbcpnetbase.com/search/pdfHits.asp?id=06_26_92&DocId=118085&hitCount=4&hits=507 366 365 155 on Nov. 5, 2014.

Janz, G.J. *Molten Salts Handbook*. Academic Press. New York, NY, 1967.

Janz, G.J., Allen, C.B., Bansal, N.P., Murphy, R.M., and Tomkins, R.P.T. "Physical Properties Data Compilations Relevant to Energy Storage. II. Molten Salts: Data on Single and Multi-Component Salt Systems." Molten Salts Data Center, Cogswell Laboratory, Rensselaer Polytechnic Institute, 1979. Retrieved from http://www.nist.gov/data/nsrds/NSRDS-NBS61-II.pdf on Nov. 10, 2014.

Janz, G.J., Krebs, U., Siegenthaler, H.F., and Tompkins, R.P.T. "Molten Salts: Volume 3, Nitrates, Nitrites, and Mixtures." Molten Salts Data Center, Department of Chemistry, Rensselaer Polytechnic Institute, 1972. Retrieved from http://www.nist.gov/data/PDFfiles/jpcrd10.pdf on Nov. 18, 2014.

Sohal, M., Ebner, M., Sabharwall, P., and Sharpe, P. "Engineering Database of Liquid Salt Thermophysical and Thermochemical Properties." Idaho National Laboratory, 2010. Retrieved from http://www.inl.gov/technicalpublications/Documents/4502650.pdf on Feb. 6, 2015.

CHAPTER 3

STEEL CYLINDRICAL SHELLS

3.1 INTRODUCTION

Molten solar salts are a great and effective way to store excess solar energy for future use due to the vast heat storage capacities of solar salts. These solar salts are contained in large insulated tanks in order to keep the molten salts in a closed system. This project examines the current method of using insulated hybrid steel cylindrical shells to store molten salt and presents a preliminary design of real life examples.

3.2 DESIGN METHODS FOR STEEL MS STORAGE TANKS

Currently, molten salt (MS) storage shells are usually cylindrical tanks made of stainless steel. The MS steel tanks have a hybrid design of A588 Carbon Steel and an inner layer of 316 Stainless Steel to protect against corrosion, varying in thickness from one inch (25 mm) for a fifty year plant life span to 0.6 in (15 mm) for a thirty year plant life span.

3.3 TANK REQUIREMENTS

For this stage of the project research, the tanks need to store enough molten solar salt, which is a 60:40 sodium nitrate ($NaNO_3$) and potassium nitrate (KNO_3) mix, to provide power for a 300 megawatt power plant for eight hours each night. Calculations determined that in order to satisfy these requirements, the two tanks need to be able to store 12,048 cubic meters of salt or 425.5×10^3 cubic feet.

In order to determine the total mass of salt required to operate the power plant, one must start with the basic energy equation, which is shown in Equation 3.1 (Holman 1986).

$$E = P_{thermal} * \Delta t_{storage} = m * c_p * \Delta T \tag{3.1}$$

In Equation 3.1 above, E represents the total energy in the system. The power generated by the power plant is $P_{thermal}$, which as stated earlier is 300 megawatts. The required time of storage is $\Delta t_{storage}$, which is 8 hours or 28,800 seconds. The required amount of solar salt needed for the power plant is represented by m. The specific heat capacity of the salt is c_p, which is 1540 joules per kilogram of salt per degree kelvin. The temperature range of the salt in the system is ΔT, which is calculated using Equation 3.2 below.

$$\Delta T = T_{salt,max} - (T_{sat} - 20\ K) \tag{3.2}$$

In Equation 3.2 above, the maximum temperature of salt in the system, or $T_{salt,max}$, is 853.15 degrees kelvin. The temperature of the Rankine cycle, or T_{sat}, is 620.55 degrees kelvin. Equation 3.2 determined that the temperature range for the salt is 252.6 degrees kelvin.

In order to determine the required mass of salt, Equation 3.1 is rearranged into Equation 3.3 as shown.

$$m = \frac{P_{thermal} * \Delta t_{storage}}{c_p * \Delta T} \tag{3.3}$$

This determined that the power plant requires 22.88 x 10^6 kilograms of salt, or 50.44 x 10^6 pounds (25,220 tons).

Equation 3.4 is used to determine the volume of solid salt required.

$$V_{salt} = \frac{m}{\rho_{salt}} \tag{3.4}$$

Equation 3.4 determined that the volume of solid salt required is 12,048 cubic meters of salt, or 425.5 x 10^6 cubic feet (12,048 cubic meters). This volume will be divided over two tanks, requiring 212.7 x 10^6 cubic feet (6,024 cubic meters) for each tank. However, a third and fourth tanks, all of carbon steel, are recommended for the storage of cooled MS after power generation and for safety and continued operations during maintenance of the other tanks.

All structural steel used is A588 Grade 50 steel. The cylindrical tank designed with a 40 feet (12.192 meters) radius at the base. This results in a height of salt of 42 feet (12.802 meters) and a height of 54 feet (16.594 meters) for the cylindrical tank.

3.4 STEEL CYLINDRICAL TANKS

The steel structural design was divided into five elements for individual analysis and design, which are the shell wall, the top cover with a central 10 feet (3.048 meters) diameter steel access dome, support columns, a steel bottom, and the concrete slab below a layer of sand. All of these structural elements are made of structural and stainless steel except the concrete slab. Shell theory was used to perform the structural analysis of the cylindrical tank and central access dome.

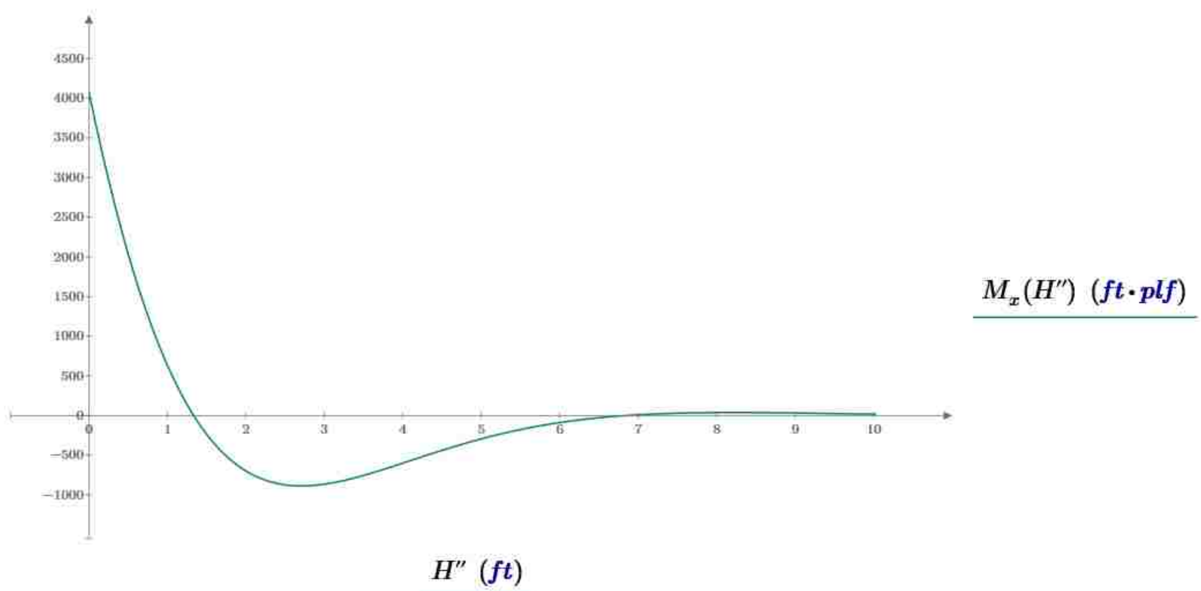

Figure 3.1: Steel Cylindrical Shell Wall M_x Bending Moment

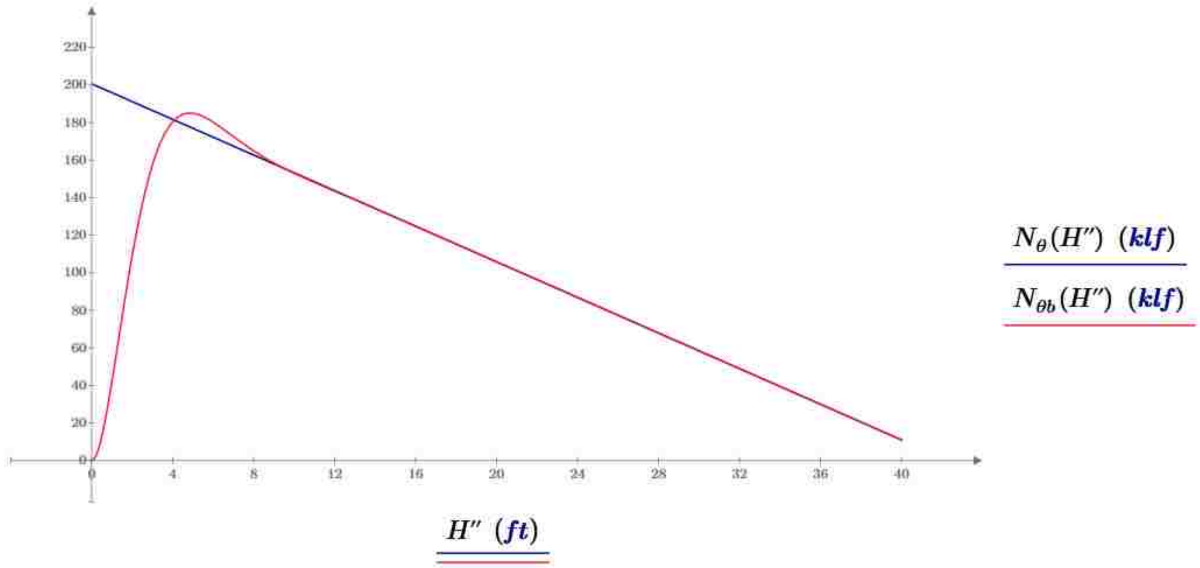

Figure 3.2: Steel Cylindrical Shell Wall N_θ Forces
The red curve is based on Bending Theory while the blue curve is based on Shell Theory

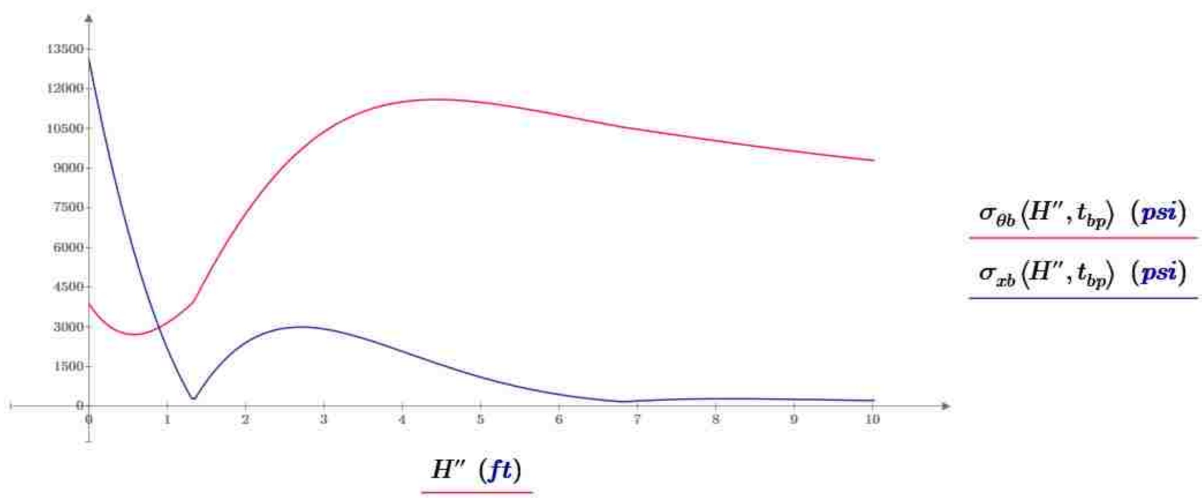

Figure 3.3: Stresses at the Bottom of the Steel Shell Wall
The red curve is the Circumferential Stress and the blue curve is the Axial Stress

The first design performed was for the shell wall. Based on shell theory, axial bending in a cylindrical shell occurs mainly at the base of the wall, at the junction with the ring and base plate, before dissipating further up the wall (Urugal 2009). Further analysis determined that axial bending dissipates nine feet above ground. The first step was to determine the bending in the shell wall as shown in Figure 3.1. The maximum positive axial bending moment is 4.085 kip-foot/foot

(18.17 kN-m/m) at the bottom of the shell, and the maximum negative bending moment is 886.2 pound-foot/foot (3.942 kN-m/m) at a height 2.7 feet (826 mm) above the bottom of the shell. Circumferential moments are equal to the Poisson ratio multiplied by the axial moments. The bottom of the wall contains the maximum circumferential tensile force, which is 177.6 kips per linear foot (klf), which is 2,593 kN/m. Tensile membrane force is determined by Equation 3.6 and Figure 3.2 (Urugal 2009). While maximum axial compressive force, N_x, in the wall at the bottom of the shell is equal to the total dead weight of the shell, top slab, live load and service dome, which is the total weight (W), divided by the circumference of the shell. Equations 3.7 through 3.12 are used to determine the bending in the shell wall (Urugal 2009).

$$p = \gamma z \tag{3.5}$$

$$N_\theta = pr \tag{3.6}$$

$$D = \frac{Et}{12(1-\nu)} \tag{3.7}$$

$$\beta = \sqrt{\frac{\sqrt{1-\nu^2}}{rt}} \tag{3.8}$$

$$C_1 = \frac{\gamma h r^2}{Et} \tag{3.9}$$

$$C_2 = \frac{\gamma r^2}{Et}\left(h - \frac{1}{\beta}\right) \tag{3.10}$$

$$w = e^{-\beta x}(C_1 \cos \beta x + C_2 \sin \beta x) + \frac{\gamma(h-x)r^2}{Et} \tag{3.11}$$

$$M_x = D\frac{d^2 w}{dx^2} \tag{3.12}$$

$$M_\theta = \nu M_x \tag{3.13}$$

$$N_x = \frac{W_x}{C} \tag{3.14}$$

In determining the applied pressure on the tank from Equation 3.5, it is the product of the salt unit weight (γ) and the depth of salt (z) at the specified point. In Equation 3.6, p is the applied pressure on the wall and r is the radius of the wall (Urugal 2009). In Equations 3.7 through 3.12, D, β, C_1, and C_2 are coefficients, E is the Young's Modulus of the shell material, t is thickness of the shell wall, ν is the Poisson's ratio of the shell material, h is the total height of molten salt, w is shell wall deflection at a height of x above ground, and the second derivative of w is used to determine the moment at that point (Urugal 2009). M_x is the axial moment at a height of x above ground, W_x is the weight of the shell including dead and live loads on its top at level above x (Urugal 2009). Figure 3.3 details the design of the cylindrical shell and the top dome.

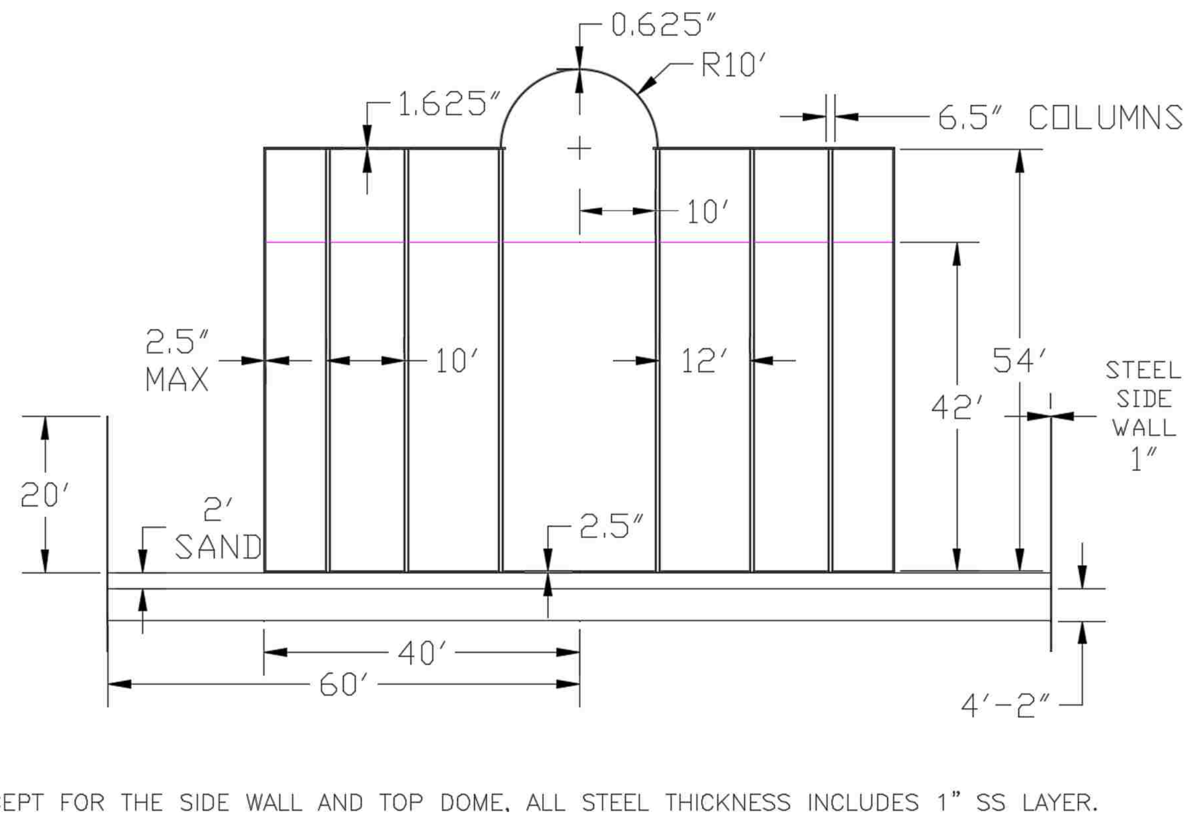

Figure 3.4: Steel Cylindrical Shell Model Including Top Dome, Supporting Rows of Columns, 2' Sand Layer, 50" Posttension Slab, and Safety Steel Walls at the Edge

The shell was designed in sections of varying thickness based on the loading. The bottom nine feet of the shell wall was designed to accommodate excess bending, require 1.5 inches of structural steel thickness due to the combined axial membrane and bending stresses. The next section of the wall, from 9 to 15 feet (2.734 to 4.572 meters) above ground, requires 0.625 inches (15.9 mm) of steel thickness. Starting from 15 feet above ground, the thickness of the shell wall is decreased by 0.125 inches (3.2 mm) every seven feet until a thickness of 0.125 inches (3.2 mm) remain. This results in the wall being 0.5 inches (12.7 mm) thick between 15 and 22 feet (4.572 to 6.706 meters), 0.375 inches (9.5 mm) between 22 and 29 feet (6.706 to 8.839 meters), 0.25 inches (6.4 mm) between 29 and 36 feet (8.839 to 10.973 meters) above ground, and 0.125 inches (3.2 mm) for the remaining portion of the wall above 36 feet (10.973 meters). Due to corrosion effects, a one inch liner of 316 Stainless Steel covers the steel wall.

The next design was for both the top steel plate and the columns supporting it in the cylindrical tank. The top plate is 0.625 inches (15.9 mm) thick and is supported by three circular rows of columns. One row of columns is located ten feet (3.048 meters) away from the center of the tank, at the tip of the opening and the 0.625 inches (15.9 mm) thick service dome. It contains eight equally spaced columns. The second row of columns is located 22 feet (6.706 meters) away from the center of the tank and contains eight equally spaced columns. Lastly, the third row of columns is located 32 feet (9.754 meters) away from center and contains 16 equally spaced columns. These columns are made of carbon steel covered with a layer of stainless steel because of the heat and corrosion from MS. When designing the columns and shell walls, an extra factor of safety is used due to the expected heat of the molten salt. At 580 degrees Celsius, steel is expected to only maintain 60% of its nominal yield strength (Salmon 2009). As a result, the final design load for the first row of columns is 6.5 kips (28.9 kN), 19.6 kips (87.2 kN) for the second row, and 11.7 kips (52.0 kN) for the third row. Ultimately, it is determined that the first row of columns be designed as HSS 4½ x 4½ x 1/8” columns, the second row as HSS 4½ x 4½ x ¼” columns, and the third row as HSS 4½ x 4½ x 1/8" columns (Steel Construction Manual 2012). Due to corrosion effects, a one inch (25.4 mm) liner of 316 Stainless Steel covers the steel column. In addition, the column will be connected to the top steel shell with a 14 inch by 14 inch (356 mm) plate that is two inches thick (50.8 mm).

In order to design for bending in the top steel flat slab, Timoshenko's method was used to design the top plate as a continuous simply supported plate over the edge of the shell and supported by rows of columns as discussed earlier. Moments at the supporting columns are found from the column pattern of annular arrays normalized as rectangular arrays. Based on Timoshenko's (1959) theory, the maximum negative bending moment in each direction is located at the column. The maximum positive moments, being the radial moments, occur at the center of the normalized annulus, and the maximum circumferential moment occur directly halfway between columns. For this shell, the maximum negative moment is 1.785 kip-foot/foot (7.940 kN-m/m) and the maximum positive radial moment is 1.040 kip-foot/foot (4.626 kN-m/m).

In addition, an opening with a 10 feet (3.048 meters) radius is carved out of the top shell so that a removable steel dome with the same radius can be placed on top of the steel plate. This opening is to allow pipes into the shell and service access into the tank.

3.5 STEEL TANK DESIGN CALCULATIONS

Figures 3.4 and 3.5 detail the calculations used to determine the tank volume. Figures 3.6 through 3.7 show how the steel shell wall was calculated. Figures 3.8 through 3.12 show how the steel top plate and steel columns were calculated. Lastly, Figure 3.13 shows how the steel top dome was calculated.

Power Plant Characteristics

$P_{thermal} := 300\ MW$ $\quad p_{sat} := 160\ bar$ $\quad T_{sat} := 347.4\ °C = 620.55\ K$ $\quad \eta := 0.30$

$P_{electrical} := \eta\ P_{thermal} = 90\ MW$ $\quad \Delta t_{storage} := 8\ hr = 28800\ s$

$Rate_{thermal} := P_{thermal}\ \Delta t_{storage} = 2400\ MW \cdot hr$ $\quad Rate_{electrical} := P_{thermal}\ \Delta t_{storage} = 2400\ MW \cdot hr$

This solar salt tank system must produce 2400 megawatt-hours worth of power (300 MW for 8 hours), which at 30% efficiency, would provide 720 megawatt-hours of electricity (90 MW for 8 hours).

Salt Properties

$T_{salt\_max} := 580\ °C = 853.15\ K$ $\quad c_p := 1495\ \frac{J}{kg \cdot K}$ $\quad \rho_{salt} := 1899\ \frac{kg}{m^3}$ $\quad \gamma_s := \rho_{salt}\ g = 118.551\ pcf$

Specific Weight of Salt

The maximum temperature that the solar salt can be in this system is 700°C. The salt has a density of 1899 kilograms per cubic meter and a specific heat of 1495 Joules per degree Kelvin per kilogram of salt.

Other Properties

$T_{melt} := 260\ °C = 533.15\ K$ $\quad T_{max} := 550\ °C = 823.15\ K$ $\quad H_{fusion} := 161000\ \frac{J}{kg}$

The melting point of the salt is 260°C and the heat of fusion is 161,000 Joules per kilogram.

Temperature Range

$\Delta T := T_{salt\_max} - (T_{sat} - 20\ K) = 252.6\ K$

The expected temperature range for the salt is 372.6 K.

Figure 3.5: Volume Calculations for the Cylindrical Steel Tank (Chapter 3) and Concrete Tank (Chapter 4) (1)

Nathan Loyd - Steel Cylindrical Tank Design

Total Mass of Salt

$$m := \frac{P_{thermal} \cdot \Delta t_{storage}}{c_p \cdot \Delta T} = 5.044 \cdot 10^7 \ \boldsymbol{lb} \qquad m = 2.288 \cdot 10^7 \ \boldsymbol{kg} \qquad m = 25219.906 \ \boldsymbol{ton}$$

Total Volume of Salt

$$V_{salt} := \frac{m}{\rho_{salt}} = 4.255 \cdot 10^5 \ \boldsymbol{ft}^3 \qquad V_{salt} = 12047.98 \ \boldsymbol{m}^3$$

Volume of Tanks

$$n_{tank} := 2 \qquad V_{tank} := \frac{V_{salt}}{n_{tank}} = 212735.2 \ \boldsymbol{ft}^3 \qquad V_{tank} = 6023.99 \ \boldsymbol{m}^3$$

Using a two tank system, the minimum required volume for each tank is 212735.200 cubic feet.

Design Parameters

$$R := 40 \ \boldsymbol{ft} \qquad H'(R') := \frac{V_{tank}}{\pi R'^2} \rightarrow \frac{67715.717186985087422 \cdot \boldsymbol{ft}^3}{R'^2} \qquad H'(R) = 42.322 \ \boldsymbol{ft}$$

$$H := 54 \ \boldsymbol{ft}$$

The radius of the tank base is 40 feet. The height of salt of for the cylinder is 42.322 feet. Overall, the total height of the wall is 54 feet

Figure 3.6: Volume Calculations for the Cylindrical Steel Tank (Chapter 3) and Concrete Tank (Chapter 4) (2)

Regular Steel Properties

$f_y := 60\ \mathbf{ksi}$ $\quad \gamma_{st} := 500\ \mathbf{pcf}$

$\nu_s := 0.3$ $\quad E_s := 29000\ \mathbf{ksi}$

$f_a := 0.6\ f_y = 36\ \mathbf{ksi}$

High Temperature Properties

$f'_y := 0.6\ f_y = 36\ \mathbf{ksi}$ (High Temperature Yield Strength)

$f'_a := 0.6\ f'_y = 21.6\ \mathbf{ksi}$ (High Temperature Allowable Stress)

$E'_s := 0.6\ E_s = 17400\ \mathbf{ksi}$ (High Temperature Young's Modulus)

The tank will use Grade 60 steel. Due to the extreme temperature of the tank, the available yield strength and Young's Modulus of steel is only 60% of its rated strength. The Young's modulus of steel is 29,000 ksi (17,400 ksi at high temperatures) and the Poisson's ratio is 0.3. The allowable stress is 60% of the yield strength.

Force Equations and Steel Thickness Design

$p(x) := \gamma_s\ (H'(R) - x)$ $\quad N_\theta(x) := p(x)\ R$ $\quad t(x) := \dfrac{N_\theta(x)}{f'_a}$

$t_{max} := \dfrac{\gamma_s\ R\ H'(R)}{f'_a} = 0.774\ \mathbf{in}$ $\quad t_u := \mathrm{Ceil}\left(t_{max}, 0.125\ \mathbf{in}\right) = 0.875\ \mathbf{in}$

Graphing Limits

$H'' := 0\ \mathbf{ft}, 0.001\ H'(R) .. H'(R)$

Maximum Thickness for Non Bending Region

Sidewall Shell Forces (Shell Bending Theory)

$D := \dfrac{E_s\ t_u^{\ 3}}{12\left(1 - \nu_s^{\ 2}\right)} = 148.258\ \mathbf{kip \cdot ft}$ $\quad \beta := \sqrt{\dfrac{\sqrt{1 - \nu_s^{\ 2}}}{R\ t_u}} = 0.572\ \mathbf{ft}^{-1}$

$h_0 := 0\ \mathbf{ft}$ (Lower Limit)

$h_1 := 9\ \mathbf{ft}$ (Upper Limit)

$C_1 := \dfrac{\gamma_s\ R^2\ H'(R)}{E'_s\ t_u} = 0.527\ \mathbf{in}$ $\quad C_2 := \dfrac{\gamma_s\ R^2}{E'_s\ t_u}\left(H'(R) - \dfrac{1}{\beta}\right) = 0.505\ \mathbf{in}$

D, β, C1, and C2 are all coefficients for shell bending equations.

$w(x) := -e^{-\beta x}\left(C_1\ \cos(\beta\ x) + C_2 \sin(\beta\ x)\right) + \dfrac{\gamma_s\ (H'(R) - x)\ R^2}{E'_s\ t_u}$ $\quad w(h_0) = 0\ \mathbf{in}$ $\quad w(h_1) = 0.417\ \mathbf{in}$

Figure 3.7: Steel Shell Wall Bending and Membrane Force Calculations (1)

Sidewall Shell Forces (Shell Bending Theory) (Continued)

$w'(x) := \frac{d}{dx} w(x)$ $w'(h_0) = 0$ $w'(h_1) = -0.001$

$w''(x) := \frac{d^2}{dx^2} w(x)$ $w''(h_0) = 0.028\ ft^{-1}$ $w''(h_1) = 0\ ft^{-1}$

$M_x(x) := D\ w''(x)$ $M_{x\_max} := M_x(h_0) = 4085.196\ plf \cdot ft$ (Maximum Positivie Bending) $\sigma_{x\_max} := \frac{6\ M_{x\_max}}{t_u^{\ 2}} = 32.015\ ksi$

$t_{0b} := \frac{\sqrt{3}\ \gamma_s\ H'(R)\ R}{f'_a} = 1.341\ in$ $t_{bp} := \mathrm{Ceil}(t_{0b}, 0.125\ in) = 1.375\ in$ **(Bending Thickness)**

$x_0 := \mathbf{root}(t(x) - (0.625\ in), x, h_0, H'(R)) = 8.16\ ft$

$M_\theta(x) := \nu_s\ M_x(x)$ $M_\theta(h_1) = 9.746\ plf \cdot ft$ $N_{\theta b}(x) := \frac{E'_s\ t_u\ w(x)}{R}$ $N_{\theta b}(h_0) = 0\ klf$ $N_{\theta b}(h_1) = 158.539\ klf$

$M_{\theta\_max} := M_\theta(h_0) = 1225.559\ plf \cdot ft$ (Maximum Circumferential Bending) (Axial Loadings at Limits)

$h_b := \mathbf{root}\left(\frac{d}{dx} M_x(x), x, 0.01\ ft, 5\ ft\right) = 2.71\ ft$ (Negative Bending Location) $M_x(h_1) = 32.487\ plf \cdot ft$ (Bending at Upper Limit)

$h_x := \mathbf{root}\left(\frac{d}{dx} N_{\theta b}(x), x, 0.01\ ft, h_1\right) = 4.853\ ft$ (Max Axial Force Location) $N_\theta(h_x) = 177.681\ klf$ (Max Axial Force)

$M_{x\_min} := |M_x(h_b)| = 886.216\ plf \cdot ft$ (Max Negative Moment)

$x(t_u) := \mathbf{root}(t(x) - t_u, x, h_0, H'(R))$ (Non Bending Region Shell Thickness Equation)

$x(0.5\ in) = 14.992\ ft$ $x(0.375\ in) = 21.825\ ft$ $x(0.25\ in) = 28.657\ ft$ $x(0.125\ in) = 35.49\ ft$

Figure 3.8: Steel Shell Wall Bending and Membrane Force Calculations (2)

Top Shell and Column Information

$t_t := 0.625\ in$ (Top Shell Thickness) $p_D := \gamma_{st}\ t_t = 26.042\ psf$ (Dead Load) $p_L := 20\ psf$ (Live Load)

$p_s := p_D + p_L = 46.042\ psf$ (Shell Service Load) $p_f := 1.2\ p_D + 1.6\ p_L = 63.25\ psf$ (Shell Factored Load)

Column Layout Information

$r_t := 10\ ft$ (Radial Distance to Ring Row of Columns) $FS := 0.6^{-1} = 1.667$ (Heat Factor of Safety)

$r_1 := 22\ ft$ (Radial Distance to Inner Middle Row of Columns) $B := 14\ in$ (Square Plate Width)

$r_2 := 32\ ft$ (Radial Distance to Outer Middle Row of Columns) $d_c := 6\ in$ (Width of HSS 6x6 Steel)

$r_{b1} := 0.5\ (r_t + r_1) = 16\ ft$ (Radial Centerline Between the Ring Row and Inner Middle Row of Columns)

$r_{b2} := 0.5\ (r_1 + r_2) = 27\ ft$ (Radial Centerline Between the Inner and Outer Middle Rows of Columns)

$r_{b3} := 0.5\ (r_2 + R) = 36\ ft$ (Radial Centerline Between the Wall and Outer Middle Row of Columns)

$r_{c1} := 0.5\ (r_t + r_{b1}) = 13\ ft$ (Radial Centerline Between the Ring Row and Inner Middle Row Centerline)

$r_{c2} := 0.5\ (r_{b1} + r_{b2}) = 21.5\ ft$ (Radial Centerline Between the Inner and Outer Middle Rows Centerlines)

$r_{c3} := 0.5\ (r_{b2} + r_{b3}) = 31.5\ ft$ (Radial Centerline Between the Wall and Outer Middle Row Centerlines)

$r_{c4} := 0.5\ (r_{b3} + R) = 38\ ft$ (Radial Centerline Between the Wall and Outer Middle Row Centerline)

$a_1 := r_1 - r_t = 12\ ft$ (Distance between the Ring Row and Inner Middle Row of Columns)

$a_2 := r_2 - r_1 = 10\ ft$ (Distance between the Inner and Outer Middle Rows of Columns)

$a_3 := R - r_2 = 8\ ft$ (Distance between the Wall and Outer Middle Row of Columns)

$a_{c1} := r_{b1} - r_t = 6\ ft$ (Distance between the Ring Row and 1st Radial Centerline)

$a_{c2} := r_{b2} - r_{b1} = 11\ ft$ (Distance between the Radial 1st and 2nd Centerlines)

$a_{c3} := r_{b3} - r_{b2} = 9\ ft$ (Distance between the Radial 2nd and 3rd Centerlines)

$a_{c4} := R - r_{b3} = 4\ ft$ (Distance between the Wall and Radial 3rd Centerline)

Figure 3.9: Top Steel Plate and Column Calculations (1)

Number of Columns per Row

$n_{c1} := 8$ (Ring Row Columns) $n_{c2} := 8$ (Inner Middle Columns) $n_{c3} := 16$ (Outer Middle Columns)

Top Shell Flexure Design

$r_{a1} := \dfrac{\pi \cdot (r_1 + r_t)}{n_{c1}} = 12.566\ ft$ (Inner Middle Row Arc Length) $\dfrac{r_{a1}}{a_1} = 1.047$ (Use b/a = 1)

$r_{a2} := \dfrac{\pi \cdot (r_2 + r_1)}{n_{c2}} = 21.206\ ft$ (Inner Middle Row Arc Length) $\dfrac{r_{a2}}{a_2} = 2.121$ (Use b/a = 2)

$r_{a3} := \dfrac{\pi \cdot (R + r_2)}{n_{c3}} = 14.137\ ft$ (Inner Middle Row Arc Length) $\dfrac{r_{a3}}{a_3} = 1.767$ (Use b/a = 2)

Bending and Shear Coefficients from Timoshenko when b/a = 1 and k = 0.1

$\beta := -0.196$ $\beta_1 := 0.0329$ $\beta_2 := -0.0182$ $\beta_3 := 0.0508$ $\gamma_{sf} := 2.73$ $k := \dfrac{B}{a_1} = 0.097$

(Use k = 0.1)

Figure 3.10: Top Steel Plate and Column Calculations (2)

Inner Section Bending and Shear Equations from Timoshenko

$M_{c1} := \beta \; p_f \; a_1^{\,2} = -1785.168 \; \mathbf{plf \cdot ft}$ (Moments in both directions at columns)

$M_{m1} := \beta_1 \; p_f \; a_1^{\,2} = 299.653 \; \mathbf{plf \cdot ft}$ (Moments in both directions at center of square formed by columns)

$M_{tx1} := \beta_2 \; p_f \; a_1^{\,2} = -165.766 \; \mathbf{plf \cdot ft}$ (Moment about axis running halfway between two columns at point directly halfway between two columns)

$M_{ty1} := \beta_3 \; p_f \; a_1^{\,2} = 462.686 \; \mathbf{plf \cdot ft}$ (Moment about axis running through two columns at point directly halfway between columns)

$Q_{m1} := \gamma_{sf} \; p_f \; a_1 = 2.072 \; \mathbf{klf}$ (Maximum Column Shear)

Bending Coefficients from Timoshenko when b/a = 2

$\alpha := 0.838$ $\beta := -0.256$ $\beta_0 := -0.0092$ $\beta_1 := 0.0411$

Middle Section Bending and Shear Equations from Timoshenko

$$M_{cx2} := \frac{-p_f \; a_2^{\,2}}{2\,\pi}\left((1-\nu_s)\,\ln\left(\frac{a_2}{B}\right) - (\alpha + \beta\,\nu_s)\right) = -747.647 \; \mathbf{plf \cdot ft}$$ (Moments in the x direction at the column)

$$M_{cy2} := \frac{-p_f \; a_2^{\,2}}{2\,\pi}\left((1-\nu_s)\,\ln\left(\frac{a_2}{B}\right) - (\beta + \alpha\,\nu_s)\right) = -1518.543 \; \mathbf{plf \cdot ft}$$ (Moments in the y direction at the column)

$M_{mx2} := 4\;\beta_0 \; p_f \; a_2^{\,2} = -232.76 \; \mathbf{lbf}$ (Moment in x direction at center of rectangle formed by columns)

$M_{my2} := 4\;\beta_1 \; p_f \; a_2^{\,2} = 1039.83 \; \mathbf{lbf}$ (Moment in y direction at center of rectangle formed by columns)

Figure 3.11: Top Steel Plate and Column Calculations (3)

Outer Section Bending and Shear Equations from Timoshenko

$M_{cx3} := \frac{-p_f\, a_3^{\,2}}{2\,\pi} \left((1-\nu_s)\, \ln\left(\frac{a_3}{B}\right) - (\alpha + \beta\, \nu_s) \right) = -377.86\ \boldsymbol{plf \cdot ft}$ (Moments in the x direction at the column)

$M_{cy3} := \frac{-p_f\, a_3^{\,2}}{2\,\pi} \left((1-\nu_s)\, \ln\left(\frac{a_3}{B}\right) - (\beta + \alpha\, \nu_s) \right) = -871.234\ \boldsymbol{plf \cdot ft}$ (Moments in the y direction at the column)

$M_{mx3} := 4\ \beta_0\ p_f\ a_3^{\,2} = -148.966\ \boldsymbol{lbf}$ (Moment in x direction at center of rectangle formed by columns)

$M_{my3} := 4\ \beta_1\ p_f\ a_3^{\,2} = 665.491\ \boldsymbol{lbf}$ (Moment in y direction at center of rectangle formed by columns)

Required Top Thickness

$M_{max} := \max\left(|M_{c1}|, |M_{m1}|, |M_{tx1}|, |M_{ty1}|, |M_{cx2}|, |M_{cy2}|, |M_{mx2}|, |M_{my2}|, |M_{cx3}|, |M_{cy3}|, |M_{mx3}|, |M_{my3}|\right)$

$M_{max} = 1785.168\ \boldsymbol{lbf}$ (Maximum Plate Moment)

$t_t := \sqrt{\frac{6\, M_{max}}{f'_y}} = 0.545\ \boldsymbol{in}$ (Required Top Thickness) $t_t := \mathrm{Ceil}\left(t_t, 0.125\ \boldsymbol{in}\right) = 0.625\ \boldsymbol{in}$ (Used Thickness)

Column Tributary Areas

$A_1 := 2\ \pi\ n_{c1}^{\,-1}\ r_{c1}\ a_{c1} = 61.261\ \boldsymbol{ft}^2$ (Tributary Area for Each Ring Row Column)

$A_2 := 2\ \pi\ n_{c2}^{\,-1}\ r_{c2}\ a_{c2} = 185.747\ \boldsymbol{ft}^2$ (Tributary Area for Each Inner Middle Row Column)

$A_3 := 2\ \pi\ n_{c3}^{\,-1}\ r_{c3}\ a_{c3} = 111.33\ \boldsymbol{ft}^2$ (Tributary Area for Each Outer Middle Row Column)

$A_4 := 2\ \pi\ r_{c1}\ a_{c4} = 326.726\ \boldsymbol{ft}^2$ (Tributary Area for the Wall)

Figure 3.12: Top Steel Plate and Column Calculations (4)

Actual Column Service Loads

$W_{s1} := A_1\ p_s = 2.821\ \boldsymbol{kip}$ (Service Load for Each Ring Row Column)
$W_{s2} := A_2\ p_s = 8.552\ \boldsymbol{kip}$ (Service Load for Each Inner Middle Row Column)
$W_{s3} := A_3\ p_s = 5.126\ \boldsymbol{kip}$ (Service Load for Each Outer Middle Row Column)
$W_{sw} := A_4\ p_s = 15.043\ \boldsymbol{kip}$ (Service Load for the Wall)

Actual Factored Column Loads

$W_{f1} := A_1\ p_f = 3.875\ \boldsymbol{kip}$ (Factored Load for Each Ring Row Column)
$W_{f2} := A_2\ p_f = 11.748\ \boldsymbol{kip}$ (Factored Load for Each Inner Middle Row Column)
$W_{f3} := A_3\ p_f = 7.042\ \boldsymbol{kip}$ (Factored Load for Each Outer Middle Row Column)
$W_{fw} := A_4\ p_f = 20.665\ \boldsymbol{kip}$ (Factored Load for the Wall)

Adjusted Factored Column Loads

$W_1 := FS\ W_{f1} = 6.458\ \boldsymbol{kip}$ (Adjusted Load for Each Ring Row Column)
$W_2 := FS\ W_{f2} = 19.581\ \boldsymbol{kip}$ (Adjusted Load for Each Inner Middle Row Column)
$W_3 := FS\ W_{f3} = 11.736\ \boldsymbol{kip}$ (Adjusted Load for Each Outer Middle Row Column)

Column Design Details

Ring Row Columns: Grade 46 HSS 4.5 x 4.5 x 1/8 for structural steel (0.116" thickness) [Capacity = 13.6 k].
Inner Middle Row: Grade 46 HSS 4.5 x 4.5 x 1/4 for structural steel (0.174" thickness) [Capacity = 24.7 k].
Outer Middle Row: Grade 46 HSS 4.5 x 4.5 x 1/8 for structural steel (0.116" thickness) [Capacity = 13.6 k].
Shop Weld: Use a 1/4" Fillet SAW Weld with Grade 60 steel.
Plate: Structural plate should be 14" x 14" x 1" thick.
Corrosion: All columns and plates will have a 1" SS 304 coating for corrosion effects.
Bolts: Use single 5/8" A325 bolts at each plate corner placed 1" from plate edge. [Capacity = 120 ksi]

Figure 3.13: Top Steel Plate and Column Calculations (5)

Dome Design

$r_d := 10\ ft$ $\quad t_d := 0.625\ in = 0.052\ ft$ $\qquad N_\phi(\phi) := \dfrac{r_d}{\sin(\phi)^2} \displaystyle\int_0^\phi \left(\left(p_L \cos(\phi)\right) + \left(\gamma_{st}\ t_d\right)\right) \cos(\phi)\ \sin(\phi)\, d\phi$

$\phi_d := 0°, 1°..90°$

Maximum Dome Forces

$$N_0 := \lim_{\phi \to 0} N_\phi(\phi) \xrightarrow{simplify} 130.20833333333333333 \cdot pcf \cdot ft^2 + 100.0 \cdot psf \cdot ft = 230.208\ plf$$

$t_0 := \dfrac{N_0}{f_a} = 0.00053\ in$ (Required Thickness)

Dome Buckling Check

$t_{cr} := \dfrac{4\ r_d\ f_a}{E_s} = 0.596\ in$ (Required Thickness) $\qquad t_d := \mathrm{Ceil}\left(t_{cr}, 0.125\ in\right) = 0.625\ in$ (Actual Thickness)

Figure 3.14: Top Steel Dome Calculations

3.6 CONCLUSION

The design of a cylindrical A588 Grade 50 steel shell, having a diameter of 80 feet (24.384 meters), for the storage of molten salts is presented. The shell is 54 feet (16.459 meters) high, has a height of salt of 42 feet (12.802 meters), and has a top access dome with a radius of 10 feet (3.048 meters). The two tank system is designed to store enough molten salt to provide 300 megawatts of power for eight hours. The shell has a one inch (25.4 mm) stainless steel liner to protect against corrosion for a 50 year design life. In addition, two foundation designs are provided for the steel cylindrical tank. Further details about the foundation design are presented in Chapter 5.

REFERENCES

Flugge, W. *Stresses in Shells*. Springer Verlag Publishing.Co, Berlin, 1960.

Holman, J.P. *Heat Transfer, Sixth Edition*. McGraw-Hill. New York, NY, 1986.

Salmon, C.G., Johnson, J.E., and Malhas, F.A. *Steel Structures: Design and Behavior*. 5th Ed. Pearson Prentice Hall, Upper Saddle River, NJ, 2009.

Steel Construction Manual. 14th Ed. American Institute of Steel Construction, 2012.

Timoshenko, S. *Theory of Plates and Shells*. McGraw-Hill, New York, 1959.

Urugal, A. C. *Theory of Beams, Plates, and Shells*. 4th Ed. CRC Press, Boca Raton, FL, 2009.

CHAPTER 4

CONCRETE CYLINDRICAL SHELLS

4.1 INTRODUCTION

Molten solar salts are a great and effective way to store excess solar energy for future use due to the vast heat storage capacities of solar salts. These solar salts are contained in large insulated tanks in order to keep the molten salts in a closed system. This chapter examines an alternative method of using insulated reinforced concrete cylindrical shells to store molten salt and presents a preliminary design of real life examples.

4.2 DESIGN METHOD FOR CONCRETE MS STORAGE TANKS

Currently, molten salt (MS) storage shells are usually cylindrical tanks made of stainless steel. This chapter presents an alternative cylindrical shell design using reinforced concrete instead of carbon steel. Like the carbon steel shell design, there will be an inner layer of 316 Stainless Steel to protect against corrosion, varying in thickness from one inch (25 mm) for a fifty year plant life span to 0.6 in (15 mm) for a thirty year plant life span.

4.3 TANK REQUIREMENTS

As with the steel cylindrical tanks, the reinforced concrete cylindrical tanks need to store enough molten solar salt, which is a 60:40 sodium nitrate ($NaNO_3$) and potassium nitrate (KNO_3) mix, to provide power for a 300 megawatt power plant for eight hours each night. Calculations determined that in order to satisfy these requirements, the two tanks need to be able to store 12,048 cubic meters of salt or 425.5 x 10^3 cubic feet. This requires 212.7 x 10^6 cubic feet (6,024 cubic meters) for each tank. The concrete cylindrical tank will have a 40 feet (12.192 meters) radius at the base, which is the same as the steel cylindrical tank. This results in a height of salt of 54 feet (16.459 meters) and a salt height of 42 feet (12.802 meters) for the concrete cylindrical tank. Like the steel cylindrical tanks, a third and fourth tanks, all of reinforced concrete, are recommended for the storage of cooled MS after power generation and for safety and continued operations during maintenance of the other tanks.

4.4 CONCRETE CYLINDRICAL TANKS

The structural design was divided into five elements for individual analysis and design, which are the concrete shell wall, the concrete top cover with a central 10 feet (3.048 meters) diameter steel access dome, steel support columns, a steel bottom, and the concrete slab below a layer of sand. Shell theory was used to perform the structural analysis of the cylindrical tank and central access dome.

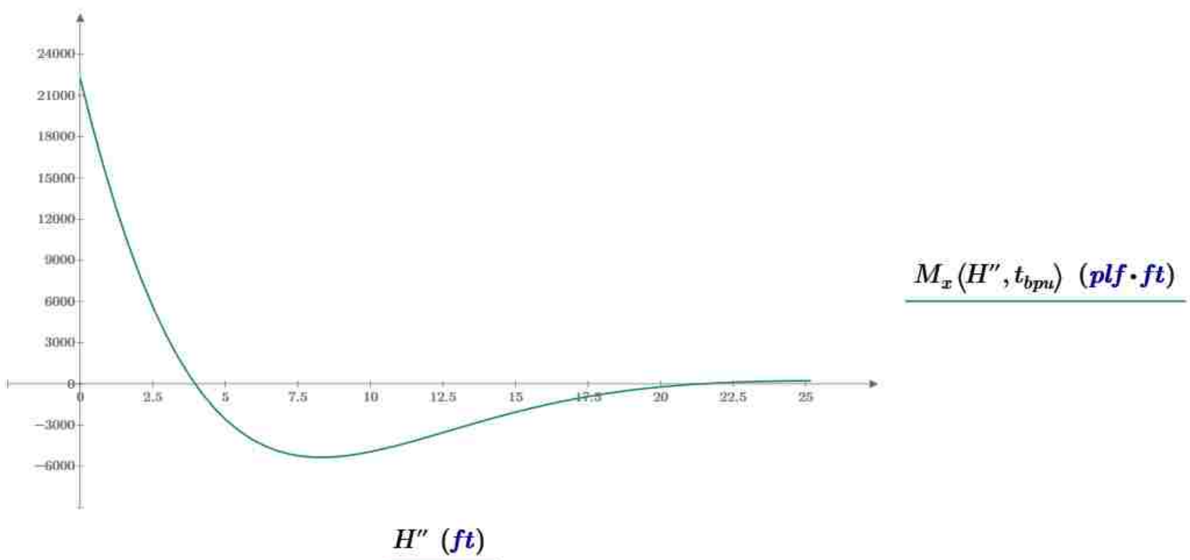

Figure 4.1: Concrete Cylindrical Shell Wall M_x Bending Moment

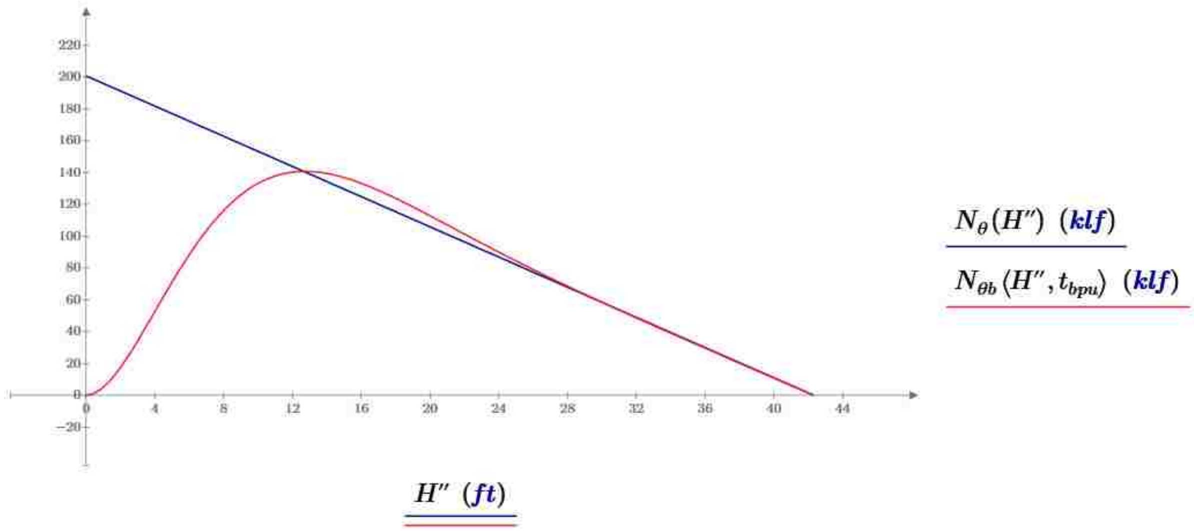

Figure 4.2: Concrete Cylindrical Shell Wall N_θ Forces
The red curve is based on Bending Theory while the blue curve is based on Shell Theory

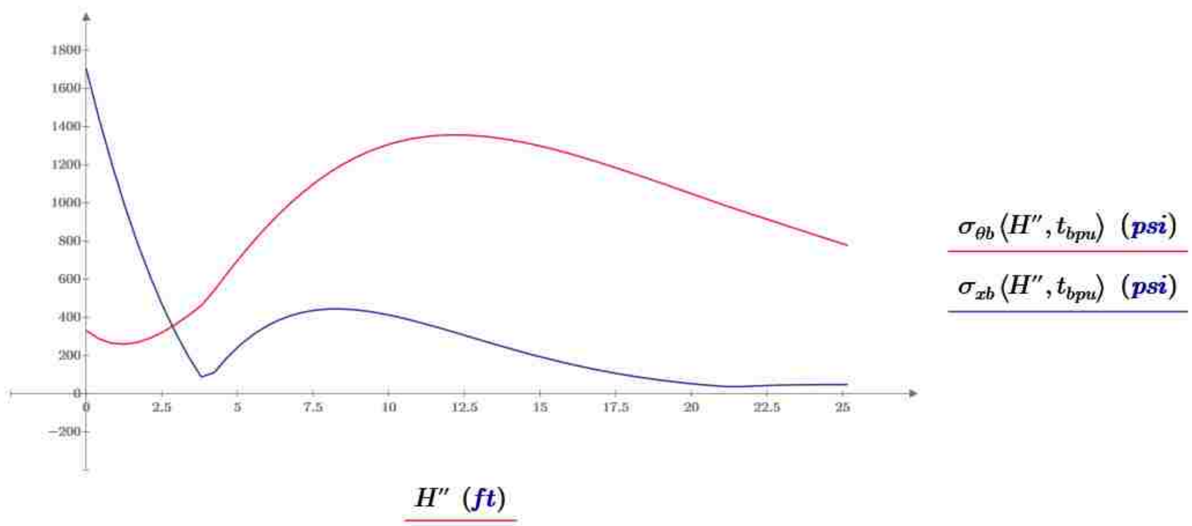

Figure 4.3: Stresses at the Bottom of the Concrete Shell Wall
The red curve is the Circumferential Stress and the blue curve is the Axial Stress

The first design performed was for the shell wall. Based on shell theory, axial bending in a cylindrical shell occurs mainly at the base of the wall, at the junction with the ring and base plate, before dissipating further up the wall (Urugal 2009). Further analysis determined that axial bending dissipates 25 feet (7.620 meters) above ground. The first step was to determine the bending in the shell wall. As shown in Figure 4.1, the maximum positive axial bending moment is 22.256 kip-foot/foot (99.00 kN-m/m) at the bottom of the shell, and the maximum negative bending moment is 5.347 kip-foot/foot (23.78 kN-m/m) at a height 8.305 feet (2.531 meters) above the bottom of the shell. Circumferential moments are equal to the Poisson ratio multiplied by the axial moments. The bottom of the wall contains the maximum circumferential tensile force, which is 140.4 kips per linear foot (klf), which is 2,053 kN/m. This results in a shell wall thickness of 9 inches (229 mm). Tensile membrane force is determined by Equation 4.2 and Figure 4.2 (Urugal 2009). While maximum axial compressive force, N_x, in the wall at the bottom of the shell is equal to the total dead weight of the shell, top slab, live load and service dome, which is the total weight (W), divided by the circumference of the shell. Equations 4.3 through 4.8 are used to determine the bending in the shell wall (Urugal 2009).

$$p = \gamma z \tag{4.1}$$

$$N_\theta = pr \tag{4.2}$$

$$D = \frac{Et}{12(1-\nu)} \tag{4.3}$$

$$\beta = \sqrt{\frac{\sqrt{1-\nu^2}}{rt}} \tag{4.4}$$

$$C_1 = \frac{\gamma h r^2}{Et} \tag{4.5}$$

$$C_2 = \frac{\gamma r^2}{Et}\left(h - \frac{1}{\beta}\right) \tag{4.6}$$

$$w = e^{-\beta x}(C_1 \cos \beta x + C_2 \sin \beta x) + \frac{\gamma(h-x)r^2}{Et} \tag{4.7}$$

$$M_x = D\frac{d^2 w}{dx^2} \tag{4.8}$$

$$M_\theta = \nu M_x \tag{4.9}$$

$$N_x = \frac{W_x}{C} \tag{4.10}$$

In determining the applied pressure on the tank from Equation 4.1, it is the product of the salt unit weight (γ) and the depth of salt (z) at the specified point. In Equation 4.2, p is the applied pressure on the wall and r is the radius of the wall (Urugal 2009). In Equations 4.3 through 4.8, D, β, C_1, and C_2 are coefficients, E is the Young's Modulus of the shell material, t is thickness of the shell wall, ν is the Poisson's ratio of the shell material, h is the total height of molten salt, w is shell wall deflection at a height of x above ground, and the second derivative of w is used to determine the moment at that point (Urugal 2009). M_x is the axial moment at a height of x above ground, W_x is the weight of the shell including dead and live loads on its top at level above x (Urugal 2009). Figure 4.3 details the design of the cylindrical shell and the top dome.

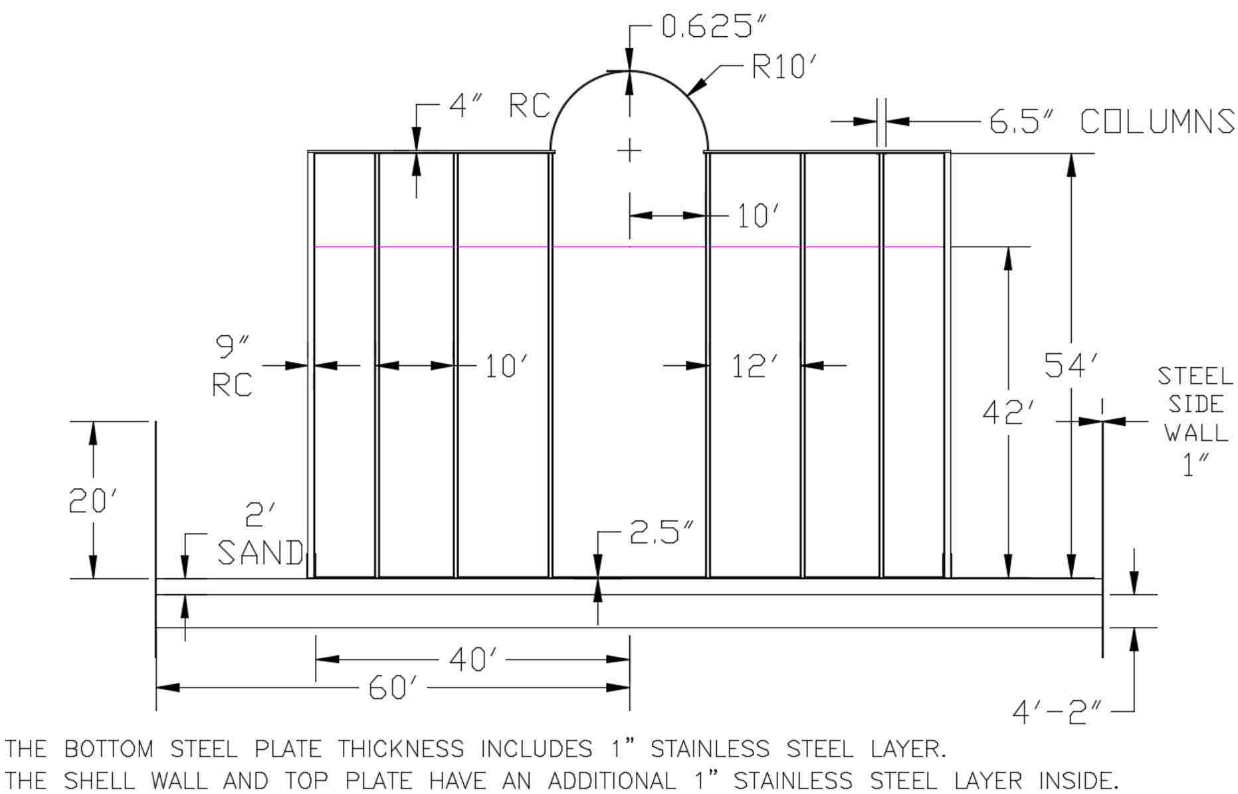

Figure 4.4: Concrete Cylindrical Shell Model Including Top Dome, Supporting Rows of Columns, 2' Sand Layer, 50" Posttension Slab, and Safety Steel Walls at the Edge

The shell was designed in sections of varying reinforcement based on the loading. The bottom 20 feet (6.048 meters) of the shell wall was designed to accommodate high circumferential tension and excess bending, requiring extra reinforcement. The bottom section of the tank requires layer of circumferential tensile reinforcement placed two inches (50.8 mm) deep from the outside of the tank with five #8 bars per linear foot. In addition, the bottom section require two vertical layers of bending reinforcement, each containing four #6 bars per linear foot, with the first layer 5.375 inches (137 mm) deep from the outside of the tank and the second layer 7.125 inches deep (181 mm). The vertical #6 bars are cut off at 20 feet (6.048 meters) above ground since the axial bending moment, M_x, dissipates around 25 feet (7.620 meters). The remaining sections only require a single layer of circumferential reinforcement, which is placed at the center of the shell wall. The next section exists from 20 to 25 feet (6.048 to 7.620 meters) above ground and requires four #8 bars per linear foot. The following section exists from 25 to 31 feet (7.620 to 9.449 meters) above ground and requires three #8 bars per linear foot. The next section exists from 31 to 37 feet (9.449 to 11.278 meters) above ground and requires two #8 bars per linear foot. The last section of the wall exists from 37 feet (11.278 meters) above ground and onward, with this section requiring only a single #8 bar per foot. Due to corrosion effects, a one inch (25.4 mm) liner of 316 Stainless Steel covers the steel wall. In addition, the bottom 3 feet (914 mm) of the concrete shell wall will have an inside and outside layer of 1.5 inch (38.1 mm) thick carbon steel surrounding the shell wall. This is to provide a connection to the 1.5 inch (38.1 mm) thick steel plate at the bottom of the tank.

The next design was for both the top concrete plate and the columns supporting it. The top concrete plate is 4 inches thick and being supported by three circular rows of columns. One row of columns is located ten feet (3.048 meters) away from the center of the tank and contains eight equally spaced columns. The second row of columns is located 22 feet (6.706 meters) away from the center of the tank and contains eight equally spaced columns. Lastly, the third row of columns is located 32 feet (9.754 meters) away from center and contains 16 equally spaced columns. These columns are made of steel because of high heat and corrosion. When designing the columns, an extra factor of safety due to the expected heat of the molten salt. At 580 degrees Celsius, steel is expected to only maintain 60% of its nominal yield strength (Salmon 2009). As a result, the final design load for the first row of columns is 9.4 kips (41.8 kN), 28.5 kips (126.8 kN) for the second row, and 17.1 kips (75.9 kN) for the third row. Ultimately, it is determined that the first row of columns be designed as HSS 4½ x 4½ x 1/8" columns, the second row as HSS 4½ x 4½ x 5/16" columns, and the third row as HSS 4½ x 4½ x 3/16" columns (<u>Steel Construction Manual</u> 2012). Due to corrosion effects, a one inch (25.4 mm) coating of SS 304 stainless steel will cover the steel column. In addition, the column will be connected to the top concrete shell with a 14 inch by 14 inch (356 mm) plate that is two inches thick (50.8 mm).

In order to design for bending in the top plate, Timoshenko's method was used to design the shell as a continuous slab due to the support columns and normalize the column pattern as a square array. Based on Timoshenko (1959), the maximum negative bending moment in each direction is located at the column. The maximum positive moments, being the radial moments, occur at the center of the normalized annulus, and the maximum circumferential moment occur directly halfway between columns. For this shell, the maximum negative moment is 2.945 kip-foot/foot (13.10 kN-m/m) and the maximum positive radial moment is 1.512 kip-foot/foot (6.726 kN-m/m). This results in the top concrete plate requiring a thickness of four inches (102 mm). The concrete plate will include four layers of reinforcement and all four layers will each contain four #3 bars per linear foot. The reinforcement for the top layer will travel in the circumferential direction, and will be placed at a depth of 0.6875 inches (17.5 mm). The reinforcement for the second layer will travel in the radial direction, and will be placed at a depth of 1.4375 inches (36.5 mm). The reinforcement for the third layer will travel in the radial direction, and will be placed at a depth of 2.5625 inches (65.1 mm). The reinforcement for the fourth layer will travel in the circumferential direction, and will be placed at a depth of 3.3125 inches (84.1 mm).

As with the steel cylindrical shell, an opening with a 10 foot (3.048 meters) radius is carved out of the top shell so that a removable steel shell with the same radius can be placed on top of the steel shell. This opening is to allow pipes into the shell and allow for service access into the tank.

4.5 CONCRETE TANK DESIGN CALCULATIONS

Figures 4.4 through 4.6 show how the concrete shell wall was calculated. In addition, Figures 4.7 through 4.13 show how the concrete top plate and steel columns were calculated.

Concrete Properties

$f'_c := 6000\ psi \quad \gamma_c := 150\ pcf \quad \nu_c := 0.2 \quad cc := 1.5\ in \quad d_v := 0.5\ in \quad \phi_b := 0.9 \quad \phi_v := 0.75$

$f_c := 0.45\ f'_c = 2700\ psi \quad E_c := 57000\ \sqrt{(1\ psi)\ f'_c} = 4415.201\ ksi \quad \sigma_t := 7.5\ \sqrt{(1\ psi)\ f'_c} = 580.948\ psi$

Sidewall Shell Forces (Shell Bending Theory)

$$C_1(t) := \frac{\gamma_s\ R^2\ H(R)}{E_c\ t} \qquad D(t) := \frac{E_c\ t^3}{12\ (1-\nu_c^{\ 2})}$$

$h_0 := 0\ ft$ (Lower Bending Limit)
$h_1 := 24\ ft$ (Upper Bending Limit)
$H' := 0\ ft, 0.01\ H(R) .. H(R)$

$$\beta(t) := \sqrt{\frac{\sqrt{1-\nu_c^{\ 2}}}{R\ t}} \qquad C_2(t) := \frac{\gamma_s\ R^2}{E_c\ t}\left(H(R) - \frac{1}{\beta(t)}\right)$$

D, β, C1, and C2 are all coefficients for shell bending equations.

$$w(x,t) := -e^{-\beta(t)\ x}\ (C_1(t)\ \cos(\beta(t)\ x) + C_2(t)\ \sin(\beta(t)\ x)) + \frac{\gamma_s\ (H(R)-x)\ R^2}{E_c\ t} \qquad N_{\theta b}(x,t) := \frac{E_c\ t\ w(x,t)}{R}$$

$$w'(x,t) := \frac{d}{dx} w(x,t) \qquad w''(x,t) := \frac{d^2}{dx^2} w(x,t) \qquad M_x(x,t) := D(t)\ w''(x,t) \qquad M_{x\_max}(t) := M_x(h_0, t)$$

$$M_\theta(x,t) := \nu_c\ M_x(x,t)$$

$$t_{bp} := \mathbf{root}\left(\sqrt{\frac{6\ M_{x\_max}(t)}{f_c}} - t, t, 0.01\ in, 12\ in\right) = 5.666\ in$$ **(Required Bending Thickness)**

$t_{bpu} := 9\ in$ **(Used Bending Thickness)** $\qquad N_\theta(x) := \gamma_s\ (H(R)-x)\ R$ (Membrane Axial Force)

$M_x(h_0, t_{bpu}) = 22256.428\ plf \cdot ft \qquad M_x(h_1, t_{bpu}) = 204.834\ plf \cdot ft \qquad N_{\theta b}(h_0, t_{bpu}) = 0\ klf$

$M_\theta(h_0, t_{bpu}) = 4451.286\ plf \cdot ft \qquad M_\theta(h_1, t_{bpu}) = 40.967\ plf \cdot ft \qquad N_{\theta b}(h_1, t_{bpu}) = 89.968\ klf$

(Bending at Lower Limit) (Bending at Upper Limit) (Axial Loadings at Limits)

Figure 4.5: Concrete Shell Wall Bending and Membrane Force Calculations (1)

Sidewall Shell Forces (Shell Bending Theory) (Continued)

$M_{\theta\_max} := M_\theta(h_0, t_{bpu}) = 4451.286\ \mathbf{plf \cdot ft}$ (Maximum Circumferential Bending) $f'(x) := \frac{d}{dx} M_x(x, t_{bpu})$

$h_b := \mathbf{root}\left(\frac{d}{dx} M_x(x, t_{bpu}), x, 0.01\ \mathbf{ft}, h_1\right) = 8.305\ \mathbf{ft}$ (Maximum Negative Bending Location)

$h_x := \mathbf{root}\left(\frac{d}{dx} N_{\theta b}(x, t_{bpu}), x, 0.01\ \mathbf{ft}, h_1\right) = 12.733\ \mathbf{ft}$ (Maximum Axial Force Location)

$N_{\theta b}(h_x, t_{bpu}) = 140.706\ \mathbf{klf}$
(Maximum Axial Force)

$M_{x\_min} := \left|M_x(h_b, t_{bpu})\right| = 5347.434\ \mathbf{plf \cdot ft}$
(Maximum Negative Moment)

Reinforcement Steel Properties

$f_y := 60\ \mathbf{ksi}$ $f'_y := 0.6\ f_y = 36\ \mathbf{ksi}$
$E_s := 29000\ \mathbf{ksi}$

$\rho_{min} := \frac{6\sqrt{(1\ \mathbf{psi})\ f'_c}}{f'_y} = 0.013$ (Minimum Steel) $n_f := \frac{f'_y}{f'_c} = 6$

Tensile Steel Reinforcement

$d_t := 1\ \mathbf{in}$ (#8 Bars)
$A_t := 0.25\ \pi\ d_t^{\ 2} = 0.785\ \mathbf{in}^2$
(Area Per Bar)

$A_{tm} := \frac{(1\ \mathbf{ft})\ N_{\theta b}(h_x, t_{bpu})}{f'_y} = 3.909\ \mathbf{in}^2$
(Required Reinforcement for Bottom)

(Required #8 Bars for Bottom)
$n_{tm} := \mathrm{Ceil}\left(\frac{A_{tm}}{A_t}, 1\right) = 5$

$x_1(n) := \mathbf{root}\left(\frac{(1\ \mathbf{ft})\ N_{\theta b}(x, t_{bpu})}{A_t\ f'_y} - n, x, 10\ \mathbf{ft}, h_1\right)$ $x_2(n) := \mathbf{root}\left(\frac{(1\ \mathbf{ft})\ N_\theta(x)}{A_t\ f'_y} - n, x, h_1, H(R)\right)$

Figure 4.6: Concrete Shell Wall Bending and Membrane Force Calculations (2)

Heights for Specified #8 Bars

$x_1(4)=19.949\ ft$ $x_2(3)=24.435\ ft$ $x_2(2)=30.397\ ft$ $x_2(1)=36.36\ ft$ $d_{ij}:=cc+0.5\ d_t=2\ in$

Bending Reinforcement (Tension Side)

$\omega_{min}:=\rho_{min}\ n_f=0.077$ $R_{min}:=\omega_{min}\ f'_c\ (1-0.5\ \omega_{min})=446.758\ psi$ $d_{min}(x,t_{bpm}):=\sqrt{\frac{|M_x(x,t_{bpm})|}{R_{min}}}$

Bending Reinforcement Calculations

$A_{min}:=t_{bpu}\ \rho_{min}\ (1\ ft)=1.394\ in^2$ (Minimum Bending Reinforcement)

$d_b:=0.75\ in$ (#6 Bars) $A_b:=0.25\ \pi\ d_b^{\ 2}=0.442\ in^2$ (Area per Bar)

$d_{max}:=t_{bpu}-cc-0.5\ d_b=7.125\ in$ (Maximum Reinforcement Depth)

$d_{bp}:=d_{min}(h_0,t_{bpu})=7.058\ in$ (Required Positive Depth) $d_{bpu}:=\mathrm{Ceil}(d_{bp},0.125\ in)=7.125\ in$

$d'_{np}:=t_{bpu}-d_{min}(h_b,t_{bpu})=5.54\ in$ (Maximum Negative Depth) $d'_{npu}:=d_{bpu}-d_b-1\ in=5.375\ in$

$n_b:=\mathrm{Ceil}\left(\frac{A_{min}}{A_b},1\right)=4$ (Minimum #6 Bars)

Wall Shear Check

$Q_x(x,t):=-\left(\frac{d}{dx}M_x(x,t)\right)$ $q_{max}:=\frac{Q_x(h_0,t_{bpu})}{t_{bpm}}=80.087\ psi$ (Actual Shell Shear Stress)

$v_c:=6\ \sqrt{(1\ psi)\ f'_c}=464.758\ psi$ (Available Concrete Shear Strength)

Figure 4.7: Concrete Shell Wall Bending and Membrane Force Calculations (3)

Top Shell and Column Information

$t_t := 4\ in$ (Top Shell Thickness) $p_D := \gamma_c\ t_t = 50\ psf$ (Dead Load) $p_L := 20\ psf$ (Live Load)

$p_s := p_D + p_L = 70\ psf$ (Shell Service Load) $p_f := 1.2\ p_D + 1.6\ p_L = 92\ psf$ (Shell Factored Load)

Column Layout Information

$r_t := 10\ ft$ (Radial Distance to Ring Row of Columns) $FS := 0.6^{-1} = 1.667$ (Heat Factor of Safety)

$r_1 := 22\ ft$ (Radial Distance to Inner Middle Row of Columns) $B := 14\ in$ (Square Plate Width)

$r_2 := 32\ ft$ (Radial Distance to Outer Middle Row of Columns) $d_c := 6\ in$ (Width of HSS 6x6 Steel)

$r_{b1} := 0.5\ (r_t + r_1) = 16\ ft$ (Radial Centerline Between the Ring Row and Inner Middle Row of Columns)

$r_{b2} := 0.5\ (r_1 + r_2) = 27\ ft$ (Radial Centerline Between the Inner and Outer Middle Rows of Columns)

$r_{b3} := 0.5\ (r_2 + R) = 36\ ft$ (Radial Centerline Between the Wall and Outer Middle Row of Columns)

$r_{c1} := 0.5\ (r_t + r_{b1}) = 13\ ft$ (Radial Centerline Between the Ring Row and Inner Middle Row Centerline)

$r_{c2} := 0.5\ (r_{b1} + r_{b2}) = 21.5\ ft$ (Radial Centerline Between the Inner and Outer Middle Rows Centerlines)

$r_{c3} := 0.5\ (r_{b2} + r_{b3}) = 31.5\ ft$ (Radial Centerline Between the Wall and Outer Middle Row Centerlines)

$r_{c4} := 0.5\ (r_{b3} + R) = 38\ ft$ (Radial Centerline Between the Wall and Outer Middle Row Centerline)

$a_1 := r_1 - r_t = 12\ ft$ (Distance between the Ring Row and Inner Middle Row of Columns)

$a_2 := r_2 - r_1 = 10\ ft$ (Distance between the Inner and Outer Middle Rows of Columns)

$a_3 := R - r_2 = 8\ ft$ (Distance between the Wall and Outer Middle Row of Columns)

$a_{c1} := r_{b1} - r_t = 6\ ft$ (Distance between the Ring Row and 1st Radial Centerline)

$a_{c2} := r_{b2} - r_{b1} = 11\ ft$ (Distance between the Radial 1st and 2nd Centerlines)

$a_{c3} := r_{b3} - r_{b2} = 9\ ft$ (Distance between the Radial 2nd and 3rd Centerlines)

$a_{c4} := R - r_{b3} = 4\ ft$ (Distance between the Wall and Radial 3rd Centerline)

Figure 4.8: Top Concrete Plate and Column Calculations (1)

Number of Columns per Row

$n_{c1} := 8$ (Ring Row Columns) $n_{c2} := 8$ (Inner Middle Columns) $n_{c3} := 16$ (Outer Middle Columns)

Top Shell Flexure Design

$r_{a1} := \dfrac{\pi \left(r_1 + r_t\right)}{n_{c1}} = 12.566\ ft$ (Inner Middle Row Arc Length) $\dfrac{r_{a1}}{a_1} = 1.047$ (Use b/a = 1)

$r_{a2} := \dfrac{\pi \left(r_2 + r_1\right)}{n_{c2}} = 21.206\ ft$ (Inner Middle Row Arc Length) $\dfrac{r_{a2}}{a_2} = 2.121$ (Use b/a = 2)

$r_{a3} := \dfrac{\pi \left(R + r_2\right)}{n_{c3}} = 14.137\ ft$ (Inner Middle Row Arc Length) $\dfrac{r_{a3}}{a_3} = 1.767$ (Use b/a = 2)

Bending and Shear Coefficients from Timoshenko when b/a = 1 and k = 0.1

$\beta := -0.196$ $\beta_1 := 0.0329$ $\beta_2 := -0.0182$ $\beta_3 := 0.0508$ $\gamma_{sf} := 2.73$ $k := \dfrac{B}{a_1} = 0.097$

(Use k = 0.1)

Figure 4.9: Top Concrete Plate and Column Calculations (2)

Inner Section Bending and Shear Equations from Timoshenko

$M_{c1} := \beta\ p_f\ a_1^{\ 2} = -2596.608\ \textbf{plf} \cdot \textbf{ft}$ (Moments in both directions at columns)

$M_{m1} := \beta_1\ p_f\ a_1^{\ 2} = 435.859\ \textbf{plf} \cdot \textbf{ft}$ (Moments in both directions at center of square formed by columns)

$M_{tx1} := \beta_2\ p_f\ a_1^{\ 2} = -241.114\ \textbf{plf} \cdot \textbf{ft}$ (Moment about axis running halfway between two columns at point directly halfway between two columns)

$M_{ty1} := \beta_3\ p_f\ a_1^{\ 2} = 672.998\ \textbf{plf} \cdot \textbf{ft}$ (Moment about axis running through two columns at point directly halfway between columns)

$Q_{m1} := \gamma_{sf}\ p_f\ a_1 = 3.014\ \textbf{klf}$ (Maximum Column Shear)

Bending and Shear Coefficients from Timoshenko when b/a = 2

$\alpha := 0.838$ $\beta := -0.256$ $\beta_0 := -0.0092$ $\beta_1 := 0.0411$

Middle Section Bending and Shear Equations from Timoshenko

$$M_{cx2} := \frac{-p_f\ a_2^{\ 2}}{2\ \pi} \left((1-\nu_c)\ \ln\left(\frac{a_2}{B}\right) - (\alpha + \beta\ \nu_c) \right) = -1364.581\ \textbf{plf} \cdot \textbf{ft}$$ (Moments in the x direction at the column)

$$M_{cy2} := \frac{-p_f\ a_2^{\ 2}}{2\ \pi} \left((1-\nu_c)\ \ln\left(\frac{a_2}{B}\right) - (\beta + \alpha\ \nu_c) \right) = -2646.071\ \textbf{plf} \cdot \textbf{ft}$$ (Moments in the y direction at the column)

$M_{mx2} := 4\ \beta_0\ p_f\ a_2^{\ 2} = -338.56\ \textbf{plf} \cdot \textbf{ft}$ (Moment in x direction at center of rectangle formed by columns)

$M_{my2} := 4\ \beta_1\ p_f\ a_2^{\ 2} = 1512.48\ \textbf{plf} \cdot \textbf{ft}$ (Moment in y direction at center of rectangle formed by columns)

Figure 4.10: Top Concrete Plate and Column Calculations (3)

Outer Section Bending and Shear Equations from Timoshenko

$M_{cx3} := \dfrac{-p_f\, a_3^{\,2}}{2\,\pi} \left((1-\nu_c)\, \ln\left(\dfrac{a_3}{B}\right) - (\alpha + \beta\, \nu_c) \right) = -706.045\ \boldsymbol{plf \cdot ft}$ (Moments in the x direction at the column)

$M_{cy3} := \dfrac{-p_f\, a_3^{\,2}}{2\,\pi} \left((1-\nu_c)\, \ln\left(\dfrac{a_3}{B}\right) - (\beta + \alpha\, \nu_c) \right) = -1526.199\ \boldsymbol{plf \cdot ft}$ (Moments in the y direction at the column)

$M_{mx3} := 4\, \beta_0\, p_f\, a_3^{\,2} = -216.678\ \boldsymbol{plf \cdot ft}$ (Moment in x direction at center of rectangle formed by columns)
$M_{my3} := 4\, \beta_1\, p_f\, a_3^{\,2} = 967.987\ \boldsymbol{plf \cdot ft}$ (Moment in y direction at center of rectangle formed by columns)

Max Bending Values

$M_{cp\_max} := \max\left(|M_{m1}|, |M_{ty1}|, |M_{my2}|\right) = 1.512\ \boldsymbol{klf \cdot ft}$ $M_{rp\_max} := M_{m1} = 435.859\ \boldsymbol{plf \cdot ft}$ $cc := 0.5\ \boldsymbol{in}$
$M_{cn\_max} := \max\left(|M_{c1}|, |M_{cy2}|\right) = 2.646\ \boldsymbol{klf \cdot ft}$ $M_{rn\_max} := \max\left(|M_{c1}|, |M_{tx1}|, |M_{cx2}|, |M_{mx2}|\right) = 2.597\ \boldsymbol{klf \cdot ft}$

Circumferential Bending Reinforcement (Positive)

$\omega_{min} := \rho_{min}\, \dfrac{f_y}{f'_c} = 0.129$ $R_{min} := \omega_{min}\, f'_c\, (1 - 0.5\, \omega_{min}) = 724.597\ \boldsymbol{psi}$ $d_{min} := \sqrt{\dfrac{M_{cp\_max}}{R_{min}}} = 1.445\ \boldsymbol{in}$

$d_{cpb} := 0.375\ \boldsymbol{in}$ (#3 Reinforcement Bars) $A_{cpb} := 0.25\, \pi\, d_{cpb}^{\,2} = 0.11\ \boldsymbol{in}^2$ (Area per Bar)

$A_{cp} := \rho_{min}\, t_t = 0.62\ \dfrac{\boldsymbol{in}^2}{\boldsymbol{ft}}$ $n_{pb} := \mathrm{Ceil}\left(\dfrac{A_{cp}}{A_{cpb}}\,(1\ \boldsymbol{ft}), 1\right) = 6$ (Required #3 Bars per foot)

$A_{pba} := n_{pb}\, A_{cpb} = 0.663\ \boldsymbol{in}^2$ (Adjusted Reinforcement Area) $d_{cp} := t_t - cc - 0.5\, d_{cpb} = 3.3125\ \boldsymbol{in}$ (Depth)

Figure 4.11: Top Concrete Plate and Column Calculations (4)

Circumferential Bending Reinforcement (Negative)

$\omega_{min} := \rho_{min} \frac{f_y}{f'_c} = 0.129$ $R_{min} := \omega_{min} f'_c (1 - 0.5\ \omega_{min}) = 724.597\ psi$ $d'_{max} := t_t - \sqrt{\frac{M_{cn\_max}}{R_{min}}} = 2.089\ in$

$d_{cnb} := 0.375\ in$ (#3 Reinforcement Bars) $A_{cnb} := 0.25\ \pi\ d_{cnb}^{\ 2} = ?\ in^2$ (Area per Bar)

$A_{cn} := \rho_{min}\ t_t = 0.62\ \frac{in^2}{ft}$ $n_{cn} := \text{Ceil}\left(\frac{A_{cn}}{A_{cnb}}(1\ ft), 1\right) = ?$ (Required #3 Bars per foot)

$A_{cna} := n_{cn}\ A_{cnb} = 0.663\ in^2$ (Adjusted Reinforcement Area) $d'_{cn} := cc + 0.5\ d_{cnb} = 0.6875\ in$
(Circumferential Reinforcement Depth)

Radial Bending Reinforcement (Positive)

$\omega_{min} := \rho_{min} \frac{f_y}{f'_c} = 0.129$ $R_{min} := \omega_{min} f'_c (1 - 0.5\ \omega_{min}) = 724.597\ psi$ $d_{min} := \sqrt{\frac{M_{rp\_max}}{R_{min}}} = 0.776\ in$

$d_{rpb} := 0.375\ in$ (#3 Reinforcement Bars) $A_{rpb} := 0.25\ \pi\ d_{rpb}^{\ 2} = 0.11\ in^2$ (Area per Bar)

$A_{rp} := \rho_{min}\ t_t = 0.62\ \frac{in^2}{ft}$ $n_{rp} := \text{Ceil}\left(\frac{A_{rp}}{A_{rpb}}(1\ ft), 1\right) = 6$ (Required #3 Bars per foot)

$A_{rpa} := n_{rp}\ A_{rpb} = 0.663\ in^2$ (Adjusted Reinforcement Area) $d_{rp} := t_t - cc - 2.5\ d_{rpb} = 2.5625\ in$
(Radial Reinforcement Depth)

Figure 4.12: Top Concrete Plate and Column Calculations (5)

Radial Bending Reinforcement (Negative)

$\omega_{min} := \rho_{min} \dfrac{f_y}{f'_c} = 0.129$ $\quad R_{min} := \omega_{min} \, f'_c \, (1 - 0.5 \, \omega_{min}) = 724.597 \, \boldsymbol{psi}$ $\quad d'_{max} := t_t - \sqrt{\dfrac{M_{rn\_max}}{R_{min}}} = 2.107 \, \boldsymbol{in}$

$d_{rnb} := 0.375 \, \boldsymbol{in}$ (#3 Reinforcement Bars) $\quad A_{rnb} := 0.25 \, \pi \, d_{rnb}^{\,2} = 0.11 \, \boldsymbol{in}^2$ (Area per Bar)

$A_{rn} := \rho_{min} \, t_t = ? \, \dfrac{\boldsymbol{in}^2}{\boldsymbol{ft}}$ $\quad n_{rn} := \mathrm{Ceil}\left(\dfrac{A_{rn}}{A_{rnb}} \, (1 \, \boldsymbol{ft}), 1\right) = 6$ (Required #3 Bars per foot)

$A_{rna} := n_{rn} \, A_{rnb} = 0.663 \, \boldsymbol{in}^2$ (Adjusted Reinforcement Area) $\quad d'_{rn} := cc + 2.5 \, d_{rnb} = 1.4375 \, \boldsymbol{in}$
(Radial Reinforcement Depth)

Column Tributary Areas

$A_1 := 2 \, \pi \, n_{c1}^{-1} \, r_{c1} \, a_{c1} = 18.672 \, \boldsymbol{ft}$ (Tributary Area for Each Ring Row Column)
$A_2 := 2 \, \pi \, n_{c2}^{-1} \, r_{c2} \, a_{c2} = 185.747 \, \boldsymbol{ft}^2$ (Tributary Area for Each Inner Middle Row Column)
$A_3 := 2 \, \pi \, n_{c3}^{-1} \, r_{c3} \, a_{c3} = 111.33 \, \boldsymbol{ft}^2$ (Tributary Area for Each Outer Middle Row Column)
$A_4 := 2 \, \pi \, r_{c1} \, a_{c4} = 326.726 \, \boldsymbol{ft}^2$ (Tributary Area for the Wall)

Actual Column Service Loads

$W_{s1} := A_1 \, p_s = 4.288 \, \boldsymbol{kip}$ (Service Load for Each Ring Row Column)
$W_{s2} := A_2 \, p_s = 13.002 \, \boldsymbol{kip}$ (Service Load for Each Inner Middle Row Column)
$W_{s3} := A_3 \, p_s = 7.793 \, \boldsymbol{kip}$ (Service Load for Each Outer Middle Row Column)
$W_{sw} := A_4 \, p_s = 22.871 \, \boldsymbol{kip}$ (Service Load for the Wall)

Figure 4.13: Top Concrete Plate and Column Calculations (6)

Actual Factored Column Loads

$W_{f1} := A_1\ p_f = 5.636\ \textbf{kip}$ (Factored Load for Each Ring Row Column)
$W_{f2} := A_2\ p_f = 17.089\ \textbf{kip}$ (Factored Load for Each Inner Middle Row Column)
$W_{f3} := A_3\ p_f = 10.242\ \textbf{kip}$ (Factored Load for Each Outer Middle Row Column)
$W_{fw} := A_4\ p_f = 30.059\ \textbf{kip}$ (Factored Load for the Wall)

Adjusted Factored Column Loads

$W_1 := FS\ W_{f1} = 9.393\ \textbf{kip}$ (Adjusted Load for Each Ring Row Column)
$W_2 := FS\ W_{f2} = 28.481\ \textbf{kip}$ (Adjusted Load for Each Inner Middle Row Column)
$W_3 := FS\ W_{f3} = 17.071\ \textbf{kip}$ (Adjusted Load for Each Outer Middle Row Column)

Column Design Details

Ring Row Columns: Grade 46 HSS 4.5 x 4.5 x 1/8 for structural steel (0.116" thickness) [Capacity = 13.6 k].
Inner Middle Row: Grade 46 HSS 4.5 x 4.5 x 5/16 for structural steel (0.291" thickness) [Capacity = 29.1 k].
Outer Middle Row: Grade 46 HSS 4.5 x 4.5 x 3/16 for structural steel (0.174" thickness) [Capacity = 19.3 k].
Shop Weld: Use a 1/4" Fillet SAW Weld with Grade 60 steel.
Plate: Structural plate should be 14" x 14" x 1" thick.
Corrosion: All columns and plates will have a 1" SS 304 coating for corrosion effects.
Bolts: Use single 5/8" A325 bolts at each plate corner placed 1" from plate edge. [Capacity = 120 ksi]

Figure 4.14: Top Concrete Plate and Column Calculations (7)

4.6 CONCLUSION

The design of a reinforced cylindrical shell, having a diameter of 80 feet (24.384 meters), for the storage of molten salts is presented. The shell is 54 feet (16.459 meters) high, has a height of salt of 42 feet (12.802 meters), and has a top access dome with a radius of 10 feet (3.048 meters). The two tank system is designed to store enough molten salt to provide 300 megawatts of power for eight hours. The shell has a one inch (25.4 mm) stainless steel liner to protect against corrosion for a 50 year design life. As with the steel cylindrical shell, two foundation designs for the concrete cylindrical tank are explored in further detail in Chapter 5.

REFERENCES

ACI 318-14. American Concrete Institute, 2014.

Flugge, W. *Stresses in Shells*. Springer Verlag Publishing.Co, Berlin, 1960.

Holman, J.P. *Heat Transfer, Sixth Edition*. McGraw-Hill. New York, NY, 1986.

Salmon, C.G., Johnson, J.E., and Malhas, F.A. *Steel Structures: Design and Behavior*. 5th Ed. Pearson Prentice Hall, Upper Saddle River, NJ, 2009.

Steel Construction Manual. 14th Ed. American Institute of Steel Construction, 2012.

Timoshenko, S. *Theory of Plates and Shells*. McGraw-Hill, New York, 1959.

Urugal, A. C. *Theory of Beams, Plates, and Shells*. 4th Ed. CRC Press, Boca Raton, FL, 2009.

CHAPTER 5

FOUNDATION DESIGN

5.1 FOUNDATION DESIGN

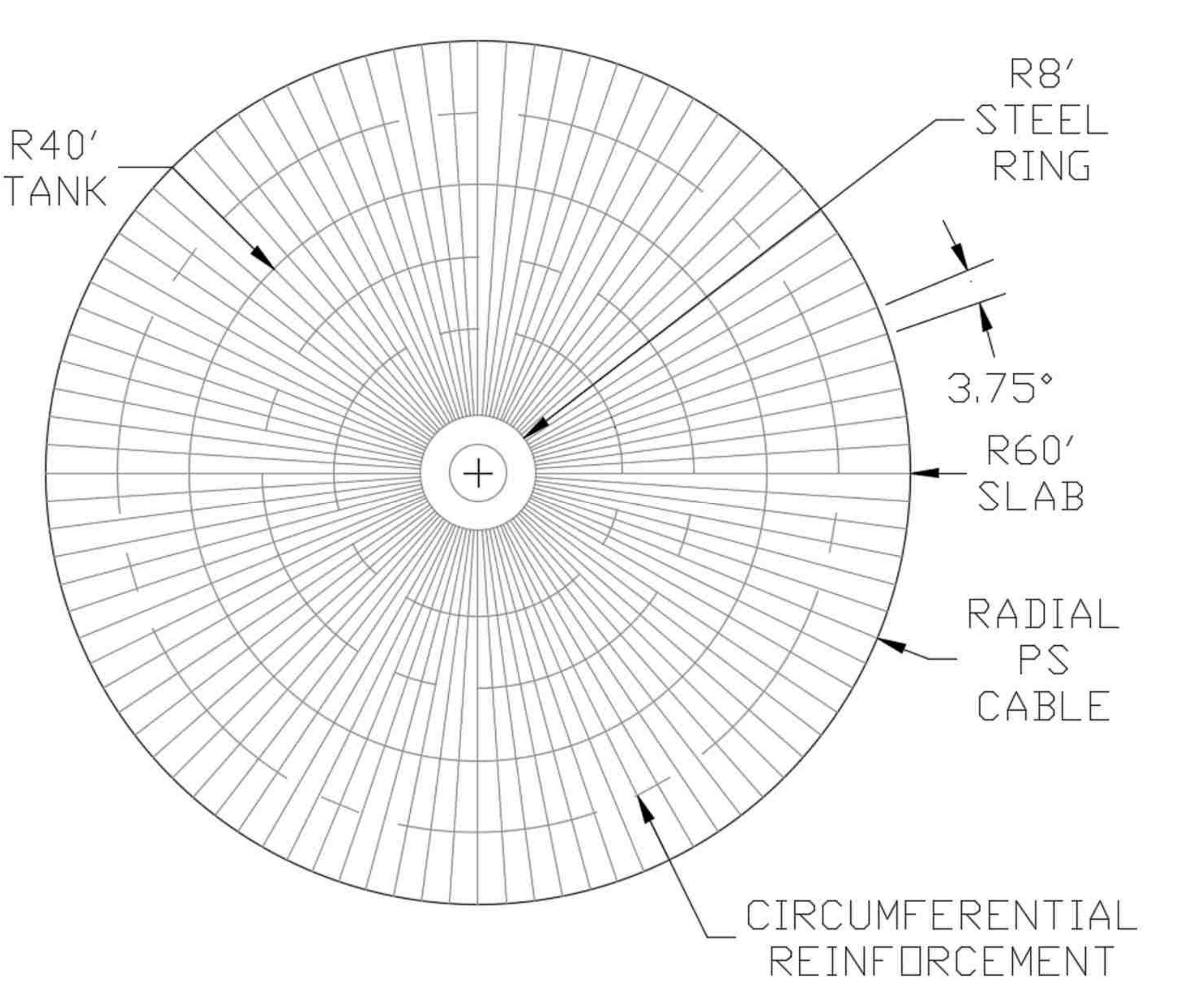

Figure 5.1: Posttensioning Cable and Circumferential Reinforcement Layout for the Circular Concrete Slab Including Inner Steel Ring

Included for the cylindrical tanks is two foundation designs, a circular foundation and a square foundation. A complete design was performed on the concrete slab sitting over dense sand. Included in the foundation design is a 2 foot (610 mm) layer of sand between the tank and the concrete slab to allow for thermal expansion of the shell. The required slab thickness for the circular slab is 50 inches (1.270 meters) while the square slab requires 63 inches (1.600 meters).

Figure 5.1 details the radial posttensioning cable layout, the steel ring, and circumferential reinforcement in the circular slab concrete slab. The steel ring is necessary because the posttensioning cables cannot intersect with each at the center of the circular concrete slab.

5.2 CIRCULAR FOUNDATION RADIAL PRE-STRESSING

The first element to the slab structural design was the radial pre-stressing of the slab. Equations 5.1 through 5.5 are used to determine the required pre-stressing for the slab.

$$M_{rm} = \frac{kqa^2}{6\phi} \tag{5.1}$$

$$d_{min} = \sqrt{\frac{M_{rm}}{\omega_p\, f_c'\,(1-0.5\omega_p)}} \tag{5.2}$$

$$f_{ps} = f_{py}\left(1 - 0.5\omega_p\right) \tag{5.3}$$

$$A_{ps} = \frac{2\pi a M_{rm}}{f_{ps}\, d\,(1-0.5\omega_p)} \tag{5.4}$$

Based on Timoshenko (1959), M_{rm} is the maximum radial moment at the edge of the tank, which is 1,688.653 kip-foot/foot (7,512 kN-m/m). Also, k is a factor based on the support condition, which is 0.410 for this structure, and q is the design load, which is 6,178 psf (295.8 kPa). Lastly, a is the slab radius of 60 feet (18.288 meters), and ϕ is the bending factor of 0.9 as specified in ACI 318-14. Equation 5.2 is used to determine the minimum depth (d_{min}) using the maximum radial moment, the compressive strength of the concrete (f_c'), which is 6,000 psi (41.4 MPa), and the amount of steel (ω_p). Based on ACI 318-14, the maximum ω_p for 6,000 psi concrete is 0.27. However, for this design, a ω_p of 0.21 is used. The required pre-stressing depth at the edge of the tank is 38.697 inches (983 mm) with a depth of 38.75 inches (984 mm) being used.

Equation 5.3 is used to determine the maximum pre-stressing for the Grade 270 cables, which determined that the maximum initial pre-stressing is 241.65 ksi (1,666.1 MPa). Equation 5.4 is used to determine the combined required cross-sectional area of all pre-stressing cables, which is 911.5 square inches (0.588 square meters).

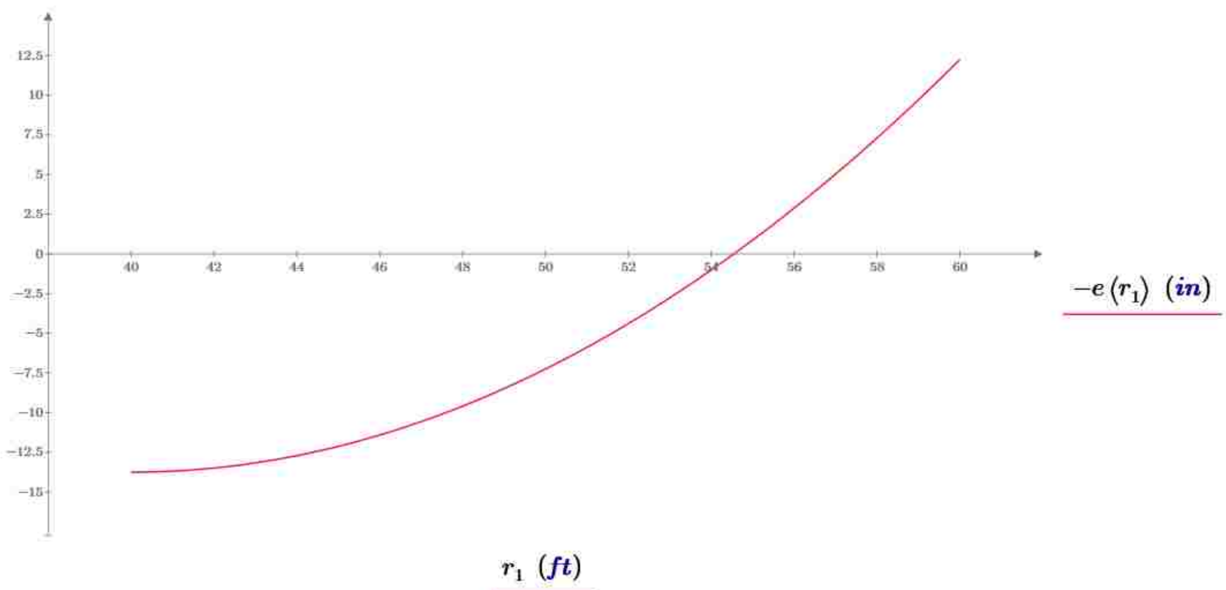

Figure 5.2: Inverted Eccentricity for the Circular Slab
A negative value corresponds to a positive eccentricity and vice versa. This is done to show the cable path.

Ultimately, this meant that the slab requires 96 radial posttensioning 55/0.5 WG cables that connect to the inner steel ring are required as shown in Figure 5.1. This pre-stressing provides a combined 221,760 kips (986,438 kN) of pre-stressing force, or 2,310 kips (10,275 kN) per cable, which results in a pre-stressing stress of 241.379 ksi (1,664.3 MPa) in each cable. In addition, the minimum radial posttensioning cables depth is 12.75 inches (324 mm) and the maximum radial posttensioning cables depth is 38.75 inches (984 mm), with the cables following a parabolic path between the edge of the slab and the edge of the tank as shown in Figure 5.2.

5.3 CIRCULAR FOUNDATION CIRCUMFERENTIAL REINFORCEMENT

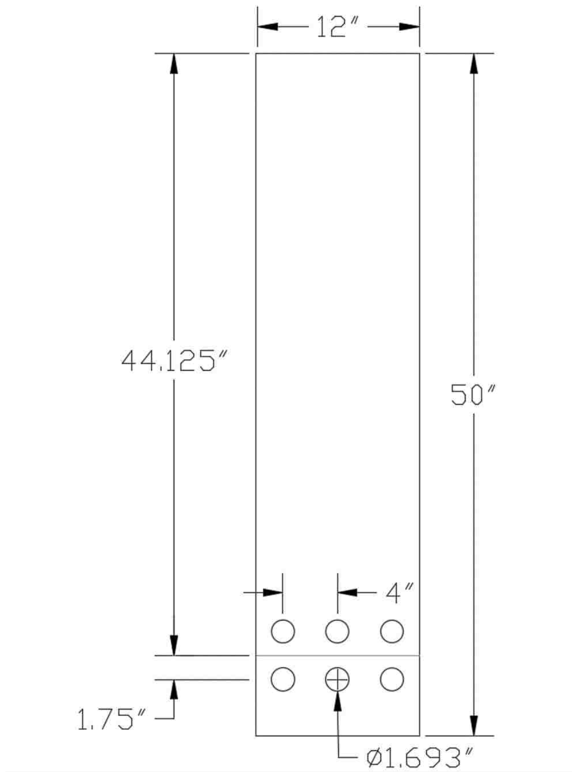

Figure 5.3: Circumferential Reinforcement Layout per Foot (Six #14 Reinforcement Bars per Foot)

The next element to the slab structural design was the circumferential reinforcement of the slab as shown in Figure 5.3. Equations 5.5 through 5.8 are used to determine the required pre-stressing for the slab.

$$M_{cm} = M_{rm}\left(\frac{(3-\upsilon_c)a^2-(1+3\upsilon_c)r^2}{(3-\upsilon_c)a^2-(3-\upsilon_c)r^2}\right) \tag{5.5}$$

$$c = \frac{d\,\varepsilon_c}{\varepsilon_s+\varepsilon_c} \tag{5.6}$$

$$a = 0.8c \tag{5.7}$$

$$A_s = \frac{0.85f_c'\,a}{f_y} \tag{5.8}$$

In these equations, M_{cm} is the maximum circumferential moment located at the edge of the tank, M_{rm} is the maximum radial moment at the edge of the tank and υ_c is the Poisson's ratio of concrete, which is 0.2. In addition, a is the radius of the slab, which is 60 feet (18.288 meters), and r is the radius of the tank, which is 40 feet (12.192 meters). This results in a required moment of 2,364.1 kip-foot/foot (10,516 kN-m/m) at the edge of the tank. The required reinforcement depth at the edge of the tank is 42.636 inches (1.083 meters). As a result, the circumferential reinforcement depth being used 44.125 inches (1.121 meters) for all reinforcement. Equation 5.6 is used to determine the depth of the neutral axis (c) in which the maximum strain of concrete (ε_c) is 0.003 and the maximum steel strain (ε_s) is 0.005. The depth of the neutral axis is 16.547 inches (420 mm). Equation 5.7 is used to determine the depth of the compression block (a) which is 13.238 inches (336 mm). Equation 5.8 is used to determine the cross-sectional area of steel per foot, which is 13.502 square inches (0.009 square meters). This area results six #14 Grade 60 reinforcement bars.

5.4 STEEL RING FOR THE CIRCULAR FOUNDATION

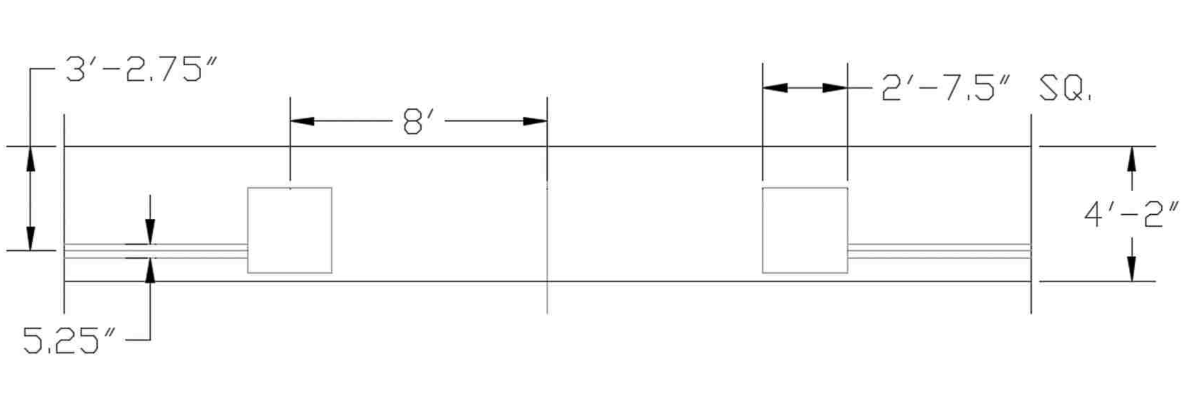

Figure 5.4: Layout of the Cable and Steel Ring Connection

The last element to the slab structural design was the steel ring connected to the pre-stressing cables. The steel cable as shown in Figure 5.4 will have a radius of 8 feet (2.438 meters), which is r_r in Equations 3a and 3b. Equations 5.9 through 5.11 are used to determine the required pre-stressing for the slab (Urugal 2009).

$$q_r = \frac{P}{2\pi r_r} \tag{5.9}$$

$$T = q_r r_r \tag{5.10}$$

$$A = \frac{T}{f_a} \tag{5.11}$$

In these equations, q_r is the uniform loading on the ring due to pre-stressing and P is the combined loading from all pre-stressing, which is 221,760 kips (986,438 kN). The uniform applied load from the pre-stressing cables on the steel ring is 4,411.8 kips/foot (64,385 kN/m). As a result, the steel ring has a tensile force (T) of 35,294 kips (156,996 kN). Using Grade 60 carbon steel, the allowable stress (f_a) in the ring is 36 ksi (248.211 MPa), meaning the steel ring requires a cross sectional area (A) of 980.4 square inches (0.633 square meters). The actual cross section of the steel ring is a square of 31.5 inches (800 mm) on each side, which has a cross sectional area of 992.25 square inches (0.640 square meters).

5.5 SQUARE FOUNDATION PRE-STRESSING DESIGN

In addition to a circular foundation design, there is also a square foundation design for the cylindrical tanks as shown is Figure 5.5. For this foundation design, it was determined that there would be two layers of pre-stressing cables, one in the x-direction and one in the y-direction, with constant eccentricity. Equations 5.2 through 5.4 from earlier were used to determine the depth and number of 55/WG 0.5 pre-stressing cables for each layer of the 63 inch (1.600 meters) square foundation. The top layer, which has cables running in the x-direction, has a depth of 45.25 inches (1.149 meters), and contains 17 cables spaced 7 feet (2.134 meters) apart. The bottom layer, which has cables running in the y-direction, has a depth of 50.5 inches (1.283 meters), and contains 15 cables spaced 8 feet (2.438 meters) apart.

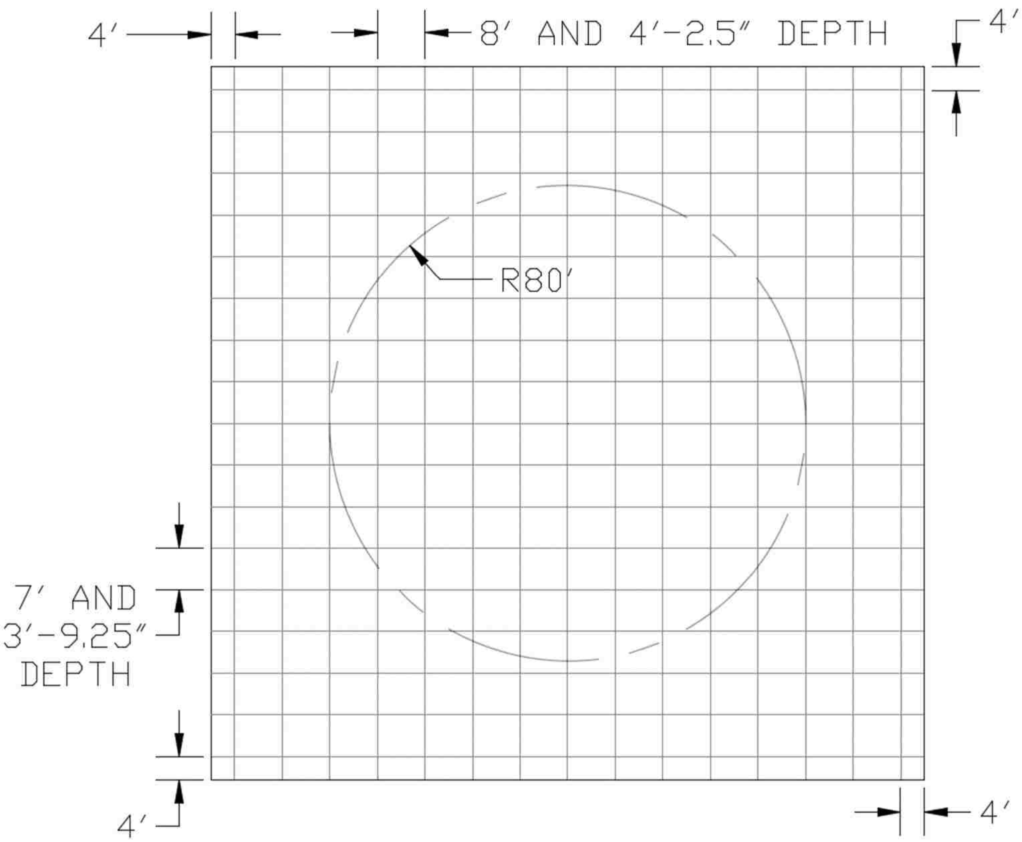

Figure 5.5: Layout of the Pre-Stressing Cable Path for the Square Foundation

5.6 FOUNDATION DESIGN CALCULATIONS

Figures 5.6 through 5.9 show the calculations for determining the radial post-tensioning of the circular slab and the cable ring. Figure 5.10 shows the calculations for determining the circumferential reinforcement for the circular slab. Lastly, Figures 5.11 through 5.16 show the calculations for the post-tensioning in both directions for the square slab.

Regular Steel Properties

$f_y := 60\ \mathbf{ksi}$ $\gamma_{st} := 500\ \mathbf{pcf}$ $\nu_s := 0.3$ $E_s := 29000\ \mathbf{ksi}$ $f_a := 0.6\ f_y = 36\ \mathbf{ksi}$

For this tank, the steel will be Grade 60 steel. The Young's modulus of steel is 29,000 ksi and the Poisson's ratio is 0.3. The allowable stress is 60% of the yield strength, resulting in 36 ksi design stress.

Concrete Properties

$f'_c := 6000\ \mathbf{psi}$ $d_v := 0.5\ \mathbf{in}$ $E_c := 57000\ \sqrt{(1\ \mathbf{psi})\ f'_c} = 4415.201\ \mathbf{ksi}$ $\rho_{min} := \dfrac{6\ \sqrt{(1\ \mathbf{psi})\ f'_c}}{f_y} = 0.008$

$\gamma_c := 150\ \mathbf{pcf}$ $cc := 1.5\ \mathbf{in}$ $\phi_b := 0.9$ $\phi_v := 0.75$ $\nu_c := 0.2$

(Minimum Steel Reinforcement)

Bottom Slab Section

$p_s := \gamma_s\ H'(R) = 5017.341\ \mathbf{psf}$ (Unfactored Salt Dead Load) $t_{bs} := 50\ \mathbf{in}$ (Slab Thickness)

$r_s := 60\ \mathbf{ft}$ (Slab Radius) $A_s := \pi\ r_s^{\ 2} = 11309.734\ \mathbf{ft}^2$ (Area of Slab)

$f_{py} := 270\ \mathbf{ksi}$ (Prestressing Stress) $r_1 := R, (R + 0.1\ \mathbf{ft}) .. r_s$ (Graphing Limits)

$p_L := 20\ \mathbf{psf}$ (Live Load) $p_{bs} := 6000\ \mathbf{psf}$ (Soil Bearing Stress)

$p_{ns} := \dfrac{1.2\ p_s\ R^2}{r_s^{\ 2}} + 1.6\ p_L = 2707.915\ \mathbf{psf}$ (Net Loading on Slab)

Slab Area Check

$p_c(d) := \gamma_c\ (d + 2\ cc)$ $p_b := 200\ \mathbf{psf}$ $p_n(d) := p_{bs} - p_b - p_c(d)$ $A_r(d) := \dfrac{p_s\ \pi\ R^2}{p_n(d)}$

$d_{max} := \mathbf{root}\left(A_s - A_r(d), d, 0\ \mathbf{ft}, 30\ \mathbf{ft}\right) = 282.606\ \mathbf{in}$

Net Soil Pressure

$p_c := \gamma_c\ t_{bs} = 625\ \mathbf{psf}$ $p_b := 200\ \mathbf{psf}$ $p_n := p_{bs} - p_b - p_c = 5175\ \mathbf{psf}$ $p_f := 1.2\ p_n - 1.6\ p_L = 6178\ \mathbf{psf}$

Figure 5.6: Circular Slab Pre-Stressing and Cable Ring Calculations (1)

Slab Design Moment

$k := 0.410$ $\quad k_1 := 0.0183$ $\quad M_{max} := \dfrac{k\ p_f\ r_s^{\ 2}}{6\ \phi_b} = 1688.653\ \boldsymbol{klf \cdot ft}$ $\quad w_{max} := \dfrac{k_1\ p_n\ r_s^{\ 4}}{E_c\ t_{bs}^{\ 3}} = 0.32\ \boldsymbol{in}$

Slab Service Moments

$M_G := \dfrac{k\ p_n\ r_s^{\ 2}}{6} = 1273.05\ \boldsymbol{klf \cdot ft}$ $\quad M_E := \dfrac{k\ p_L\ r_s^{\ 2}}{6} = 4.92\ \boldsymbol{klf \cdot ft}$ $\quad M_T := M_G - M_E = 1268.13\ \boldsymbol{klf \cdot ft}$

Slab Prestressing

$k_c := \dfrac{t_{bs}}{6} = 8.333\ \boldsymbol{in}$ $\quad \sigma_c := 0.45\ f'_c = 2700\ \boldsymbol{psi}$ $\quad \sigma_t := 6\ \sqrt{(1\ \boldsymbol{psi})\ f'_c} = 464.758\ \boldsymbol{psi}$ $\quad f'_{ci} := 3600\ \boldsymbol{psi}$

$\beta_1 := 0.75$ $\quad \eta := 0.75$ $\quad \omega_{max} := 0.36\ \beta_1 = 0.27$ $\quad \omega_p := 0.21$

$R_p := \omega_p\ f'_c\ (1 - 0.5\ \omega_p) = 1127.7\ \boldsymbol{psi}$ $\quad A_{ps\_b} := 0.174\ \boldsymbol{in}^2$ (Area per Tendon)

$m := 55$ (Tendons per Anchor)

$d_c := \sqrt{\dfrac{M_{max}}{R_p}} = 38.697\ \boldsymbol{in}$ (Required Depth) $\quad d := \mathrm{Ceil}\left(d_c, 0.25\ \boldsymbol{in}\right) = 38.75\ \boldsymbol{in}$ (Used Depth)

$f_{ps\_c} := f_{py}\ (1 - 0.5\ \omega_p) = 241.65\ \boldsymbol{ksi}$ (Maximum Initial Prestressing Stress) $\quad A_c := 2\ \pi\ r_s\ t_{bs} = 1570.796\ \boldsymbol{ft}^2$ (Total Slab Side Surface Area)

$A_{ps\_c} := \dfrac{2\ \pi\ r_s\ M_{max}}{f_{ps\_c}\ d\ (1 - 0.5\ \omega_p)} = 911.531\ \boldsymbol{in}^2$ (Required Cable Area) $\quad P_{max} := A_{ps\_c}\ f_{ps\_c} = 220271.406\ \boldsymbol{kip}$ (Required Prestressing Force)

Figure 5.7: Circular Slab Pre-Stressing and Cable Ring Calculations (2)

Slab Prestressing (Continued)

$n_c := \frac{A_{ps\_c}}{A_{ps\_b}} = 5238.682$ (Required Number of Tendons) $n := \mathrm{Ceil}\left(\frac{n_c}{m}, 1\right) = 96$ (Number of Anchors)

$A_{ps} := m\ n\ A_{ps\_b} = 918.72\ \mathbf{in}^2$ (Resultant Design Cable Area) $e_{max} := d - 0.5\ t_{bs} = 13.75\ \mathbf{in}$ (Eccentricity)

$P_c := A_{ps}\ f_{ps\_c} = 222008.688\ \mathbf{kip}$ $P_{si} := \mathrm{Floor}\left(P_c, m\ n\ \mathbf{kip}\right) = 221760\ \mathbf{kip}$ (Design Prestressing Force)

$f_{ps} := \frac{P_{si}}{A_{ps}} = 241.379\ \mathbf{ksi}$ (Design Prestressing Stress)

Per Cable Loading

$P_{sic} := \frac{P_{si}}{n} = 2310\ \mathbf{kip}$

Per Tendon Loading

$P_{sit} := \frac{P_{si}}{m\ n} = 42\ \mathbf{kip}$

Effective Prestressing

$f_c := \frac{P_{si}}{A_c} = 980.394\ \mathbf{psi}$

Minimum Design Checks

$\sigma_{st} := \left(\frac{-P_{si}}{A_c}\right)\left(\frac{e_{max}}{k_c} - 1\right) + \frac{6\ M_T}{{t_{bs}}^2} = 2406.256\ \mathbf{psi}$ $\sigma_{st} \le \sigma_c = 1$ (Successful Compression Check for the Top of Concrete)

$\sigma_{sb} := \left(\frac{-P_{si}}{A_c}\right)\left(\frac{e_{max}}{k_c} + 1\right) + \frac{6\ M_T}{{t_{bs}}^2} = 445.467\ \mathbf{psi}$ $\sigma_{sb} \le \sigma_t = 1$ (Successful Tension Check for the Bottom of Concrete)

Figure 5.8: Circular Slab Pre-Stressing and Cable Ring Calculations (3)

Punching Shear Check

$$v_c := \left(2\ \sqrt{(1\ \mathbf{psi})\ f'_c}\right)\left(1+\frac{P_{si}}{(2000\ \mathbf{psi})\ A_c}\right)=230.86\ \mathbf{psi} \qquad V_u(d):=\pi\ p_{ns}\ \left((R+0.5\ d)^2-R^2\right)$$

$$b_0(d):=\pi\ (2\ R+d) \qquad V_c(d):=v_c\ d\ b_0(d) \qquad d_p:=\mathbf{root}\left(\phi_v\ V_c(d)-V_u(d), d, 0\ \mathbf{ft}, 3\ \mathbf{ft}\right)=0\ \mathbf{in}$$

One-Way Shear Check

$$\theta(d):=2\ \operatorname{acos}\left(\frac{R+d}{r_s}\right) \qquad A_v(d):=\frac{\theta(d)\ r_s^2}{2}-\frac{r_s^2\ \sin(\theta(d))}{2} \qquad b_w(d):=2\ r_s\ \sin\left(\frac{\theta(d)}{2}\right)$$

$$V_u(d):=p_{ns}\ A_v(d) \qquad V_c(d):=v_c\ d\ b_w(d) \qquad d_{min}:=\mathbf{root}\left(\phi_v\ V_c(d)-V_u(d), d, 0\ \mathbf{ft}, 3\ \mathbf{ft}\right)=16.744\ \mathbf{in}$$

End Zone Prestress Check

$$e_0:=-k_e-\frac{A_c\ k_c\ \sigma_t}{P_{si}}=-12.284\ \mathbf{in} \qquad e_0:=\operatorname{Ceil}(e_0, 0.25\ \mathbf{in})=-12.25\ \mathbf{in} \qquad d:=\frac{t_{bs}}{2}+e_0=12.75\ \mathbf{in}$$

Prestress Cable Path

$$e(r):=e_{max}-\frac{(e_{max}-e_0)\ (r-R)^2}{(r_s-R)^2} \qquad d_r(r):=e(r)+\frac{t_{bs}}{2}$$

Cable Ring

$$r_r:=8\ \mathbf{ft} \qquad q_r:=\frac{P_{si}}{2\ \pi\ r_r}=4411.775\ \frac{\mathbf{kip}}{\mathbf{ft}} \qquad T_r:=q_r\ r_r=35294.2\ \mathbf{kip} \qquad A_{tr}:=\frac{T_r}{f_a}=980.394\ \mathbf{in}^2$$

Figure 5.9: Circular Slab Pre-Stressing and Cable Ring Calculations (4)

Slab Circumferential Bending Reinforcement

$$M_{\theta m} := \left(\frac{(3+\nu_c)\ r_s^{\ 2} - (1+3\ \nu_c)\ R^2}{(3+\nu_c)\ r_s^{\ 2} - (3+\nu_c)\ R^2} \right) M_{max} = 2364.115\ \boldsymbol{klf \cdot ft}$$

$\varepsilon_s := 0.005$

$\varepsilon_c := 0.003$

$d := 44.125\ \boldsymbol{in}$ (Used Depth)

$d_{cnb} := 1.693\ \boldsymbol{in}$

$$c := \frac{\varepsilon_c\ d}{\varepsilon_s + \varepsilon_c} = 16.547\ \boldsymbol{in} \qquad a := 0.8\ c = 13.238\ \boldsymbol{in} \qquad A_{cnb} := 0.25\ \pi\ d_{cnb}^{\ 2} = 2.251\ \boldsymbol{in}^2$$

$$d_{min} := \mathbf{root}\left(M_{\theta m} - \left(\left(0.136\ d^2\ f'_c\right) \left(\frac{\varepsilon_c}{\varepsilon_s + \varepsilon_c} \right) \left(5 - \frac{2\ \varepsilon_c}{\varepsilon_s + \varepsilon_c} \right) \right), d, 0\ \boldsymbol{in}, t_{bs} \right) = 42.636\ \boldsymbol{in}$$ (Required Depth)

$$T := (1\ \boldsymbol{ft})\ 0.85\ f'_c\ a = 810.135\ \boldsymbol{kip} \qquad A_s := \frac{T}{f_y} = 13.502\ \boldsymbol{in}^2 \qquad n_{cn} := \mathrm{Ceil}\left(\frac{A_s}{A_{cnb}}, 1 \right) = 6$$

$$M := T\ (d - 0.5\ a) = 2532.094\ \boldsymbol{kip \cdot ft}$$

Inner Slab Top Layer Bending Reinforcement

$\varepsilon_c := 0.003$ $\quad \varepsilon_s := 0.003$ (New Steel Strain) $\quad d := 38.75\ \boldsymbol{in}$ (Used Depth) $\quad c := \dfrac{\varepsilon_c\ d}{\varepsilon_s + \varepsilon_c} = 19.375\ \boldsymbol{in}$

$a := 0.8\ c = 15.5\ \boldsymbol{in}$

$$d_{min} := \mathbf{root}\left(M_{\theta m} - \left(\left(0.136\ d^2\ f'_c\right) \left(\frac{\varepsilon_c}{\varepsilon_s + \varepsilon_c} \right) \left(5 - \frac{2\ \varepsilon_c}{\varepsilon_s + \varepsilon_c} \right) \right), d, 0\ \boldsymbol{in}, t_{bs} \right) = 38.06\ \boldsymbol{in}$$ (Required Depth)

$$T := (1\ \boldsymbol{ft})\ 0.85\ f'_c\ a = 948.6\ \boldsymbol{kip} \qquad A_s := \frac{T}{f_y} = 15.81\ \boldsymbol{in}^2 \qquad n_{cn} := \mathrm{Ceil}\left(\frac{A_s}{A_{cnb}}, 1 \right) = 8$$

$$M := T\ (d - 0.5\ a) = 2450.55\ \boldsymbol{kip \cdot ft}$$

Figure 5.10: Circular Slab Circumferential Reinforcement Calculations

Regular Steel Properties

$f_y := 60\ \mathbf{ksi}$ $\gamma_{st} := 500\ \mathbf{pcf}$ $\nu_s := 0.3$ $E_s := 29000\ \mathbf{ksi}$ $f_a := 0.6\ f_y = 36\ \mathbf{ksi}$

For this tank, the steel will be Grade 60 steel. The Young's modulus of steel is 29,000 ksi and the Poisson's ratio is 0.3. The allowable stress is 60% of the yield strength, resulting in 36 ksi design stress.

Concrete Properties

$f'_c := 6000\ \mathbf{psi}$ $d_v := 0.5\ \mathbf{in}$ $E_c := 57000\ \sqrt{(1\ \mathbf{psi})\ f'_c} = 4415.201\ \mathbf{ksi}$ $\rho_{min} := \dfrac{6\ \sqrt{(1\ \mathbf{psi})\ f'_c}}{f_y} = 0.008$

$\gamma_c := 150\ \mathbf{pcf}$ $cc := 1.5\ \mathbf{in}$ $\phi_b := 0.9$ $\phi_v := 0.75$ $\nu_c := 0.2$

(Minimum Steel Reinforcement)

Bottom Slab Section

$p_s := \gamma_s\ H'(R) = 5017.341\ \mathbf{psf}$ (Unfactored Salt Dead Load) $t_{bs} := 63\ \mathbf{in}$ (Slab Thickness)

$l_s := 120\ \mathbf{ft}$ (Slab Width) $A_s := l_s^{\ 2} = 14400\ \mathbf{ft}^2$ (Area of Slab)

$f_{py} := 270\ \mathbf{ksi}$ (Prestressing Stress) $x_1 := R, (R + 0.1\ \mathbf{ft}) .. 0.5\ l_s$ (Graphing Limits)

$p_L := 20\ \mathbf{psf}$ (Live Load) $p_{ba} := 6000\ \mathbf{psf}$ (Soil Bearing Stress)

$$p_{ns} := \frac{1.2\ \pi\ p_s\ R^2}{A_s} + 1.6\ p_L = 2133.659\ \mathbf{psf}$$ (Net Loading on Slab)

Slab Area Check

$p_c(d) := \gamma_c\ (d + 2\ cc)$ $p_b := 200\ \mathbf{psf}$ $p_n(d) := p_{ba} - p_b - p_c(d)$ $A_r(d) := \dfrac{p_s\ \pi\ R^2}{p_n(d)}$

$d_{max} := \mathbf{root}\,(A_s - A_r(d), d, 0\ \mathbf{ft}, 30\ \mathbf{ft}) = 320.889\ \mathbf{in}$

Net Soil Pressure

$p_c := \gamma_c\ t_{bs} = 787.5\ \mathbf{psf}$ $p_b := 200\ \mathbf{psf}$ $p_n := p_{ba} - p_b - p_c = 5012.5\ \mathbf{psf}$ $p_f := 1.2\ p_n - 1.6\ p_L = 5983\ \mathbf{psf}$

Figure 5.11: Square Slab Pre-Stressing and Shear Calculations (1)

Center Slab Design Moment

$x_s := \frac{l_s}{2} - R = 20\ ft$ $\quad$ $M_{MC} := \frac{p_f\ x_s^2}{2} = 1196.6\ klf \cdot ft$

Center Slab Service Moments

$M_{GC} := \frac{p_n\ x_s^2}{2} = 1002.5\ klf \cdot ft$ $\quad$ $M_{EC} := \frac{p_L\ x_s^2}{2} = 4\ klf \cdot ft$ $\quad$ $M_{TC} := M_{GC} - M_{EC} = 998.5\ klf \cdot ft$

Slab Prestressing Information

$\sigma_c := 0.45\ f'_c = 2700\ psi$ $\quad$ $\sigma_t := 6\ \sqrt{(1\ psi)\ f'_c} = 464.758\ psi$ $\quad$ $f'_{ci} := 3600\ psi$

$k_c := \frac{t_{bs}}{6} = 10.5\ in$ $\quad$ $\beta_1 := 0.75$ $\quad$ $\eta := 0.75$ $\quad$ $\omega_{max} := 0.36\ \beta_1 = 0.27$

$A_{ps\_b} := 0.174\ in^2$ (Area per Tendon) $\quad$ $m := 55$ (Tendons per Anchor)

One-Way Shear Check

$v_c := \left(2\ \sqrt{(1\ psi)\ f'_c}\right) = 154.919\ psi$ $\quad$ $A_v(d) := (0.5\ l_s - R - d)\ l_s$

$V_u(d) := p_{ns}\ A_v(d)$ $\quad$ $V_c(d) := v_c\ l_s\ d$ $\quad$ $d_{min} := \mathbf{root}\left(\phi_v\ V_c(d) - V_u(d), d, 0\ ft, t_{bs}\right) = 27.144\ in$

Figure 5.12: Square Slab Pre-Stressing and Shear Calculations (2)

Slab Prestressing in the X-Direction

$\omega_p := 0.103$ $\quad R_p := \omega_p\, f'_c\, (1 - 0.5\, \omega_p) = 586.173\ \textbf{psi}$

$d_c := \sqrt{\dfrac{M_{MC}}{R_p}} = 45.182\ \textbf{in}$ (Required Depth) $\quad d := \mathrm{Ceil}\left(d_c, 0.25\ \textbf{in}\right) = 45.25\ \textbf{in}$ (Used Depth)

$f_{ps\_c} := f_{py}\, (1 - 0.5\, \omega_p) = 256.095\ \textbf{ksi}$ (Maximum Initial Prestressing Stress) $\quad A_c := l_s\, t_{bs} = 630\ \textbf{ft}^2$ (Total Slab Side Surface Area)

$A_{ps\_c} := \dfrac{l_s\, M_{MC}}{f_{ps\_c}\, d\, (1 - 0.5\, \omega_p)} = 156.767\ \textbf{in}^2$ (Required Cable Area) $\quad P_{max} := A_{ps\_c}\, f_{ps\_c} = 40147.229\ \textbf{kip}$ (Required Prestressing Force)

$n_c := \dfrac{A_{ps\_c}}{A_{ps\_b}} = 900.959$ (Required Number of Tendons) $\quad n := \mathrm{Ceil}\left(\dfrac{n_c}{m}, 1\right) = 17$ (Number of Anchors)

$A_{ps} := m\, n\, A_{ps\_b} = 162.69\ \textbf{in}^2$ (Resultant Design Cable Area) $\quad e_{max} := d - 0.5\, t_{bs} = 13.75\ \textbf{in}$ (Eccentricity)

$P_c := A_{ps}\, f_{ps\_c} = 41664.096\ \textbf{kip}$ $\quad P_{si} := \mathrm{Floor}\left(P_c, m\, n\ \textbf{kip}\right) = 41140\ \textbf{kip}$ (Design Prestressing Force)

$f_{ps} := \dfrac{P_{si}}{A_{ps}} = 252.874\ \textbf{ksi}$ (Design Prestressing Stress)

Per Cable Loading

$P_{mc} := \dfrac{P_{si}}{n} = 2420\ \textbf{kip}$

Per Tendon Loading

$P_{stt} := \dfrac{P_{si}}{m\, n} = 44\ \textbf{kip}$

Effective Prestressing

$f_c := \dfrac{P_{si}}{A_c} = 453.483\ \textbf{psi}$

Figure 5.13: Square Slab Pre-Stressing Calculations (X-Direction) (1)

Minimum Design Checks

$$\sigma_{st} := \left(\frac{-P_{si}}{A_c}\right)\left(\frac{e_{max}}{k_c} - 1\right) + \frac{6\ M_{TC}}{t_{bs}^{\ 2}} = 1369.084\ \textbf{psi}$$ $\sigma_{st} \le \sigma_c = 1$ (Successful Compression Check for the Top of Concrete)

$$\sigma_{sb} := \left(\frac{-P_{si}}{A_c}\right)\left(\frac{e_{max}}{k_c} + 1\right) + \frac{6\ M_{TC}}{t_{bs}^{\ 2}} = 462.118\ \textbf{psi}$$ $\sigma_{sb} \le \sigma_t = 1$ (Successful Tension Check for the Bottom of Concrete)

$$\sigma_{st} := \left(\frac{P_{si}}{A_c}\right)\left(\frac{e_{max}}{k_c} - 1\right) = 140.364\ \textbf{psi}$$ $\sigma_{st} \le \sigma_t = 1$ (Successful Tension Check for the Top of Concrete)

$$\sigma_{sb} := \left(\frac{P_{si}}{A_c}\right)\left(\frac{e_{max}}{k_c} + 1\right) = 1047.33\ \textbf{psi}$$ $\sigma_{sb} \le \sigma_c = 1$ (Successful Compression Check for the Bottom of Concrete)

Figure 5.14: Square Slab Pre-Stressing Calculations (X-Direction) (2)

Slab Prestressing for the Center Section in the Y-Direction

$\omega_p := 0.082$ $\quad R_p := \omega_p\, f'_c\, (1 - 0.5\, \omega_p) = 471.828\ \mathbf{psi}$

$d_c := \sqrt{\dfrac{M_{MC}}{R_p}} = 50.36\ \mathbf{in}$ (Required Depth) $\quad d := \mathrm{Ceil}\,(d_c, 0.25\ \mathbf{in}) = 50.5\ \mathbf{in}$ (Used Depth)

$f_{ps\_c} := f_{py}\, (1 - 0.5\, \omega_p) = 258.93\ \mathbf{ksi}$ (Maximum Initial Prestressing Stress) $\quad A_c := l_s\, t_{bs} = 630\ \mathbf{ft}^2$ (Total Slab Side Surface Area)

$A_{ps\_c} := \dfrac{l_s\, M_{MC}}{f_{ps\_c}\, d\, (1 - 0.5\, \omega_p)} = 137.41\ \mathbf{in}^2$ (Required Cable Area) $\quad P_{max} := A_{ps\_c}\, f_{ps\_c} = 35579.636\ \mathbf{kip}$ (Required Prestressing Force)

$n_c := \dfrac{A_{ps\_c}}{A_{ps\_b}} = 789.714$ (Required Number of Tendons) $\quad n := \mathrm{Ceil}\left(\dfrac{n_c}{m}, 1\right) = 15$ (Number of Anchors)

$A_{ps} := m\, n\, A_{ps\_b} = 143.55\ \mathbf{in}^2$ (Resultant Design Cable Area) $\quad e_{max} := d - 0.5\, t_{bs} = 19\ \mathbf{in}$ (Eccentricity)

$P_c := A_{ps}\, f_{ps\_c} = 37169.402\ \mathbf{kip}$ $\quad P_{si} := \mathrm{Floor}\,(P_c, m\, n\ \mathbf{kip}) = 37125\ \mathbf{kip}$ (Design Prestressing Force)

$f_{ps} := \dfrac{P_{si}}{A_{ps}} = 258.621\ \mathbf{ksi}$ (Design Prestressing Stress)

Per Cable Loading

$P_{mc} := \dfrac{P_{si}}{n} = 2475\ \mathbf{kip}$

Per Tendon Loading

$P_{sit} := \dfrac{P_{si}}{m\, n} = 45\ \mathbf{kip}$

Effective Prestressing

$f_c := \dfrac{P_{si}}{A_c} = 409.226\ \mathbf{psi}$

Figure 5.15: Square Slab Pre-Stressing Calculations (Y-Direction) (1)

Minimum Design Checks

$\sigma_{st} := \left(\frac{-P_{si}}{A_c}\right)\left(\frac{e_{max}}{k_e} - 1\right) + \frac{6\ M_{TC}}{t_{bs}^{\ 2}} = 1178.17\ \textbf{psi}$ $\quad \sigma_{st} \le \sigma_c = 1$ (Successful Compression Check for the Top of Concrete)

$\sigma_{sb} := \left(\frac{-P_{si}}{A_c}\right)\left(\frac{e_{max}}{k_e} + 1\right) + \frac{6\ M_{TC}}{t_{bs}^{\ 2}} = 359.717\ \textbf{psi}$ $\quad \sigma_{sb} \le \sigma_t = 1$ (Successful Tension Check for the Bottom of Concrete)

$\sigma_{st} := \left(\frac{P_{si}}{A_c}\right)\left(\frac{e_{max}}{k_e} - 1\right) = 331.278\ \textbf{psi}$ $\quad \sigma_{st} \le \sigma_t = 1$ (Successful Tension Check for the Top of Concrete)

$\sigma_{sb} := \left(\frac{P_{si}}{A_c}\right)\left(\frac{e_{max}}{k_e} + 1\right) = 1149.731\ \textbf{psi}$ $\quad \sigma_{sb} \le \sigma_c = 1$ (Successful Compression Check for the Bottom of Concrete)

Figure 5.16: Square Slab Pre-Stressing Calculations (Y-Direction) (2)

5.7 CONCLUSION

For both the steel and concrete cylindrical shells, there are two foundation designs presented, which are a circular foundation and square foundation. The circular foundation has a 120 feet (36.576 meters) diameter concrete foundation with posttensioning, a 50 inch (1.270 meters) thickness, and steel side walls that are 20 feet (6.048 meters) high for safety in case of an accident. The circular slab has 96 radial posttensioning 55/0.5 WG cables connect to a steel ring. These cables will follow a parabolic path between the edge of the slab and the edge of the tank. Along this path, the minimum radial posttensioning cables depth is 12.75 inches (324 mm) and the maximum radial posttensioning cables depth is 38.75 inches (984 mm). The circumferential reinforcement will have a depth of 44.125 inches (1.121 meters). Lastly, the Grade 60 carbon steel ring connecting the pre-stressing will have a radius of 8 feet (2.438 meters) and have a square cross section of 31.5 inches (800 mm) on each side. The square foundation has a 120 feet (36.576 meters) side length concrete foundation with posttensioning, a 63 inch (1.600 meters) thickness, and steel side walls that are 20 feet (6.048 meters) high for safety in case of an accident. The square slab has two layers of pre-stressing, one layer for each direction.

REFERENCES

ACI 318-14. American Concrete Institute, 2014.

Timoshenko, S. *Theory of Plates and Shells*. McGraw-Hill, New York, 1959.

Urugal, A. C. *Theory of Beams, Plates, and Shells*. 4th Ed. CRC Press, Boca Raton, FL, 2009.

CHAPTER 6

CONCLUSIONS AND FUTURE RESEARCH

6.1 CONCLUSIONS

After performing a survey of various molten salts, it has been determined that the most suitable molten salt is a mixture commonly referred to as Solar Salt. This mixture contains in proportion 60% sodium nitrate and 40% potassium nitrate. A survey of molten salt storage tanks reveal that current methods for storing molten salt involve using steel cylindrical tanks.

A sample design of a steel cylindrical tank is explored. The design of a cylindrical A588 Grade 50 steel shell, having a diameter of 80 feet (24.384 meters), for the storage of molten salts is presented. The shell is 54 feet (16.459 meters) high, has a height of salt of 42 feet (12.802 meters), and has a top access dome with a radius of 10 feet (3.048 meters). The two tank system is designed to store enough molten salt to provide 300 megawatts of power for eight hours. The steel shell has a one inch (25.4 mm) stainless steel liner to protect against corrosion for a 50 year design life.

In addition, a concrete cylindrical tank design is presented. The design of a reinforced cylindrical shell, having a diameter of 80 feet (24.384 meters), for the storage of molten salts is presented. The shell is 54 feet (16.459 meters) high, has a height of salt of 42 feet (12.802 meters), and has a top access dome with a radius of 10 feet (3.048 meters). The concrete shell also has a one inch (25.4 mm) stainless steel liner to protect against corrosion for a 50 year design life.

Lastly, two foundation designs are performed for both the steel and concrete cylindrical tanks, a circular foundation design and a square foundation design. The circular foundation have a 120 feet (36.576 meters) diameter concrete foundation with posttensioning, which has a 50 inch

(1.270 meters) thickness and steel side walls that are 20 feet (6.048 meters) high for safety in case of an accident. This slab will have 96 radial posttensioning 55/0.5 WG cables connect to a steel ring following parabolic path between the edge of the slab and the edge of the tank. Along this path, the minimum radial posttensioning cables depth is 12.75 inches (324 mm) and the maximum radial posttensioning cables depth is 38.75 inches (984 mm). The circumferential reinforcement will have a depth of 44.125 inches (1.121 meters). Lastly, the Grade 60 carbon steel ring connecting the pre-stressing will have a radius of 8 feet (2.438 meters) and have a square cross section of 31.5 inches (800 mm) on each side. The square foundation has a 120 feet (36.576 meters) side length concrete foundation with posttensioning, a 63 inch (1.600 meters) thickness, and steel side walls that are 20 feet (6.048 meters) high for safety in case of an accident. The square slab has two layers of pre-stressing, one layer for each direction.

6.2 FUTURE RESEARCH

The main purpose of the future research in this field is to determine if there are better ways to store molten salt. In particular, two alternatives are being considered as a possible replacement for cylindrical shells. These alternatives are drop shell tanks and spherical shell tanks. With both of these types of shells, steel and reinforced concrete designs will be examined.

Drop shell tanks have lower MS pressures than their cylindrical shell counterparts, thus much thinner walls and better surface area to volume ratio, this a decrease in heat loss from MS and great saving in the volume of steel. The concept is a modified constant stress liquid storage tank shell designs, using two smoothly joined toroidal shells of two different radii, instead of a variable meridional radius, as in the nonlinear theory of liquid tanks of constant stress (Flugge 1960). Figure 6.1 depicts the drop shell and its dimensions.

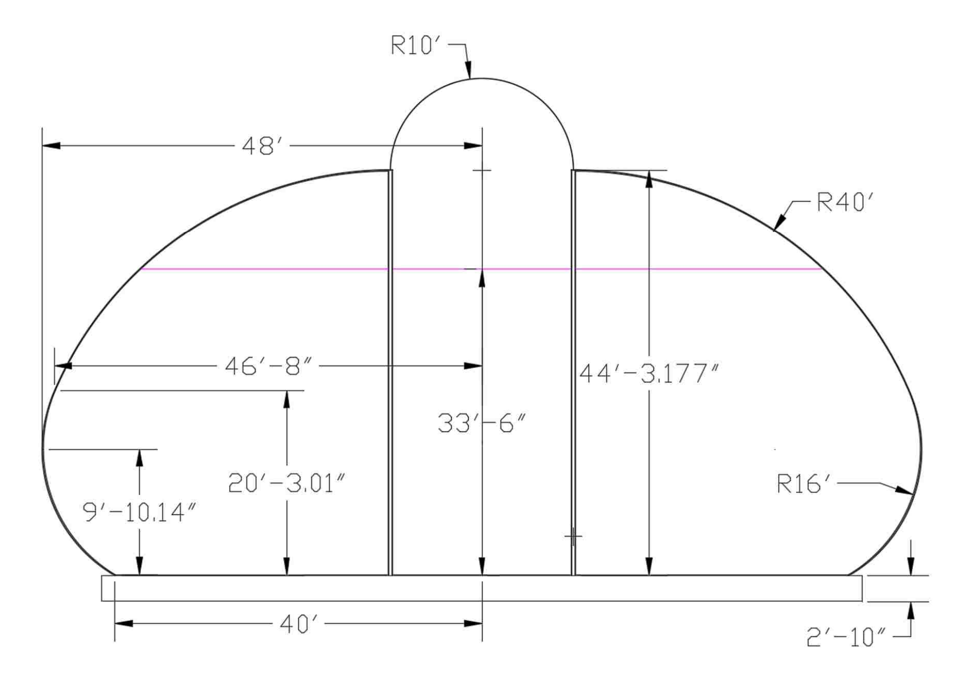

Figure 6.1: Drop Shell Model

One of the unique features of an egg drop shell is that the stress in the shell at any point is directly proportional to the product of both the radius of curvature and the vertical depth of salt at that point. In order to properly use this effect while providing for constructability, this tank is designed by combining two circular arcs into a continuous curve. The top curve maintains a larger radius than the bottom curve. The radii are designed such that the ratio between these radii is approximately inversely related to the ratio of maximum depths for the corresponding curves, which is outlined in Equation 6.1.

$$\frac{R_1}{R_2} \approx \frac{Z_2}{Z_1} \tag{6.1}$$

The other structural alternative is to explore the design of spherical shells, which is shown in Figure 6.2. In this structure, a spherical shell filled with molten salt and rests on a cylindrical ring support (Urugal 2009). Ideally, the cylindrical ring support should intersect the spherical shell at the same point that the radial tensile stress is zero.

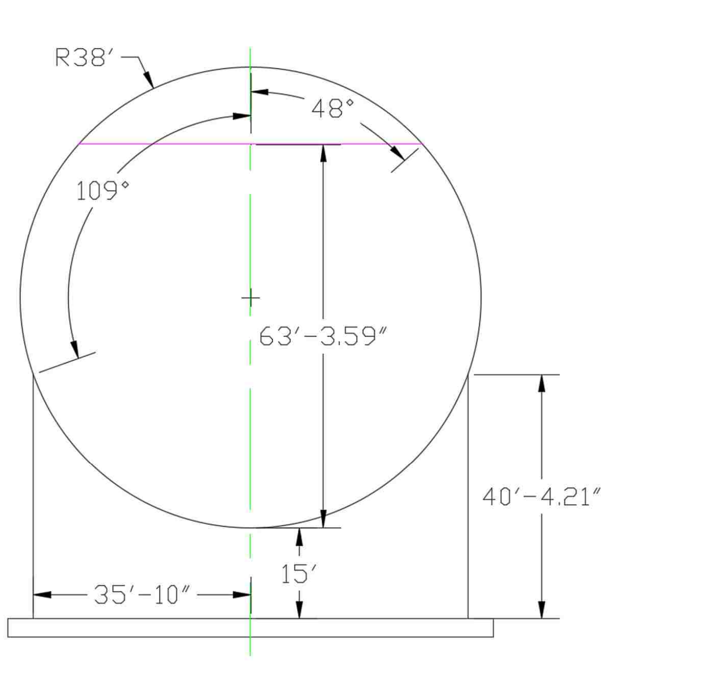

Figure 6.2: Spherical Shell Model

Lastly, one other design alternative that will be explored is whether reinforced concrete designs will use masonry cements in the concrete instead of Portland cement. Based on Kodur (2014), Portland cement concrete disintegrates between 500°C and 600°C. Refractory cements have the ability to withstand temperatures up to 800°C. This would ensure that the concrete tanks would be able to withstand the effects of some molten salts that can reach 700°C.

REFERENCES

Flugge, W. *Stresses in Shells*. Springer Verlag Publishing.Co, Berlin, 1960.

Kodur, Venkatesh. "Properties of Concrete at Elevated Temperatures." Hindawi Publishing Corporation, 2014. Retrieved from http://downloads.hindawi.com/journals/isrn/2014/468510.pdf on June 15, 2015.

Urugal, A. C. *Theory of Beams, Plates, and Shells*. 4th Ed. CRC Press, Boca Raton, FL, 2009.

APPENDIX A

CHARACTERISTICS OF MOLTEN SALTS AND RECOMMENDATIONS FOR USE IN SOLAR POWER STATIONS

Written By

Dr. Samaan G. Ladkany, PE

Dr. William G. Culbreth, PE,

Nathan Loyd, EI

This paper has been adapted from this thesis and will be published and presented at the 1st Annual EURO-MED-ISEC Conference in Istanbul, Turkey, from May 24 to 29, 2016.

CHARACTERISTICS OF MOLTEN SALTS AND RECOMMENDATIONS FOR USE IN SOLAR POWER STATIONS

Samaan G. Ladkany, William G. Culbreth, and Nathan Loyd

HRH College of Engineering, University of Nevada Las Vegas, Las Vegas, NV, USA

Molten salts (MS) in the 580°C range could be used to store excess energy from solar power stations and possibly from nuclear or coal. The energy can be stored up to a week in large containers at elevated temperature to generate eight hours of electricity to be used at night or during peak demand hours. This helps to reduce the fluctuation experienced at thermal solar power stations due to weather conditions. Our research supported by Office of Naval Research (ONR), presents a survey of salts to be used in molten salt technology. The physical characteristics of these salts such as density, melting temperature, viscosity, electric conductivity, surface tension, thermal capacity and cost are discussed. Cost is extremely important given the large volumes of salt required for energy storage at a commercial power station. Formulas are presented showing the amount of salt needed per required megawatts of stored energy depending on the type of salt. The estimated cost and the size of tanks required and the operating temperatures are presented. Recommendations are made regarding the most efficient type of molten salt to use. Commercial thermal solar power stations have been constructed in the US and overseas mainly in Spain for which molten salt is being considered. A field of flat mirrors together with collection towers are used in some designs and parabolic troughs used in others.

Keywords: Commercial electric station, energy storage, energy production, molten salt technology, solar salts, thermal solar power.

1 INTRODUCTION

Molten solar salts are a great and effective way to store excess solar energy for future use due to the vast heat storage capacities of solar salts. In order for the solar salts to effectively store heat, the salts must be contained. This is done by storing the solar salts in large insulated tanks in order to keep the molten salts in a closed system.

This project examines the current method of using insulated stainless steel cylindrical shells to store molten salt and presents a preliminary design of real life examples. In addition, this design solution is compared to alternative shell designs that are expected to be more efficient in reducing shell thicknesses and stainless steel using hybrid shell design and shapes other than cylindrical shells.

2 TYPES OF MOLTEN SALTS

There are various kinds of salts, all of which can be melted for use as a molten salt. This report will mostly focus on five salts: sodium nitrate, lithium nitrate, potassium nitrate, sodium chloride, and a mixture of 60% sodium nitrate and 40% potassium nitrate. These salts have been most prominently mentioned in the literature and are being used in experimental thermal sun storage facilities since they are cost effective (Janz 1967). Other salts that can be used in these applications, both alone and in mixture form, include calcium nitrate, potassium chloride, and lithium chloride (Janz 1967).

3 PHYSICAL PROPERTIES OF MOLTEN SALTS

The first aspect of solar salts that must be considered are there physical properties, including melting point, density, viscosity, surface tension, heat capacity and electrical conductance. The density of these solar salts directly affect the loading exhibited by the storage tanks and any piping used. The melting point reflects an approximation of the temperatures these storage tanks will experience, which can be used to determine thermal expansion, ultimate strength and thickness along with heat shielding requirements of the tanks. The viscosity determines the resistance of the molten salt while flowing through any pipes used. Surface tension is the measure of force a liquid exerts on a surface by interacting with the surface. Lastly, the electrical conductance determines the salt's ability to conduct electricity. Table 1 compares the densities and melting points of these various salts.

Table 1: Physical Properties of Solar Salts (Haynes 2012a) (Janz et. al. 1972)

Compound or Mixture	Melting Point (°C)	Density at MP (g/cm3)
Sodium Nitrate – $NaNO_3$	306.5	1.900
Lithium Nitrate – $LiNO_3$	253.0	1.781
Potassium Nitrate – KNO_3	334.0	1.865
Sodium Chloride – NaCl	800.7	1.556
60 % $NaNO_3$ / 40 % KNO_3	225 (approximate)	1.870 (at 625 K)

Comparing the melting points, the 60% sodium nitrate and 40% potassium nitrate mixture has the lowest melting point with an approximate melting point of 225°C (Janz et. al. 1972). The next lowest melting point is lithium nitrate at 253°C (Haynes 2012a). On the other side of the spectrum, sodium chloride (basic table salt) has the highest melting point considered at 800.7°C (Haynes 2012a). The melting point of a salt is an important consideration for solar salt applications, which means that based on melting point, the best salt, for our applications is the 60% sodium nitrate and 40% potassium nitrate mixture since it has the lowest melting point considered while sodium chloride is the worst salt considered since it has the highest melting point.

Comparing the densities of these salts, the salt with the lowest density considered is sodium chloride with a density of 1.556 g/cm3 (Haynes 2012a). The salt with the next lowest density is lithium nitrate with a density of 1.781 g/cm3 (Haynes 2012a). At the other end, the salt with the highest density considered is sodium nitrate with a density of 1.900 g/cm3 (Haynes 2012a). Unlike melting point, density is not as important of a consideration, especially since the relative difference in densities between these salts is small.

Table 2 compares the viscosities, surface tensions, and electrical conductance of various solar salts.

Table 2: Physical Properties of Solar Salts at Melting Point (Janz 1967) (Janz et. al. 1972)

Compound or Mixture	Viscosity (mPa-s)	Surface Tension (mN/m)	Electrical Conductance (S/cm)
Sodium Nitrate – $NaNO_3$	3.038	116.35	0.9713
Lithium Nitrate – $LiNO_3$	7.469	115.51	0.3958
Potassium Nitrate – KNO_3	2.965	109.63	0.6324
Sodium Chloride – NaCl	1.459	116.36	0.8709
60 % $NaNO_3$ / 40 % KNO_3	3.172*	121.80 (at 510 K)	0.7448*

Note: Values with a single asterisk (*) have been extrapolated for the 60% $NaNO_3$ mix at 580 K

Comparing the viscosities, the salt with the lowest viscosity is sodium chloride with 1.459 mPa-s (Janz 1967). The next lowest salt is potassium nitrate with 2.965 mPa-s (Janz 1967). Conversely, the salt with the highest viscosity is lithium nitrate with 7.469 mPa-s (Janz 1967). In comparison with other physical properties considered, viscosity is not the most important property to consider in comparing molten salts. However, it is a property of some importance as the viscosity compares the resistance exerted against the molten salts while flowing through a pipe, which is something the molten salts will have to do in the containment units.

Comparing the surface tension, the salt with the lowest surface tension is potassium nitrate with 109.63 mN/m (Janz 1967). The next lowest salt is lithium nitrate with 115.51 mN/m (Janz 1967). On the other side, the salt with the highest surface tension is the 60% sodium nitrate and 40% potassium nitrate mixture with 121.80 mN/m (Janz et. al. 1972). In comparison with other properties considered, surface tension is also not one of the most important properties to consider in comparing molten salts to be used in our applications. However, it is a property of some importance because it affects the tanks and piping of the containment units

Comparing the electrical conductance, the salt with the highest electrical conductance is sodium nitrate with 0.9713 S/cm (Janz 1967). The next highest salt is sodium chloride with 0.8709 S/cm (Janz 1967). On the other side, the salt with the lowest electrical conductance is lithium nitrate with 0.3958 S/cm (Janz 1967). Compared to the other physical and thermodynamic properties considered, electrical conductance is a minor consideration when comparing solar salts for energy storage applications.

4 THERMODYNAMIC PROPERTIES OF MOLTEN SALTS

Solar salts are known for their ability to store heat for long periods of time. The heat of fusion measures the required amount of heat needed to convert a substance from a solid state to a liquid state, or simply the amount of heat needed to melt a substance. The specific heat capacity measures a substance's ability to store heat. Lastly, thermal conductivity measures a substance's ability to conduct heat through said substance. All three properties considered are of major importance since these properties compare how the salts conduct and store heat. Table 3 compares the thermodynamic properties of solar salts.

Table 3: Thermodynamic Properties of Solar Salts (Janz 1967) (Cornwell 1970) (Haynes 2012b) (Janz et. al. 1979)

Compound or Mixture	Specific Heat Capacity (J/mol/K)	Thermal Conductivity (kW/mol/K)	Heat of Fusion (kJ/mol)
Sodium Nitrate – $NaNO_3$	131.8	5.66	15.50
Lithium Nitrate – $LiNO_3$	99.6	5.82	26.70
Potassium Nitrate – KNO_3	115.9	4.31	9.60
Sodium Chloride – NaCl	48.5	8.80	28.16
60 % $NaNO_3$ / 40 % KNO_3	167.4 (at 510 K)	3.80	13.77
Note: Since some values were given in calories in some sources, they were converted into joules for this table (1 cal = 4.184 J or 1 kcal = 4.184 kJ) (IUPAC).			

Comparing the specific heat capacity, the salt with the highest specific heat capacity is the 60% sodium nitrate and 40% potassium nitrate mixture with 167.4 J/mol/K (Janz et. al. 1979). The next highest salt is sodium nitrate with 131.8 J/mol/K (Janz 1967). On the other side, the salt with the lowest specific heat capacity is sodium chloride with 48.5 J/mol/K (Janz 1967). Based on this comparison, the best salt to use for energy storage is the 60% sodium nitrate and 40% potassium nitrate mixture since it has the highest heat capacity considered while sodium chloride is the worst salt considered since it has the lowest heat capacity.

Comparing the thermal conductivity, the salt with the highest thermal conductivity is sodium chloride with 8.80 kW/mol/K (Cornwell 1970). The next highest salt is lithium nitrate with 5.82 kW/mol/K (Cornwell 1970). On the other side, the salt with the lowest thermal conductivity is the 60% sodium nitrate and 40% potassium nitrate mixture with 3.80 kW/mol/K (Cornwell 1970).

Comparing the heat of fusion, the salt with the lowest heat of fusion is potassium nitrate with 9.60 kJ/mol (Haynes 2012b). The next lowest salt is the 60% sodium nitrate and 40% potassium nitrate mixture with 13.77 kJ/mol (Janz et. al. 1979). On the other side, the salt with the highest heat of fusion is sodium chloride with 28.16 kJ/mol (Haynes 2012b). Based on the comparison of salt characteristics presented in Table 1.3, the 60%/40% sodium/potassium nitrates present, for now the most interesting option for molten salt energy storage. However other options will be considered, such as, the addition of Nano silica to the salt mix in order to improve its specific heat capacity by 30% or more.

5 COST OF SOLAR SALTS

Ultimately, compared to the other considered salts, the most promising solar salt to use, so far, in molten salt energy storage, is the 60% Sodium Nitrate and 40% Potassium Nitrate mixture since it compares favorably against other salts in terms of thermodynamic and heating properties, which are the primary factors to consider for use as a solar salt.

However, when considering the use of solar salts, one must consider the costs of various types of salts. Table 4 compares the 60% sodium nitrate and 40% potassium nitrate mixture to various other solar salt substitutes that are available in the marketplace.

Table 4: Costs of Solar Salts (Kearney & Associates 2001)

Compound or Mixture	ΔT (°C)	Cost of Salts ($/kg)	Cost of Power ($/kWH)
Hitec XL in 59% Water (42:15:43 Ca:Na:K)	200	1.43	18.20
	200	3.49 (w/o H_2O)	18.20
Hitec (7:53 Na:K: Nitrate, 40 Na Nitrate)	200	0.93	10.70
Solar Salt (60:40 Na:K Nitrate)	200	0.49	5.80
Calcium Nitrate Mixture Dewatered (42:15:43 Ca:Na:K Mixture)	200	1.19	15.20
	150	1.19	20.10
	100	1.19	30.00
Therminol VP-1 (Diphenyl Biphenyl Oxide)	3.96	100.00	57.50

The solar salt mixture (60% NaNO3 – 40% KNO3) is both the least expensive in terms of cost to purchase, which is 49 cents per kilogram, and the costs per kilowatt-hour of power generated, which is $5.80 per kilowatt-hour (Kearney & Associates 2001). The next best priced mixture in both aspects is the Hitec mixture, which costs 93 cents per kilogram to purchase and has a power cost of kilowatt-hour of $10.70 (Kearney & Associates 2001). In addition, the mixture that is the most expensive in both aspects is the Therminol VP-1, which costs $100 per kilogram to purchase and has a power cost of $57.50 per kilowatt-hour (Kearney & Associates 2001).

6 CORROSION FROM MOLTEN SALTS

In addition to being able to hold large quantities of heat, molten salts can be corrosive. Table 5 examines the corrosion properties of stainless steel exposed to various molten salts.

Table 5: Corrosion Properties of Stainless Steel Using Molten Salts (Sohal et. al. 2010) (Bradshaw and Goods 2001)

Compound or Mixture	Temp (°C)	Corrosion Rate (mm/y)	
		SS 304	SS 316
60 % $NaNO_3$ / 40 % KNO_3	580	------	0.5
Sodium Chloride – NaCl	845	7.2	7.2
Hitec Salt	538	0.21	<0.03
	430	------	0.007
	505	------	0.008
	550	------	0.074

The solar salt mixture at a temperature of 580°C corrodes both the SS 316 stainless steel at 0.5 millimeters per year (Bradshaw and Goods 2001). The sodium chloride at a temperature of 845°C corrodes both types of stainless steel at 7.2 millimeters per year (Sohal et. al. 2010). At 538°C, the Hitec Salt corrodes through SS 304 steel at 0.21 millimeters per year, and through the SS 316 steel at less than 0.03 millimeters per year (Sohal et. al. 2010). In addition, the Hitec Salt corrodes through SS 316 steel 0.007 millimeters per year at 430°C, 0.008 millimeters per year at 505°C, and 0.074 millimeters per year at 550°C (Sohal et. al. 2010).

7 CONCLUSION

A survey of molten solar salts for use in energy storage shells is presented, to provide electric generation stations with power for eight hours. Tables are shown providing the characteristics of various molten salts to be used in thermal solar energy stations. Recommendations for the selection of an economical molten salt compound is made using various characteristics, including thermal capacity, availability, melting temperature, and the cost of salts.

REFERENCES

"1.6 Conversion tables for units." IUPAC. Retrieved from http://iupac.org/publications/analytical_compendium/Cha01sec6.pdf on Feb. 3, 2015.

Bradshaw, R.W. and S.H. Goods. "Corrosion Resistance of Stainless Steels during Thermal Cycling in Alkali Nitrate Molten Salts." Sandia National Laboratory, 2001.

Cornwell, K. "The Thermal Conductivity of Molten Salts." Department of Mechanical Engineering, Heriot-Watt University, 1970. Retrieved from http://iopscience.iop.org/0022-3727/4/3/313/pdf/0022-3727_4_3_313.pdf on Nov. 6, 2014.

"Engineering Evaluation of a Molten Salt HTF in a Parabolic Trough Solar Field", pg. 7. Kearney & Associates and Flabeg Solar International, 2001. Retrieved from http://www.nrel.gov/csp/troughnet/pdfs/ulf_herrmann_salt.pdf on Dec. 13, 2014.

Haynes, W. "Density of Molten Elements and Representative Salts". *CRC Handbook of Chemistry and Physics*, 2012. Retrieved from http://www.hbcpnetbase.com//articles/04_07_92.pdf#xml=http://www.hbcpnetbase.com/search/pdfHits.asp?id=04_07_92&DocId=118023&hitCount=10&hits=1984 1980 1969 1965 1386 1382 160 159 141 41 on Nov. 5, 2014.

Haynes, W. "Enthalpy of Fusion." *CRC Handbook of Chemistry and Physics*, 2012. Retrieved from http://www.hbcpnetbase.com//articles/06_26_92.pdf#xml=http://www.hbcpnetbase.com/search/pdfHits.asp?id=06_26_92&DocId=118085&hitCount=4&hits=507 366 365 155 on Nov. 5, 2014.

Janz, G.J. *Molten Salts Handbook*. Academic Press. New York, NY, 1967.

Janz, G.J., Allen, C.B., Bansal, N.P., Murphy, R.M., and Tomkins, R.P.T. "Physical Properties Data Compilations Relevant to Energy Storage. II. Molten Salts: Data on Single and Multi-Component Salt Systems." Molten Salts Data Center, Cogswell Laboratory, Rensselaer Polytechnic Institute, 1979. Retrieved from http://www.nist.gov/data/nsrds/NSRDS-NBS61-II.pdf on Nov. 10, 2014.

Janz, G.J., Krebs, U., Siegenthaler, H.F., and Tompkins, R.P.T. "Molten Salts: Volume 3, Nitrates, Nitrites, and Mixtures." Molten Salts Data Center, Department of Chemistry, Rensselaer Polytechnic Institute, 1972. Retrieved from http://www.nist.gov/data/PDFfiles/jpcrd10.pdf on Nov. 18, 2014.

Sohal, M., Ebner, M., Sabharwall, P., and Sharpe, P. "Engineering Database of Liquid Salt Thermophysical and Thermochemical Properties." Idaho National Laboratory, 2010. Retrieved from http://www.inl.gov/technicalpublications/Documents/4502650.pdf on Feb. 6, 2015.

APPENDIX B

DESIGN OF MOLTEN SALT SHELLS FOR USE IN ENERGY STORAGE AT SOLAR POWER PLANTS

Written By

Dr. Samaan G. Ladkany, PE

Dr. William G. Culbreth, PE,

Nathan Loyd, EI

This paper has been adapted from this thesis and will be published and presented at the 1st Annual EURO-MED-ISEC Conference in Istanbul, Turkey, from May 24 to 29, 2016.

DESIGN OF MOLTEN SALT SHELLS FOR USE IN ENERGY STORAGE AT SOLAR POWER PLANTS

Dr. Samaan G. Ladkany, PE, Dr. William G. Culbreth, PE, and Nathan Loyd, EI

HRH College of Engineering, University of Nevada Las Vegas, Las Vegas, NV, USA
Tel: +1 (702) 301-7895, +1 (702) 895-3438, +1 (702) 738-5013

Design of a steel tank for the storage of excess energy from thermal solar power plants using molten salts (MS) at 580°C is presented. Energy can be stored up to a week in large containers to generate eight hours of electricity for use at night or to reduce weather related fluctuation at solar thermal energy plants. Our research supported by Office of Naval Research (ONR) presents a detailed design of a cylindrical shell for the storage of high temperature molten salts. The storage shell consists of an inner stainless steel layer designed to resist corrosion and an external steel structural layer to contain the large pressures resulting from the molten salt. The cylindrical tank is 54 feet (16.459 meters) high and has an 80 feet (48.768 meters) diameter, with the salt level at a height of 42 feet (12.802 meters). Given the heat of the molten salt and the size of the tank, the design includes a flat shell cover supported on stainless steel columns and a semispherical utility access dome at the center. Considerations are made for the reduction of strength of steel at elevated temperatures. Layers of external insulation materials are used to reduce heat loss in the storage shell. The design presents a posttensioned concrete foundation analysis for the storage tank, which sits on a layer of sand to allow for thermal expansion.

Keywords: Commercial electric station, energy production, molten salt tanks, posttensioned concrete slabs, solar salts, steel cylindrical shells

1 INTRODUCTION

Molten solar salts are a great and effective way to store excess solar energy for future use due to the vast heat storage capacities of solar salts. These solar salts are contained in large insulated tanks in order to keep the molten salts in a closed system. This project examines the current method of using insulated hybrid steel cylindrical shells to store molten salt and presents a preliminary design of real life examples.

2 DESIGN METHODS FOR MS STORAGE TANKS

Currently, molten salt (MS) storage shells are usually cylindrical tanks made of stainless steel. The MS steel tanks have a hybrid design of A588 Carbon Steel and an inner layer of 316 Stainless Steel to protect against corrosion, varying in thickness from one inch (25 mm) for a fifty year plant life span to 0.6 in (15 mm) for a thirty year plant life span.

3 TANK REQUIREMENTS

For this stage of the project research, the tanks need to store enough molten solar salt, which is a 60:40 sodium nitrate ($NaNO_3$) and potassium nitrate (KNO_3) mix, to provide power for a 300 megawatt power plant for eight hours each night. Calculations determined that in order to satisfy these requirements, the two tanks need to be able to store 12,048 cubic meters of salt or 425.5 x 10^3 cubic feet.

In order to determine the total mass of salt required to operate the power plant, one must start with the basic energy equation, which is shown in Equation 1 (Holman 1986).

$$E = P_{thermal} * \Delta t_{storage} = m * c_p * \Delta T \tag{1}$$

In Equation 1 above, E represents the total energy in the system. The power generated by the power plant is $P_{thermal}$, which as stated earlier is 300 megawatts. The required time of storage is $\Delta t_{storage}$, which is 8 hours or 28,800 seconds. The required amount of solar salt needed for the power plant is represented by m. The specific heat capacity of the salt is c_p, which is 1540 joules per kilogram of salt per degree kelvin. The temperature range of the salt in the system is ΔT, which is calculated using Equation 2 below.

$$\Delta T = T_{salt,max} - (T_{sat} - 20\ K) \tag{2}$$

In Equation 2 above, the maximum temperature of salt in the system, or $T_{salt,max}$, is 853.15 degrees kelvin. The temperature of the Rankine cycle, or T_{sat}, is 620.55 degrees kelvin. Equation 2 determined that the temperature range for the salt is 252.6 degrees kelvin.

In order to determine the required mass of salt, Equation 1 is rearranged into Equation 3 as shown.

$$m = \frac{P_{thermal} * \Delta t_{storage}}{c_p * \Delta T} \tag{3}$$

This determined that the power plant requires 22.88 x 10^6 kilograms of salt, or 50.44 x 10^6 pounds (25,220 tons).

Equation 4 is used to determine the volume of solid salt required.

$$V_{salt} = \frac{m}{\rho_{salt}} \tag{4}$$

Equation 4 determined that the volume of solid salt required is 12,048 cubic meters of salt, or 425.5 x 10^6 cubic feet (12,048 cubic meters). This volume will be divided over two tanks, requiring 212.7 x 10^6 cubic feet (6,024 cubic meters) for each tank. However, a third and fourth tanks, all of carbon steel, are recommended for the storage of cooled MS after power generation and for safety and continued operations during maintenance of the other tanks.

All structural steel used is A588 Grade 50 steel. The cylindrical tank designed with a 40 feet (12.192 meters) radius at the base. This results in a height of salt of 42 feet (12.802 meters) and a height of 54 feet (16.459 meters) for the cylindrical tank.

4 STEEL CYLINDRICAL TANKS

The steel structural design was divided into five elements for individual analysis and design, which are the shell wall, the top cover with a central 10 feet (3.048 meters) diameter steel access dome, support columns, a steel bottom, and the concrete slab below a layer of sand. All of these structural elements are made of structural and stainless steel except the concrete slab. Shell theory was used to perform the structural analysis of the cylindrical tank and central access dome.

The first design performed was for the shell wall. Based on shell theory, axial bending in a cylindrical shell occurs mainly at the base of the wall, at the junction with the ring and base plate, before dissipating further up the wall (Urugal 2009). Further analysis determined that axial bending dissipates nine feet above ground. The first step was to determine the bending in the shell wall. The maximum positive axial bending moment is 4.085 kip-foot/foot (18.17 kN-m/m) at the bottom of the shell, and the maximum negative bending moment is 886.2 pound-foot/foot (3.942 kN-m/m) at a height 2.7 feet (826 mm) above the bottom of the shell. Circumferential moments are equal to the Poisson ratio multiplied by the axial moments. The bottom of the wall contains the maximum circumferential tensile force, which is 177.6 kips per linear foot (klf), which is 2,593 kN/m. Tensile membrane force is determined by Equation 5b (Urugal 2009). While maximum axial compressive force, N_x, in the wall at the bottom of the shell is equal to the total dead weight of the shell, top slab, live load and service dome, which is the total weight (W), divided by the circumference of the shell. Equations 5c through 5h are used to determine the bending in the shell wall (Urugal 2009).

$$p = \gamma z \tag{5a}$$

$$N_\theta = pr \tag{5b}$$

$$D = \frac{Et}{12(1-\nu)} \tag{5c}$$

$$\beta = \sqrt{\frac{\sqrt{1-\nu^2}}{rt}} \tag{5d}$$

$$C_1 = \frac{\gamma h r^2}{Et} \tag{5e}$$

$$C_2 = \frac{\gamma r^2}{Et}\left(h - \frac{1}{\beta}\right) \tag{5f}$$

$$w = e^{-\beta x}(C_1 \cos \beta x + C_2 \sin \beta x) + \frac{\gamma (h-x) r^2}{Et} \tag{5g}$$

$$M_x = D\frac{d^2 w}{dx^2} \tag{5h}$$

$$M_\theta = \nu M_x \tag{5i}$$

$$N_x = \frac{W_x}{C} \tag{5j}$$

In determining the applied pressure on the tank from Equation 5a, it is the product of the salt unit weight (γ) and the depth of salt (z) at the specified point. In Equation 5b, p is the applied pressure on the wall and r is the radius of the wall (Urugal 2009). In Equations 5c through 5h, D, β, C_1, and C_2 are coefficients, E is the Young's Modulus of the shell material, t is thickness of the shell wall, ν is the Poisson's ratio of the shell material, h is the total height of molten salt, w is shell wall deflection at a height of x above ground, and the second derivative of w is used to determine the moment at that point (Urugal 2009). M_x is the axial moment at a height of x above ground, W_x is the weight of the shell including dead and live loads on its top at level above x (Urugal 2009). Figure 1 details the design of the cylindrical shell and the top dome.

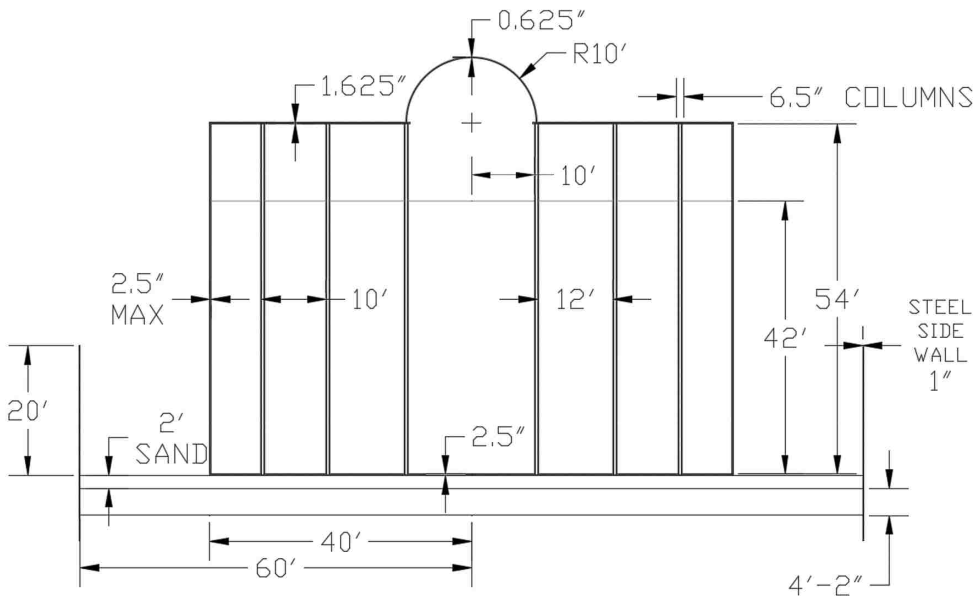

EXCEPT FOR THE SIDE WALL AND TOP DOME, ALL STEEL THICKNESS INCLUDES 1” SS LAYER.

Figure 1: Steel Cylindrical Shell Model Including Top Dome, Supporting Rows of Columns, 2’ Sand Layer, 50” Posttension Slab, and Safety Steel Walls at the Edge

The shell was designed in sections of varying thickness based on the loading. The bottom nine feet of the shell wall was designed to accommodate excess bending, require 1.5 inches of structural steel thickness due to the combined axial membrane and bending stresses. The next section of the wall, from 9 to 15 feet (2.734 to 4.572 meters) above ground, requires 0.625 inches (15.9 mm) of steel thickness. Starting from 15 feet above ground, the thickness of the shell wall is decreased by 0.125 inches (3.2 mm) every seven feet until a thickness of 0.125 inches (3.2 mm) remain. This results in the wall being 0.5 inches (12.7 mm) thick between 15 and 22 feet (4.572 to 6.706 meters), 0.375 inches (9.5 mm) between 22 and 29 feet (6.706 to 8.839 meters), 0.25 inches (6.4 mm) between 29 and 36 feet (8.839 to 10.973 meters) above ground, and 0.125 inches (3.2 mm) for the remaining portion of the wall above 36 feet (10.973 meters). Due to corrosion effects, a one inch liner of 316 Stainless Steel covers the steel wall.

The next design was for both the top steel plate and the columns supporting it in the cylindrical tank. The top plate is 0.625 inches (15.9 mm) thick and is supported by three circular rows of columns. One row of columns is located ten feet (3.048 meters) away from the center of the tank, at the tip of the opening and the 0.625 inches (15.9) thick service dome. It contains eight equally spaced columns. The second row of columns is located 22 feet (6.706 meters) away from the center of the tank and contains eight equally spaced columns. Lastly, the third row of columns is located 32 feet (9.754 meters) away from center and contains 16 equally spaced columns. These columns are made of carbon steel covered with a layer of stainless steel because of the heat and corrosion from MS. When designing the columns and shell walls, an extra factor of safety is used due to the expected heat of the molten salt. At 580 degrees Celsius, steel is expected to only maintain 60% of its nominal yield strength (Salmon 2009). As a result, the final design load for the first row of columns is 6.5 kips (28.9 kN), 19.6 kips (87.2 kN) for the second row, and 11.7 kips (52.0 kN) for the third row. Ultimately, it is determined that the first row of columns be designed as HSS 4½ x 4½ x 1/8" columns, the second row as HSS 4½ x 4½ x ¼" columns, and the third row as HSS 4½ x 4½ x 1/8" columns (Steel Construction Manual 2012). Due to corrosion effects, a one inch (25.4 mm) liner of 316 Stainless Steel covers the steel column. In addition, the column will be connected to the top steel shell with a 14 inch by 14 inch (356 mm) plate that is two inches thick (50.8 mm).

In order to design for bending in the top steel flat slab, Timoshenko's method was used to design the top plate as a continuous simply supported plate over the edge of the shell and supported by rows of columns as discussed earlier. Moments at the supporting columns are found from the column pattern of annular arrays normalized as rectangular arrays. Based on Timoshenko's (1959) theory, the maximum negative bending moment in each direction is located at the column. The maximum positive moments, being the radial moments, occur at the center of the normalized annulus, and the maximum circumferential moment occur directly halfway between columns. For this shell, the maximum negative moment is 1.785 kip-foot/foot and the maximum positive radial moment is 1.040 kip-foot/foot.

In addition, an opening with a 10 feet (3.048 meters) radius is carved out of the top shell so that a removable steel dome with the same radius can be placed on top of the steel plate. This opening is to allow pipes into the shell and service access into the tank.

5 FOUNDATION DESIGN

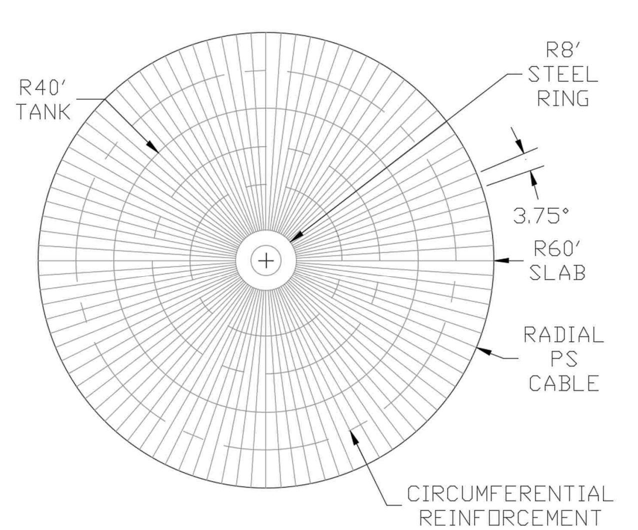

Figure 2: Posttensioning Cable and Circumferential Reinforcement Layout for Concrete Slab Including Inner Steel Ring

A complete design was performed on the concrete slab sitting over dense sand. Included in the foundation design is a 2 feet (610 mm) layer of sand between the tank and the concrete slab as shown in Figure 1 to allow for thermal expansion of the shell. Figure 2 details the radial posttensioning cable layout, the steel ring, and circumferential reinforcement in the concrete slab. The steel ring is necessary because the posttensioning cables cannot intersect with each at the center of the 50 inch concrete slab.

For the slab, 96 radial posttensioning 55/0.5 WG cables that connect to the inner steel ring are required as shown in Figure 2. In addition, six #14 circumferential bars per foot are required under the MS tank, with number of bars decreasing toward the free edge. In addition, the minimum radial posttensioning cables depth is 12.75 inches (324 mm), the maximum radial posttensioning cables depth is 38.75 inches (984 mm), and the circumferential reinforcement depth is 44.125 inches (1.121 meters). This requires a slab thickness of 50 inches (1.270 meters) as shown in Figure 1.

6 CONCLUSION

The design of a cylindrical A588 Grade 50 steel shell, having a diameter of 80 feet (24.384 meters), for the storage of molten salts is presented. The shell is 54 feet (16.459 meters) high, has a height of salt of 42 feet (12.802 meters), and has a top access dome with a radius of 10 feet (3.048 meters). The two tank system is designed to store enough molten salt to provide 300 megawatts of power for eight hours. The shell has a one inch (25.4 mm) stainless steel liner to protect against corrosion for a 50 year design life. Also shown is a 120 feet (36.576 meters) diameter concrete foundation with posttensioning, which has a 50 inch (1.270 meters) thickness and steel side walls that are 20 feet (6.048 meters) high for safety in case of an accident.

REFERENCES

Flugge, W. *Stresses in Shells*. Springer Verlag Publishing.Co, Berlin, 1960.

Holman, J.P. *Heat Transfer, Sixth Edition*. McGraw-Hill. New York, NY, 1986.

Salmon, C.G., Johnson, J.E., and Malhas, F.A. *Steel Structures: Design and Behavior*. 5th Ed. Pearson Prentice Hall, Upper Saddle River, NJ, 2009.

Steel Construction Manual. 14th Ed. American Institute of Steel Construction, 2012.

Timoshenko, S. *Theory of Plates and Shells*. McGraw-Hill, New York, 1959.

Urugal, A. C. *Theory of Beams, Plates, and Shells*. 4th Ed. CRC Press, Boca Raton, FL, 2009.

BIBLIOGRAPHY

"1.6 Conversion tables for units." IUPAC. Retrieved from http://iupac.org/publications/analytical_compendium/Cha01sec6.pdf on Feb. 3, 2015.

"Engineering Evaluation of a Molten Salt HTF in a Parabolic Trough Solar Field", pg. 7. Kearney & Associates and Flabeg Solar International, 2001. Retrieved from http://www.nrel.gov/csp/troughnet/pdfs/ulf_herrmann_salt.pdf on Dec. 13, 2014.

ACI 318-14. American Concrete Institute, 2014.

Bauer, Thomas, Nils Breidenbach, Nicole Pfleger, Doerte Laing, and Markus Eck. "Overview of Molten Salt Storage Systems and Material Development for Solar Thermal Power Plants". Institute of Technical Thermodynamics, German Aerospace Center, 2012.

Bradshaw, R.W. and S.H. Goods. "Corrosion Resistance of Stainless Steels during Thermal Cycling in Alkali Nitrate Molten Salts." Sandia National Laboratory, 2001.

Cordaro, Joseph, Alan Kruizenga, Rachel Altmaier, Matthew Sampson, and April Nissen. "Thermodynamic Properties of Molten Nitrate Salts". Sandia National Laboratories, 2011.

Cornwell, K. "The Thermal Conductivity of Molten Salts." Department of Mechanical Engineering, Heriot-Watt University. <http://iopscience.iop.org/0022-3727/4/3/313/pdf/0022-3727_4_3_313.pdf>. (1970). (Nov. 6, 2014).

Flugge, W. *Stresses in Shells*. Springer Verlag Publishing.Co, Berlin, 1960.

Haynes, W. "Density of Molten Elements and Representative Salts". *CRC Handbook of Chemistry and Physics*, 2012. Retrieved from http://www.hbcpnetbase.com//articles/04_07_92.pdf#xml=http://www.hbcpnetbase.com/search/pdfHits.asp?id=04_07_92&DocId=118023&hitCount=10&hits=1984 1980 1969 1965 1386 1382 160 159 141 41 on Nov. 5, 2014.

Haynes, W. "Enthalpy of Fusion." *CRC Handbook of Chemistry and Physics*, 2012. Retrieved from http://www.hbcpnetbase.com//articles/06_26_92.pdf#xml=http://www.hbcpnetbase.com/search/pdfHits.asp?id=06_26_92&DocId=118085&hitCount=4&hits=507 366 365 155 on Nov. 5, 2014.

Holman, J.P. *Heat Transfer, Sixth Edition*. McGraw-Hill. New York, NY, 1986.

Janz, G.J. *Molten Salts Handbook*. Academic Press. New York, NY, 1967.

Janz, G.J., Allen, C.B., Bansal, N.P., Murphy, R.M., and Tomkins, R.P.T. "Physical Properties Data Compilations Relevant to Energy Storage. II. Molten Salts: Data on Single and Multi-Component Salt Systems." Molten Salts Data Center, Cogswell Laboratory, Rensselaer Polytechnic Institute, 1979. Retrieved from http://www.nist.gov/data/nsrds/NSRDS-NBS61-II.pdf on Nov. 10, 2014.

Janz, G.J., Krebs, U., Siegenthaler, H.F., and Tompkins, R.P.T. "Molten Salts: Volume 3, Nitrates, Nitrites, and Mixtures." Molten Salts Data Center, Department of Chemistry, Rensselaer Polytechnic Institute, 1972. Retrieved from http://www.nist.gov/data/PDFfiles/jpcrd10.pdf on Nov. 18, 2014.

Kodur, Venkatesh. "Properties of Concrete at Elevated Temperatures." Hindawi Publishing Corporation, 2014. Retrieved from http://downloads.hindawi.com/journals/isrn/2014/468510.pdf on June 15, 2015.

Salmon, C.G., Johnson, J.E., and Malhas, F.A. *Steel Structures: Design and Behavior*. 5th Ed. Pearson Prentice Hall, Upper Saddle River, NJ, 2009.

Sohal, M., Ebner, M., Sabharwall, P., and Sharpe, P. "Engineering Database of Liquid Salt Thermophysical and Thermochemical Properties." Idaho National Laboratory, 2010.

Retrieved from http://www.inl.gov/technicalpublications/Documents/4502650.pdf on Feb. 6, 2015.

Steel Construction Manual. 14th Ed. American Institute of Steel Construction, 2012.

Timoshenko, S. *Theory of Plates and Shells*. McGraw-Hill, New York, 1959.

Urugal, A. C. *Theory of Beams, Plates, and Shells*. 4th Ed. CRC Press, Boca Raton, FL, 2009.

CURRICULUM VITAE

Graduate College
University of Nevada, Las Vegas

Nathan David Tyrrell Loyd

Degrees:

Bachelor of Science, Civil Engineering, 2013
University of Nevada, Reno – Reno, Nevada

Conference Publications

Loyd, Nathan and Samaan G. Ladkany (2016). “Characteristics of Molten Salts and Recommendations for Use in Solar Power Stations”, EURO-MED-ISEC Conference, May 2016, Istanbul, Turkey.

Loyd, Nathan and Samaan G. Ladkany (2016). “Design of Molten Salt Shells for Use in Energy Storage at Solar Power Plants”, EURO-MED-ISEC Conference, May 2016, Istanbul, Turkey.

Thesis Title:

Solar Energy Storage in Molten Salt Shell Structures

Thesis Examination Committee:

Chairperson, Samaan G. Ladkany, Ph. D.
Committee Member, Nader Ghafoori, Ph. D.
Committee Member, Ying Tian, Ph. D.
Graduate Faculty Representative, William Culbreth, Ph. D.